

**Harnessing SABRE to polarise water, biologically
significant amines and plant oils as a prelude to
their use in MRI**

Adel Mohammed M Alshehri

Doctor of Philosophy

University of York

Chemistry

January 2023

Abstract

In this study, a new range of biological compounds were explored as targets for SABRE. The thesis starts with examining a group of important amines, phenethylamine, ethanolamine, benzylamine and ammonia. All of the studied amines generate dihydride-amine complexes, which are characterised, and proved to be SABRE active. The conditions were then optimised to achieve signal enhancements levels for their proton resonances of 200-916 fold.

These amines were utilised in the next chapter as agents for SABRE RELAY where a group of plant based natural products (essential oils) are hyperpolarised. The measurements showed significant enhancement levels for their ^1H resonances of between 2544-2953 fold. The same SABRE protocol led to the hyperpolarisation and detection of all the ^{13}C signals for citronellol, rhodinol, and menthol within seconds rather than hours as would normally be required.

During the measurements of chapters 2 and 3 it was noted that some of the results were affected by the presence of water in the NMR solvent. Since water is a fundamental molecule and was not previously examined by SABRE at the time this work started, it was decided to use it as a substrate in the 4th chapter. The work on water started by significantly improving the lifetime of the hyperpolarised water signal from 3.7 s to 30 s by using mixtures of D_2O and DMSO. Benzylamine and ammonia were used as SABRE-RELAY agents for these measurements and HOD enhancement levels of 700-fold were obtained.

The critical evolution of the data presented in this thesis suggests that hyperpolarisation transfer from a polarised OH into a wide range of target analytes is possible. The spin-topology of the analyte is critical, as polarisation transfer stops at quaternary centres. The relaxation times of the associated groups played a role in mediating detected signal strengths.

Contents

Abstract.....	3
Contents	5
List of Tables	9
List of Figures.....	12
Acknowledgements.....	17
Author Declaration	19
Chapter 1: Introduction.....	21
1.1 Nuclear magnetic resonance	21
1.2 Sensitivity issue	22
1.3 Methods of hyperpolarisation and signal enhancement.....	23
1.3.1 Hyperpolarisation by brute force	23
1.3.2 Hyperpolarisation by optical pumping.....	24
1.3.3 Hyperpolarisation by dynamic nuclear polarisation (DNP).....	25
1.3.4 Hyperpolarisation by parahydrogen induced polarization (PHIP).....	29
Chapter 2: SABRE with phenylethylamine, ethanolamine, benzylamine, and ammonia.....	36
2.1 Introduction.....	36
2.2 Developing SABRE for phenylethylamine.....	38
2.2.1 Characterisation of phenylethylamine.....	39
2.2.2 T_1 relaxation time of phenethylamine	40
2.2.3 Reaction of phenylethylamine with Ir(Cl)(COD)(IMes) (2).....	41
2.2.4 SABRE of 1 achieved by the catalyst [Ir(H) ₂ (IMes)(1) ₃]Cl (3).....	45
2.3 SABRE Optimisation.....	47
2.3.1 Effect of substrate loading on the ¹ H polarisation level in 2 when its concentration is kept constant.....	47
2.3.2 Temperature effect on polarisation	49

2.3.3 SABRE at variable magnetic field strengths.....	50
2.4 Developing SABRE for Ethanolamine	51
2.4.1 T_1 relaxation time of ethanolamine	52
2.4.2 Reaction of ethanolamine with Ir(Cl)(COD)(IMes) (2).....	52
2.5 SABRE Optimisation of Ethanolamine	54
2.5.1 Effect of ethanolamine concentration on the ^1H NMR based polarisation level when the concentration of precatalyst 2 is kept constant	54
2.5.2 SABRE under low and high temperature experiments	55
2.5.3 SABRE at variable magnetic field strengths.....	56
2.6 Developing SABRE for benzylamine and ammonia	57
2.6.1 Effect on SABRE polarisation by substrate-catalyst ratio	63
2.6.2 Effect on SABRE polarisation by temperature.....	63
2.7 Summary	64
2.8 Conclusion	65
Chapter 3: Hyperpolarisation of essential oils.....	66
3.1 Results and Discussion	67
3.1.1 NMR Characterisation of Citronellol through SABRE-RELAY	67
3.1.2 SABRE-RELAY of Citronellol with the sensitizer Phenethylamine.....	68
3.1.3 SABRE-RELAY of citronellol with the sensitizer ethanolamine	69
3.1.4 SABRE-RELAY with the sensitizer ammonia	69
3.1.5 SABRE-RELAY with deuterated phenethylamine (PEA- d_4)	71
3.1.6 SABRE-RELAY with deuterated benzylamine- d_7	72
3.1.7 Effect of the concentration of transfer agent and substrate on the enhancement level of SABRE-RELAY	73
3.1.7.1 SABRE Relay with different concentrations of ammonia	73
3.1.7.2 SABRE-RELAY with different loadings of citronellol	74
3.1.8 NMR Characterisation of nerol through SABRE-RELAY	76
3.1.9 SABRE-RELAY with ammonia	77
3.1.10 SABRE-RELAY of nerol with deuterated benzylamine- d_7	78
3.1.11 NMR Characterisation of Geraniol through SABRE-RELAY	79
3.1.12 SABRE-RELAY with deuterated benzylamine- d_7	80
3.1.13 SABRE-RELAY with deuterated phenethylamine (PEA- d_4)	80
3.1.14 SABRE-RELAY with ammonia	81
3.2 ^{13}C NMR signal enhancements for Citronellol, Nerol and Geraniol.....	81
3.3 Effect of T_1 relaxation	87
3.4 Increasing the substrate range	90
3.4.1 SABRE-RELAY of Menthol	90

3.4.2 SABRE-RELAY of Verbenol.....	92
3.4.3 SABRE-RELAY of Rhodinol.....	95
3.5 Conclusions and Perspective.....	98
Chapter 4: Hyperpolarisation of Water with SABRE	100
4.1 Introduction.....	100
4.2 Results and discussion	101
4.2.1 Control NMR Spectra	101
4.2.2 Characterisation of $[\text{Ir}(\text{H})_2(\text{IMes})(\text{BnNH}_2)_3]\text{Cl}$	103
4.2.3 Effect of added D_2O on the appearance of the SABRE-RELAY polarisation derived from BnNH_2	107
4.2.4 Utilisation of DMSO as a co-ligand with benzylamine for the hyperpolarisation of H_2O	110
4.2.4.1 SABRE Relay using $\text{Ir}(\text{IMes})(\text{COD})\text{Cl}$, BnNH_2 , DMSO and H_2O	111
4.2.5 Effect of D_2O on the level of H_2O signal gain and T_1	113
4.2.6 SABRE Relay using $\text{IrCl}(\text{COD})(\text{IMes})$, NH_3 and H_2O	114
4.3 Conclusion	115
Chapter 5: Conclusions and future work	117
Chapter 6: Experimental	120
6.1 Instrumentation	120
6.1.1 NMR spectrometers	120
6.1.2 Generation of <i>para</i> - H_2	120
6.2 Summary of the SABRE NMR method.....	120
6.2.1 Preparation of a SABRE NMR sample.....	120
6.2.2 SABRE NMR measurement	121
6.2.3 SABRE enhancement calculations.....	121
6.2.4 Measurement of T_1 relaxation time	122
6.2.5 Measurement of hyperpolarised T_1	122
Appendix A.....	123
7.1 Characterisation of substrates	123
Phenylethylamine	123
Ethanolamine	124
Benzylamine	124
Citronellol	125
Nerol	126

Geraniol	126
Menthol	127
Verbenol	128
Rhodniol	128
7.2 Characterisation of SABRE complexes	129
[Ir(H) ₂ (IMes)(phenethylamine) ₃]Cl	129
[Ir(H) ₂ (IMes)(ethanolamine) ₃]Cl	130
[Ir(H) ₂ (IMes)(NH ₃) ₃]Cl.....	131
[Ir(H) ₂ (IMes)(BnNH ₂) ₃]Cl	132
[Ir(H) ₂ (IMes)(BnNH ₂) ₂ (DMSO)]Cl.....	133
Appendix B	134
Abbreviations.....	142
References	144

List of Tables

Table 2.1: NMR characterisation data for phenethylamine in dichloromethane- d_2 at 298 K with labelling according to the inset structure.	39
Table 2.2: NMR characterisation data for square planar IrCl(COD)(IMes) (2) in dichloromethane- d_2 at 298 K with resonances attributed according to the labelling of the inset structure.	42
Table 2.3: NMR characterisation data for octahedral [Ir(H) ₂ (IMes)(1) ₃]Cl (3) that forms when phenylethylamine (1) and H ₂ react with Ir(Cl)(COD)(IMes) (2) in dichloromethane- d_2 at 298 K with the labels according to the inset structure.....	44
Table 2.4: ¹ H NMR SABRE enhancements, per proton for the indicated groups of 1 for 5 and 10-fold excesses relative to 2 , based on 3 averages.....	48
Table 2.5: NMR characterisation data for ethanolamine in dichloromethane- d_2 at 298 K with labelling according to the inset structure.	52
Table 2.6: NMR characterisation data for [Ir(H) ₂ (ethanolamine) ₃ (IMes)]Cl (4) in dichloromethane- d_2 at 253 K alongside the labelled structure.....	53
Table 2.7: ¹ H NMR SABRE enhancement levels for ethanolamine obtained from 5 mM IMes samples with 10- and 20-fold excess of ethanolamine, three measurements were taken.	55
Table 2.8: NMR characterisation data of [Ir(H) ₂ (IMes)(BnNH ₂) ₃]Cl (5) in dichloromethane- d_2 at 298 K with resonances attributed according to the labelling of the inset structure.	59
Table 2.9: NMR characterisation data for benzylamine in dichloromethane- d_2 at 298 K.....	60
Table 2.10: NMR characterisation data for [Ir(H) ₂ (IMes)(BnNH ₂) ₃]Cl (6) in dichloromethane- d_2 at 298 K with the labels according to the inset structure.....	61
Table 3.1: NMR characterisation data for citronellol in dichloromethane- d_2 at 298 K.....	68

Table 3.2: NMR characterisation data for nerol in dichloromethane- d_2 at 298 K.....	76
Table 3.3: ^1H NMR enhancement levels for nerol using ammonia after a delay time of 3.5 s and the corresponding values after correction for T_1 without this delay.	78
Table 3.4 : NMR characterisation data for geraniol in dichloromethane- d_2 at 298 K.	80
Table 3.5: Comparison of the ^1H NMR signal enhancement levels achieved for the protons in geraniol as a function of resonance according to the relay substrate NH_3 , PEA- d_4 and Benzylamine- d_7	81
Table 4.1: Characterization data for $[\text{Ir}(\text{H})_2(\text{IMes})(\text{BnNH}_2)_3]\text{Cl}$, 2-BnNH $_2$	106
Table 4.2: Characterization of $[\text{Ir}(\text{H})_2(\text{IMes})(\text{BnNH}_2)_2(\text{DMSO})]\text{Cl}$ complex.....	111
Table 6.1: NMR characterisation data for phenethylamine in dichloromethane- d_2 at 298 K with labelling according to the inset structure.	123
Table 6.2: NMR characterisation data for ethanolamine in dichloromethane- d_2 at 298 K with labelling according to the inset structure.	124
Table 6.3: NMR characterisation data for benzylamine in dichloromethane- d_2 at 298 K.....	124
Table 6.4: NMR characterisation data for citronellol in dichloromethane- d_2 at 298 K.....	125
Table 6.5: NMR characterisation data for nerol in dichloromethane- d_2 at 298 K...	126
Table 6.6 : NMR characterisation data for geraniol in dichloromethane- d_2 at 298 K.	127
Table 6.7: NMR characterisation data for octahedral $[\text{Ir}(\text{H})_2(\text{IMes})(\mathbf{1})_3]\text{Cl}$ (3) that forms when phenylethylamine (1) and H_2 react with $\text{Ir}(\text{Cl})(\text{COD})(\text{IMes})$ (2) in dichloromethane- d_2 at 298 K with the labels according to the inset structure.....	129

Table 6.8: NMR characterisation data for $[\text{Ir}(\text{H})_2(\text{ethanolamine})_3(\text{IMes})]\text{Cl}$ (**4**) in dichloromethane- d_2 at 253 K alongside the labelled structure..... 130

Table 6.9: NMR characterisation data of $[\text{Ir}(\text{H})_2(\text{IMes})(\text{NH}_3)_3]\text{Cl}$ (**5**) in dichloromethane- d_2 at 298 K with resonances attributed according to the labelling of the inset structure. 131

Table 6.10: NMR characterisation data for $[\text{Ir}(\text{H})_2(\text{IMes})(\text{BnNH}_2)_3]\text{Cl}$ (**6**) in dichloromethane- d_2 at 298 K with the labels according to the inset structure..... 132

Table 6.11: Characterization of $[\text{Ir}(\text{H})_2(\text{IMes})(\text{BnNH}_2)_2(\text{DMSO})]\text{Cl}$ complex. 133

List of Figures

- Figure 1.1: Illustration for the effect of spin population difference on the NMR signal strength..... 22
- Figure 1.2: MRI images of lungs of a healthy volunteer (on the left) compared to images from a COPD patient (on the right). Images were obtained after inhalation of hyperpolarised ^{129}Xe gas, and the purple colour represent the data from the hyperpolarisation process.³³ 25
- Figure 1.3: An illustration of a typical d-DNP setup for NMR investigations. The numbering shows the sequence in which the experimental procedures are performed. (1) loading a sample into a polariser. (2) achieving hyperpolarisation through microwave irradiation at 1 K. (3) a heated solvent rapidly dissolves the sample in the hyperpolarised state. (4) transferring the liquid sample to the NMR instrument. (5) measurement of hyperpolarised signal.⁴⁷ 27
- Figure 1.4: A) Histological sections of a healthy mouse prostate, early-stage, and late-stage tumour, hyperpolarised $[1-^{13}\text{C}]$ pyruvate was injected, and a representative hyperpolarised ^{13}C spectrum is shown below the histological sections. An obvious increase in the ratio of hyperpolarised lactate to hyperpolarised pyruvate was seen in the spectra as disease progressed from normal to early and late stages of tumour. B) Late-stage primary tumour in a mouse as seen on an axial T_2 ^1H image with an overlaid image of hyperpolarised $[1-^{13}\text{C}]$ lactate following injection of hyperpolarised $[1-^{13}\text{C}]$ pyruvate. Increases in hyperpolarized $[1-^{13}\text{C}]$ lactate was seen in the midst of the transformation from healthy to cancerous prostate and throughout the development of the disease. Images taken from Kurhanewicz *et. al.*⁵⁵ 28
- Figure 1.5: The four spin states combinations of hydrogen..... 29
- Figure 1.6: Energy levels and their representative NMR spectra with natural abundance hydrogen (a) and *para*- H_2 (b). In the upper photos, the population of each spin state is illustrated by the line thickness. Image from Duckett *et al.*, 2012¹⁶ 31
- Figure 1.7: Schematic representation of SABRE hyperpolarisation transfer mechanism. Green colour represents hyperpolarised state and red represents thermal state. 32
- Figure 1.8: SABRE-RELAY achieved by polarised proton exchange. 33

Figure 1.9: MR images of ^{15}N for hyperpolarised solution of ^{15}N -labelled metronidazole in 5 mm NMR tube. (a) axial view of the hyperpolarised metronidazole sample. (b) coronal view of the hyperpolarised metronidazole sample. Image taken from Birchall *et al.*, 2020. ⁷⁷34

Figure 2.1: Structure of phenethylamine (a) and ethanolamine (b).37

Figure 2.2: T_1 values for the ^1H NMR signals of free phenethylamine (1) (green) and (1) in the presence of H_2 (orange), at 9.4 T (due to phenyl ring signal overlap the T_1 is for the multiplet). The concentrations used were 2.65 mM of 1 and 2 mM of iridium.41

Figure 2.3: ^1H NMR spectra showing the effect of SABRE on the ^1H NMR response of phenethylamine (1). (b) single scan control spectrum, (a) single scan SABRE NMR spectrum. The SABRE precatalyst was $\text{Ir}(\text{Cl})(\text{COD})(\text{IMes})$ (2) (5mM), 1 concentration was 5.3mM, *para*- H_2 was present at 3 bar and transfer undertaken at 60 G. (c) a two broad peaks of NH and OH when precautions were taken to eliminate water contamination. (d) the two peaks of NH and OH are coalescing into a single broad peak due to limited water contamination.46

Figure 2.4: SABRE enhancement levels for the indicated (see inset structure) ^1H NMR resonances of free phenethylamine (1) after polarisation transfer at 273, 283, 298, 303, and 313 K.50

Figure 2.5: ^1H NMR SABRE enhancement levels for 1 (resonances indicated) at 50, 60, 70, 80, and 90 G.51

Figure 2.6: T_1 values for the ^1H NMR signals of free ethanolamine (green labelled), and ethanolamine in the presence of H_2 (orange labelled), at 9.4 T. The concentrations used were 2.35 mM of ethanolamine and 2 mM loading of IMes (2).52

Figure 2.7: ^1H NMR spectra showing the effect of SABRE on the ^1H NMR response of phenethylamine, signal scan control (top) spectrum, single scan SABRE NMR (bottom) spectrum. The SABRE precatalyst was $\text{Ir}(\text{Cl})(\text{COD})(\text{IMes})$ (5mM), the ligand was present in a 5 fold excess, *para*- H_2 was present at 3 bar and polarisation transfer undertaken at 60 G. The affected resonances are indicated in the structure. 54

Figure 2.8: ^1H NMR signal enhancement levels for the indicated resonances of ethanolamine under SABRE at 278, 288, 298, and 308 K respectively.56

Figure 2.9: ^1H NMR enhancement levels for the indicated resonances of ethanolamine using SABRE at: 40, 50, 60, 70, 80, and 90 G.....	57
Figure 2.10: (a) Thermally polarised ^1H NMR spectra of (5) scaled by x32 (b) Hyperpolarised ^1H NMR spectra of 4 (single scan) showing polarised free and bound NH_3 , and residual water signal indicated.....	58
Figure 2.11: (a) ^1H NMR spectra of BnNH_2 , hyperpolarised (bottom) and thermal polarised (top) (b) ^1H NMR spectra of $\text{BnNH}_2\text{-}d_7$ hyperpolarised (bottom) and thermal polarised (top). ¹⁰⁸	62
Figure 2.12: Temperature effect on SABRE polarisation of 2- BnNH_2 adapted from lali <i>et al.</i> ¹⁰⁸	64
Figure 3.1: a) ^1H NMR spectra to illustrate the enhancement of citronellol's ^1H responses achieved with SABRE-RELAY using NH_3 as the carrier. Thermally polarised NMR spectrum (upper) alongside single scan SABRE-RELAY response (lower). The inset structure can be used to link these resonances to their origin in Citronellol. b) The enhancement of citronellol's ^1H responses achieved using SABRE-RELAY with 1 as the carrier is demonstrated through ^1H NMR spectra. The upper spectrum represents the thermally polarized NMR response, while the lower spectrum shows the result of a single scan using SABRE-RELAY. The inset structure at (a) provides a means to correlate these resonances with their corresponding positions in citronellol.....	70
Figure 3.2: Comparison of citronellol signal enhancements per proton for the three SABRE-RELAY carriers PEA- d_4 , Benzlammine- d_7 , and NH_3 samples.	72
Figure 3.3: ^1H NMR signal enhancement level for the indicated Citronellol protons (per proton) achieved with the excesses of NH_3 relative to 5 being 12, 8 and 4 fold as indicated.....	74
Figure 3.4: ^1H NMR signal enhancements seen for citronellol with 1.5, 2.5, 5, 10 and 15 equivalents relative to (2).....	75
Figure 3.5: Typical ^1H NMR spectra of Nerol under SABRE-RELAY.....	78
Figure 3.6: ^{13}C NMR responses for citronellol. Top, 2048 scan spectrum, middle single scan hyperpolarised spectrum and bottom hyperpolarised single scan refocused and decoupled INEPT spectrum using a $\text{cns}t_2$ of 122 Hz.	85

Figure 3.7: Comparison of the average signal enhancement levels for ^{13}C of citronellol, nerol, and geraniol.	86
Figure 3.8: T_1 relaxation times, at 9.4 T, for the indicated ^1H NMR groups in citronellol, nerol and geraniol.	88
Figure 3.9: NMR responses of menthol when dissolved in dichloromethane- d_2 at 298 K.	90
Figure 3.10: Enhancement of menthol ^1H responses with SABRE-RELAY.....	91
Figure 3.11: Single scan hyperpolarised ^{13}C responses of menthol using refocussed INEPT with a $\text{cns}t_2$ of 122 Hz, top spectrum, and SABRE-RELAY bottom spectrum.	92
Figure 3.12: NMR responses of verbenol when dissolved in dichloromethane- d_2 at 298 K.	93
Figure 3.13: ^1H NMR spectra of verbenol with SABRE-RELAY showing enhancement level of ^1H responses.....	94
Figure 3.14: Single scan ^{13}C NMR spectra of verbenol with SABRE-RELAY (bottom) and refocussed INEPT (top).....	95
Figure 3.15: NMR responses of rhodinol when dissolved in dichloromethane- d_2 at 298 K.	96
Figure 3.16: ^1H NMR spectra of rhodinol with SABRE-RELAY showing enhancement level of ^1H responses.....	97
Figure 3.17: Single scan hyperpolarised ^{13}C responses of rhodinol obtained in 1 second (top) and through refocussed INEPT (bottom).	98
Figure 4.1: Effect of the addition of H_2O on the appearance of the ^1H NMR spectra of three different samples of benzylamine in dichloromethane- d_2	103
Figure 4.2: 3-dimensional representation of the structure of 2-BnNH $_2$, with numbering according to Table 4.1.	104

Figure 4.3: ^1H NMR spectrum of $[\text{Ir}(\text{H})_2(\text{IMes})(\text{BnNH}_2)_3]\text{Cl}$ complex alongside resonance assignments (below).....	105
Figure 4.4: Hyperpolarised ^1H NMR signals seen when a sample of BnNH_2 and $\text{Ir}(\text{COD})(\text{IMes})(\text{Cl})$ are examined under SABRE conditions.	107
Figure 4.5: The signals at δ 3.65 for $\text{CH}_{12\text{a}}$ and δ 3.30 for $\text{CH}_{12\text{b}}$ due to $[\text{Ir}(\text{H})_2(\text{IMes})(\text{BnNH}_2)_3]\text{Cl}$ simplify into doublets after replacement of the NH proton by ND.....	108
Figure 4.6: ^1H NMR signals at δ 4.80, 4.64 and δ 1.66 which correspond to the water and NH resonances that are hyperpolarised when a solution of $[\text{Ir}(\text{H})_2(\text{IMes})(\text{BnNH}_2)_3]\text{Cl}$ containing a 265-fold excess of D_2O and a 5-fold excess of BnNH_2 is examined under SABRE.	109
Figure 4.7: Effect of D_2O amount on the T_1 relaxation time of the water response under SABRE.....	114
Figure 6.1: Diagram of the inversion-recovery experiment's pulse sequence used for the measurements of T_1 . ¹³⁹	122
Figure 6.2: NMR responses of menthol when dissolved in dichloromethane- d_2 at 298 K.....	127
Figure 6.3: NMR responses of verbenol when dissolved in dichloromethane- d_2 at 298 K.....	128
Figure 6.4: NMR responses of rhodinol when dissolved in dichloromethane- d_2 at 298 K.....	128

Acknowledgements

Firstly, I am very grateful to my supervisor Professor Simon Duckett for his guidance, and support throughout my PhD. I would also like to thank my TAP professor Seth Davis for his advice and insightful comments throughout our TAP meetings.

Special thanks to Dr Wissam who helped me to improve my lab skills and assisted me learning and performing SABRE measurements. I would also like to thank Dr Marianna for her assistance either in the lab or with NMR work. To Dr Peter Rayner for helping me in the lab and providing the compounds needed for my thesis. And thanks to all CHyM members who have helped me directly or indirectly by their contributions.

Major thanks to Richard for assisting me with NMR and answering my questions, and for always being helpful and cheerful. Also, many thanks to Fadi for his technical assistance. To Vicky for providing me with everything needed for lab work.

Thanks to my fellow PhD students who have helped me to understand things better Ahmed, Olga, Jennifer, Ben, Liz, Kate, and Aminata. Wishing all the best of luck in your future.

Finally, my deepest thanks go out to my father, mother, and to my wife for believing in me and encouraging me to keep going not only through my PhD but through everything in my life.

Author Declaration

I declare that this thesis is a presentation of original work and I am the sole author. This work has not previously been presented for an award at this, or any other, University. All sources are acknowledged as References.

Chapter 1: Introduction

1.1 Nuclear magnetic resonance

Nuclear magnetic resonance (NMR) is a spectroscopic approach that is widely used for analysing chemical compounds. In fact, NMR spectra can be generated from signals that are detected from many types of nuclei, such as: ^1H , ^{15}N , ^{19}F and ^{13}C .¹ Furthermore, NMR has multiple applications that provide information to support many areas such as drug design² and vaccine production,³ the food industry,⁴ the identification of natural products⁵ and the characterisation of plant extracts.⁶ In addition, NMR forms the basis of an imaging modality, which is known as magnetic resonance imaging (MRI).

MRI is a very powerful NMR application that has been used widely in the study of biological systems.^{4, 7} Its images are 3 dimensional and ideally provide the user with high spatial resolution (200–500 μm). It is also non-invasive and thus, information can be obtained without harm or change. Although MRI commonly obtains static information, it can also be used to provide dynamic information. Therefore, MRI allows for the imaging of the structure/anatomy of plants, whilst simultaneously delivering information about biochemical changes that occur inside the plant itself.⁸

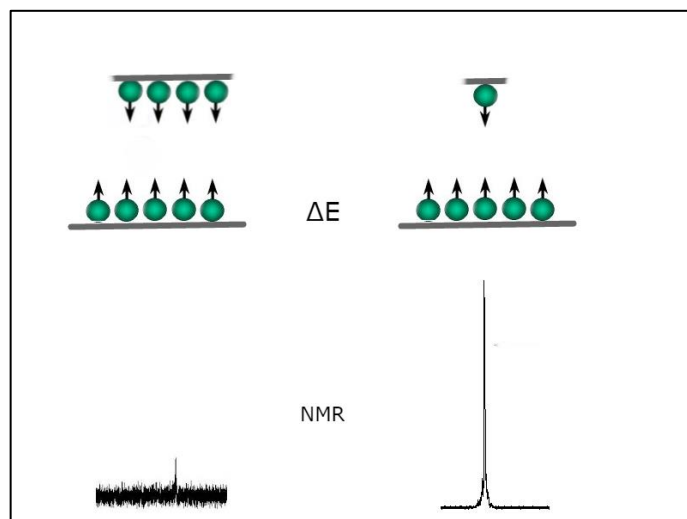
Currently, MRI and NMR are used in various applications in plant studies, which involve the comprehensive evaluation of plant traits.¹ More specifically, it is used in the application of measuring water content and its distribution, and in the estimation of water transport and flow velocity through the plant's vascular system.⁹ It is also used in the identification of plant extracts,⁶ the study of plant metabolism,¹⁰ the study of root systems,¹¹ and the examination of plant seeds.¹² In addition, it is used in the imaging of whole plants as MRI.¹³

Despite the advantages of NMR, it is limited by the inherent issue of low sensitivity.¹³⁻¹⁴ However, in order to understand the process of signal generation in MRI it is essential to know the reason behind this limitation and how to overcome it.

1.2 Sensitivity issue

Nuclei with spin $\frac{1}{2}$ form the basis of signal generation in MRI. When they interact with a magnetic field their spins become aligned parallel $+\frac{1}{2}$ or anti-parallel $-\frac{1}{2}$ to the direction of the applied magnetic field, according to the sign of the magnetogyric ratio. The parallel state is the low energy state (α) whereas the anti-parallel state is the high energy state (β).¹⁵ In a molecule with two coupled but distinct spins, there are four possible spin combinations and hence four possible energies. The resulting four energy levels are simply denoted as $\alpha\alpha$, $\alpha\beta$, $\beta\alpha$ and $\beta\beta$ when the two spins are distinct. Signal generation relies on probing the difference between spin populations for states that are connected by an allowed transition. An allowed transition is associated with the selection rule $\Delta m = \pm 1$ so in this case, one α can be changed to β . One further consequence of this is that if the energy levels associated with an NMR transition have equal populations there will be no resultant NMR signal. In the case of Figure 1.1. a schematic illustrating the concept of energy level populations for a simpler one spin system can be seen.¹⁶ On the left, is the situation where the energy levels have almost the same populations, and a weak signal results, while on the right we have a large population excess in the lower energy state and a large signal will be seen.

Figure 1.1: Illustration for the effect of spin population difference on the NMR signal strength.



In a regular MRI or NMR experiment, the spin population distribution between the two states β and α is defined by the Boltzmann distribution (Equation 1.1).

Equation 1.1: The Boltzmann distribution equation.

$$\frac{N_{\alpha}}{N_{\beta}} = e \left[\frac{\Delta E}{k_B T} \right]$$

In fact, N_{α} and N_{β} can be defined as the number of spins in each state of these two states with energy difference ΔE . ΔE is directly proportional to the strength of the applied magnetic field and the gyromagnetic ratio. The population difference stems from the Boltzmann equation which includes k_B the Boltzmann constant, and T , the temperature according to Equation 1.1.¹⁷ Upon placing the appropriate constants into this equation for a field of 9.4 T and a temperature of 298 K, the population difference becomes 2 for every 62,000 ^1H nuclei in a sample. Thus, only 2 ^1H spins can contribute positively to the detected signal in every 62,000 nuclei if the measurement takes place at 400 MHz (9.4 T) and 298 K. This simple relationship explains the low sensitivity of NMR and MRI since the signal stems from only the small number of nuclei leading to the population difference rather than the bulk population. Consequently, several techniques have been invented to produce non-Boltzmann distributions of these spins. These include hyperpolarisation by brute force, dynamic nuclear polarisation (DNP), optical pumping, and Parahydrogen Induced Polarisation (PHIP).^{16, 18-20}

1.3 Methods of hyperpolarisation and signal enhancement

1.3.1 Hyperpolarisation by brute force

Brute force is a simple technique that leads to hyperpolarisation as first defined in 1934 by Gorter.²¹ Several years of research and development were necessary before its use became increasingly widespread.²²⁻²³ However, it is currently considered as an outdated technique.²⁴ Brute force can achieve its hyperpolarisation in two ways. First, by exposing a sample to a strong magnetic field, which is stronger than that of the detection field. This will increase the number of polarised spins as the energy difference between spins states will increase. Second, by using very low temperatures, now the population difference between spins states is increased as thermal energy is limited, and thus the NMR signal is improved.²⁵ A signal enhancement of 1000-fold was reported when the temperature was 4 K and the magnetic field was 20 T, up from 1.5 T.²⁶ A much higher signal enhancement level of 200,000-fold was

achieved by Owers-Bradley *et al.* by using an ultra-low temperature of 7 millikelvin with a 16 T magnetic field.²⁷ Despite the fact that this is a significant improvement, there are two factors to consider. First, the hyperpolarisation state can only be created at very low temperatures, and will quickly return to Boltzmann equilibrium when warmed to diagnostically relevant temperatures. In addition, these challenging conditions make it a very demanding and costly technique.

It should be clear therefore that biological samples may be affected severely by the low temperatures as denaturation may result. Consequently, this method has limited applicability for highly ordered systems. At low temperatures, low solubility may become an issue and flash cooling is required. From an NMR perspective relaxation is a key issue as there is a time lag between dissolution and any measurement. It is therefore desirable that low viscosity media are employed.

Progress however continues, and recent studies by Hirsch *et al.* reported ~1500-fold of signal enhancements for ^{13}C using this approach.²⁸ However, this enhancement is still lower than that which can be created by some of the other hyperpolarisation techniques now detailed.

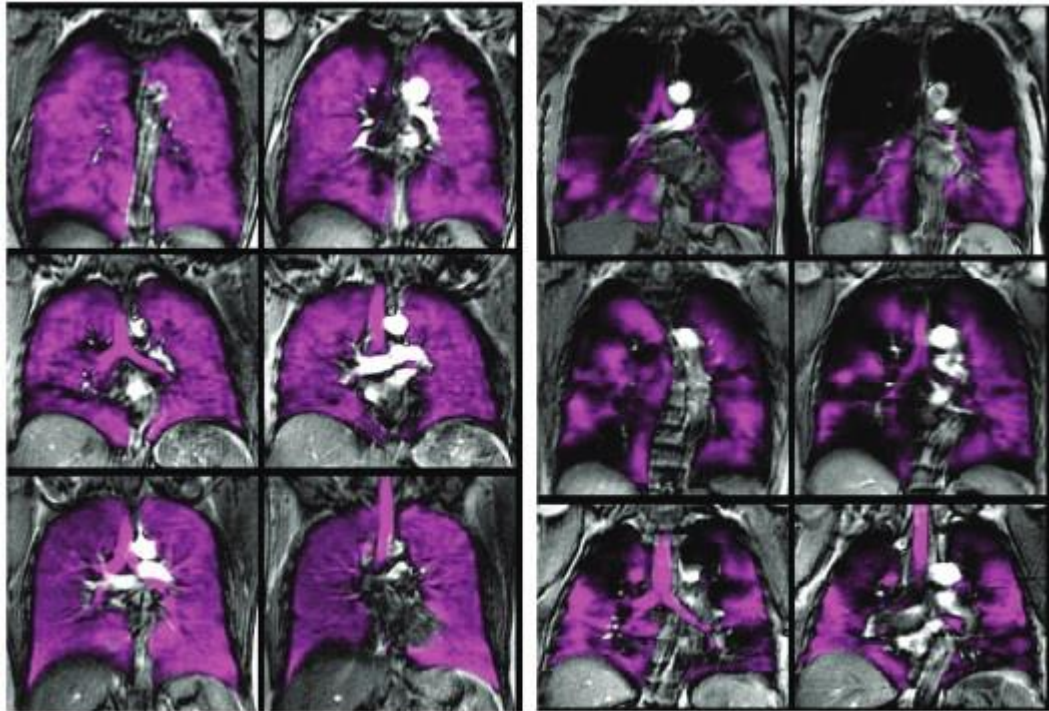
1.3.2 Hyperpolarisation by optical pumping

Optical pumping is a technique used to hyperpolarise the noble gases ^3He and ^{129}Xe using light to create spin polarisations.²⁹ During this process, the polarised laser light excites the electrons of an alkali metal, which is usually rubidium vapour, located inside a glass cell containing the noble gas. This causes the electronic spin state of rubidium to become polarised.¹⁸ The ^{129}Xe gas in the gas cell then collides with the rubidium vapour and through a process of spin order exchange it becomes hyperpolarised.³⁰ The hyperpolarised ^{129}Xe gas can then be separated from the rubidium vapour by simply cooling the cell to condense the rubidium onto the cell wall; the hyperpolarised gas can then be extracted into a container for subsequent use in imaging applications. For example, hyperpolarised imaging methods were created to harness these gases in 1994 by Albert *et al.*, during their study of mice lungs.³¹

Subsequently, clinical applications, using hyperpolarised ^3He and ^{129}Xe gases in MRI of the lung have shown to be extremely useful for detecting pathological changes such

as Chronic Obstructive Pulmonary Disease COPD (Figure 1.2).³²⁻³³ Since conventional MRI delivers insufficient anatomical information, this could provide a solution to the restricted use of MRI for lung imaging.³⁴

Figure 1.2: MRI images of lungs of a healthy volunteer (on the left) compared to images from a COPD patient (on the right). Images were obtained after inhalation of hyperpolarised ^{129}Xe gas, and the purple colour represent the data from the hyperpolarisation process.³³



However, the main disadvantage of the optical pumping method is that it is currently limited to applications like lung imaging, as well as some perfusion studies.³⁵⁻³⁷

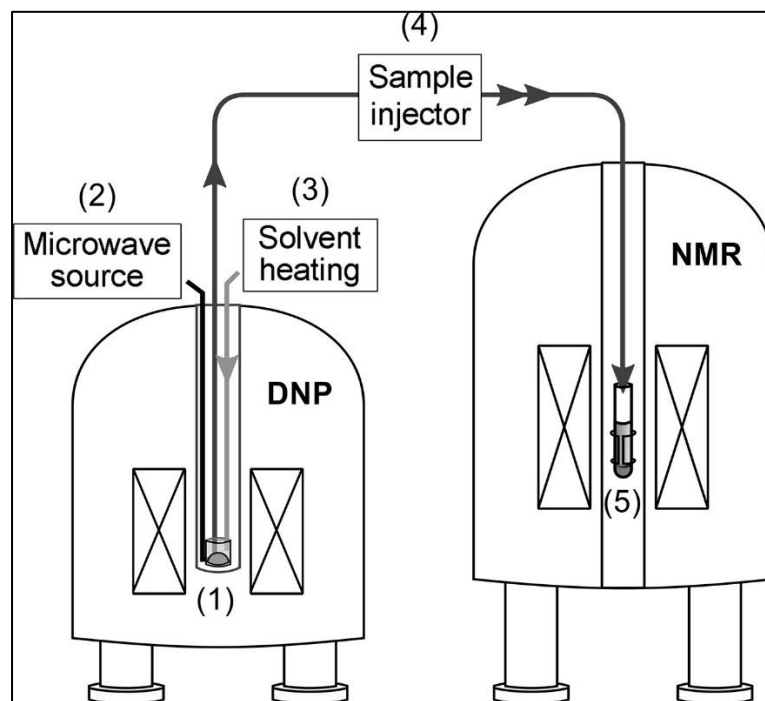
1.3.3 Hyperpolarisation by dynamic nuclear polarisation (DNP)

Dynamic nuclear polarisation (DNP) is a hyperpolarisation method in which polarisation is transferred from an unpaired electron by interaction with nuclear spins to produce a non-Boltzmann nuclear spin distribution. This transfer happens when irradiating with microwave frequencies that correspond to the electron paramagnetic resonance (EPR) signal of the free radical.³⁸ The basic DNP principle was originally presented in 1953 by Overhauser,³⁹ and experimentally proven by Carver and Slichter.⁴⁰

The process of polarisation transfer can occur in solids and liquids, but since this thesis only uses liquid samples, the focus of discussion for DNP will lie in the liquid-state. The details of the polarisation transfer mechanisms are beyond the scope of this thesis, and this is in fact a complicated subject that has yet to be fully understood. Some papers have been published to better understand the mechanics underlying it.⁴¹⁻⁴³ They state there are four main types for polarisation transfer. For solids, the solid effect,⁴⁴ the cross effect,⁴⁵ or the thermal mixing.³⁸ For liquids, the Overhauser effect is the only effect directly applicable.³⁹ However, the Overhauser effect is limited by solvent heating resulting from the high microwave powers that are required to saturate the EPR line. Therefore, it may be difficult to conduct experiments on compounds with biological relevance. Additionally, the method is performed at room temperature which produces low polarisation levels when compared to that of low temperature DNP.

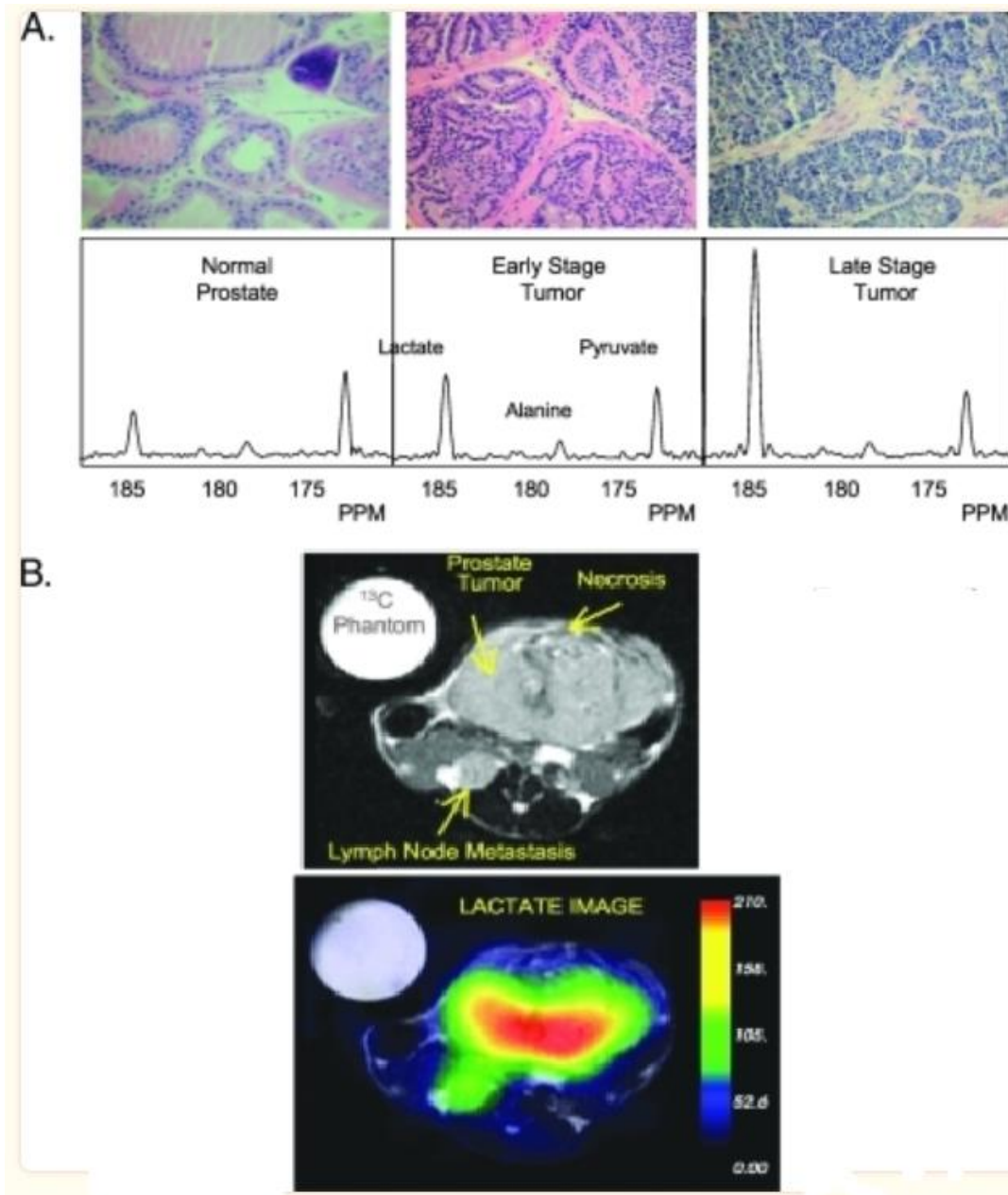
In fact, it was 2003, that saw a new DNP technique called dissolution-DNP (d-DNP) described that was innovated by Ardenkjær-Larsen *et. al.*⁴⁶ In this technique, a substrate is dissolved in a radical and then frozen by exposing the sample to extremely low temperatures (~1K), during that period microwave irradiation occurs such that all the nuclear spins become hyperpolarised at low temperatures. After that, the sample is thawed in hot water prior to NMR monitoring (Figure 1.3).⁴⁷⁻⁴⁸ This study reported using the technique for the hyperpolarisation of a sample of urea. This resulted in polarisation level of >10,000 fold.

Figure 1.3: An illustration of a typical d-DNP setup for NMR investigations. The numbering shows the sequence in which the experimental procedures are performed. (1) loading a sample into a polariser. (2) achieving hyperpolarisation through microwave irradiation at 1 K. (3) a heated solvent rapidly dissolves the sample in the hyperpolarised state. (4) transferring the liquid sample to the NMR instrument. (5) measurement of hyperpolarised signal.⁴⁷



The development of d-DNP enabled the successful hyperpolarisation of several compounds.⁴⁹ This allowed some compounds to be *in vivo* studied especially those with long T_1 relaxation time, which is essential for maintaining the hyperpolarisation during the transfer of samples to the scanning field. These findings have revealed astonishing insights into their metabolic processes. Pyruvate is one of these compounds that has interested DNP research.⁵⁰⁻⁵³ In 1927 a study about cancer metabolism noted higher amounts of glucose uptake occur within tumour cells in comparison to normal unaffected cells,⁵⁴ which then led to higher amounts of the product lactate.⁵⁴⁻⁵⁵ Using the d-DNP technique has allowed monitoring and analysing pyruvate metabolism *in vivo* (Figure 1.4),⁵⁵ which could help improving the diagnosis and monitoring of tumour treatment. Pyruvate is also a key molecule in the krebs cycle that is essential for generating energy of cells in plants, animals, and humans.⁵⁶

Figure 1.4: A) Histological sections of a healthy mouse prostate, early-stage, and late-stage tumour, hyperpolarised [1-¹³C] pyruvate was injected, and a representative hyperpolarised ¹³C spectrum is shown below the histological sections. An obvious increase in the ratio of hyperpolarised lactate to hyperpolarised pyruvate was seen in the spectra as disease progressed from normal to early and late stages of tumour. B) Late-stage primary tumour in a mouse as seen on an axial T₂ ¹H image with an overlaid image of hyperpolarised [1-¹³C] lactate following injection of hyperpolarised [1-¹³C] pyruvate. Increases in hyperpolarized [1-¹³C] lactate was seen in the midst of the transformation from healthy to cancerous prostate and throughout the development of the disease. Images taken from Kurhanewicz *et. al.*⁵⁵



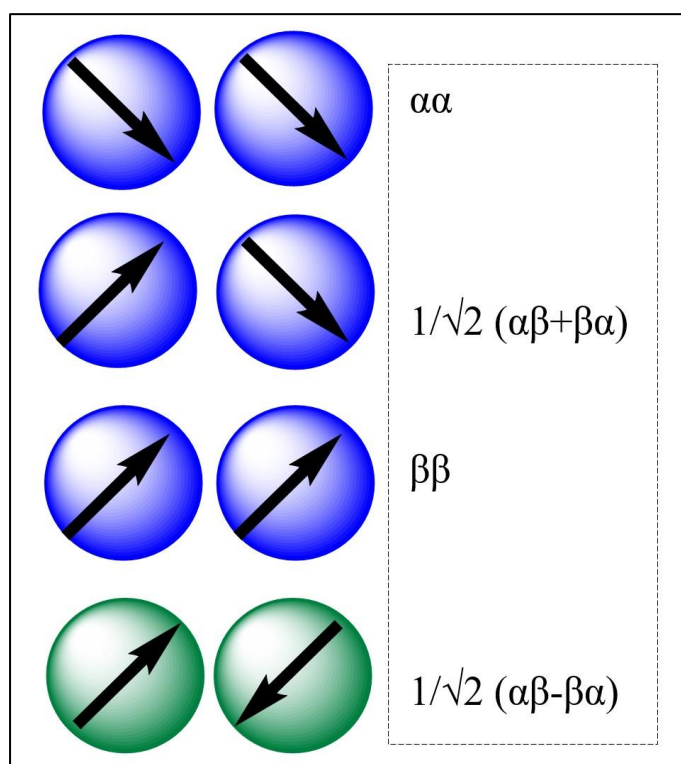
However, the main limitation of DNP is its non-equilibrium nature, which affects both the reproducibility of the method and makes it a single-shot approach.⁵⁷ In this

context, the measurement process uses up the magnetisation that DNP creates, so identical measurements cannot be repeated without rehyperfolarisation. Furthermore, as the NMR signals are inherently weak, the expectation is that no signal will be detected if the hyperpolarization step were to fail.

1.3.4 Hyperpolarisation by parahydrogen induced polarization (PHIP)

Hydrogen molecules are composed of two ^1H atoms joined together by a single covalent bond. The ^1H nucleus has a spin of $\frac{1}{2}$ which makes it visible to NMR spectroscopy. There are therefore two possible configurations for a proton's spin which are spin up and spin down. This means that there are four distinct combinations of spin states that can result from a given pair of spins (Figure 1.5).

Figure 1.5: The four spin states combinations of hydrogen.

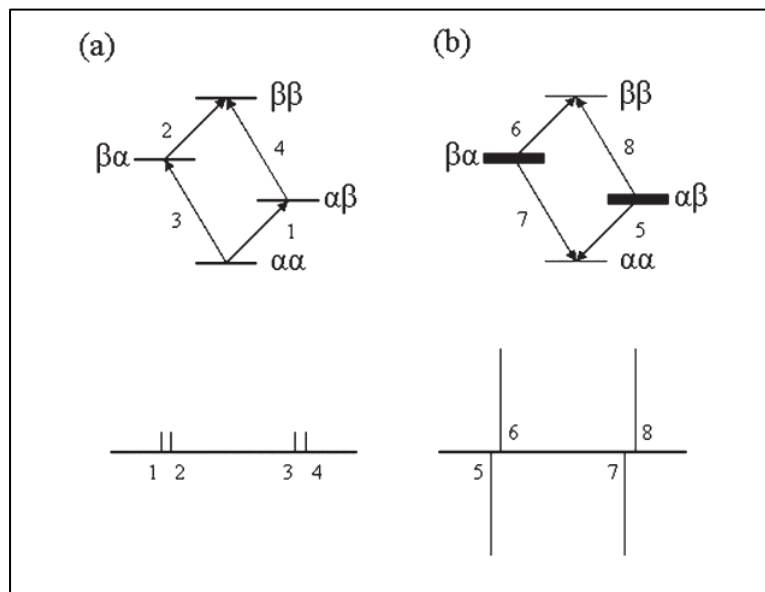


Among these, the top three combinations are known as *ortho* H_2 and reflect the triplet spin manifold. The bottom spin state linear combination where the spins are formally anti-parallel is known as *para*- H_2 . This is a singlet spin-state and has lower energy than the triplet forms, and it is the source of hyperpolarisation in PHIP.

Parahydrogen induced polarisation (PHIP) is an alternative to DNP and perhaps one of the simplest and most efficient methods for hyperpolarisation. In *para*-H₂ the two nuclear spins are aligned anti-parallel ($\alpha\beta$ - $\beta\alpha$), a fact that is reflective of its identity as the molecular singlet. *Para*-H₂ can be formed by simply cooling H₂ gas in the presence of a suitable catalyst and once it is created it has a long lifetime in the absence of O₂, which makes it useful. This is reflective of the fact that the second form of H₂ known as *ortho*-H₂ cannot equilibrate with *para*-H₂ without changing two quantum numbers, one associated with a spin flip and the second a rotational state change. The simultaneous change of these two quantum numbers is forbidden and leads to the long lifetime of *para*-H₂.

When forming a reaction product by taking isolated *para*-H₂ and placing its nuclei into the product, a non-Boltzmann distribution can be created in the product's nuclear spin configuration. In the simplest case, this means that the product spins derived from *para*-H₂ can only take up $\alpha\beta$ and $\beta\alpha$ terms as the initial $\alpha\beta$ - $\beta\alpha$ connection must be preserved (Figure 1.6). Clearly if the *para*-H₂ used was pure and its relative nuclear spin alignment efficiently maintained, the result is a significantly increased population difference across transitions that are connected by a change in Δm of ± 1 . Hence there is a dramatic boost in detected MRI or NMR signal sensitivity.¹⁶ Since the $\alpha\beta$ and $\beta\alpha$ state transitions can occur in either absorption or emission, the corresponding NMR spectra exhibit a distinctive pair of antiphase doublets.

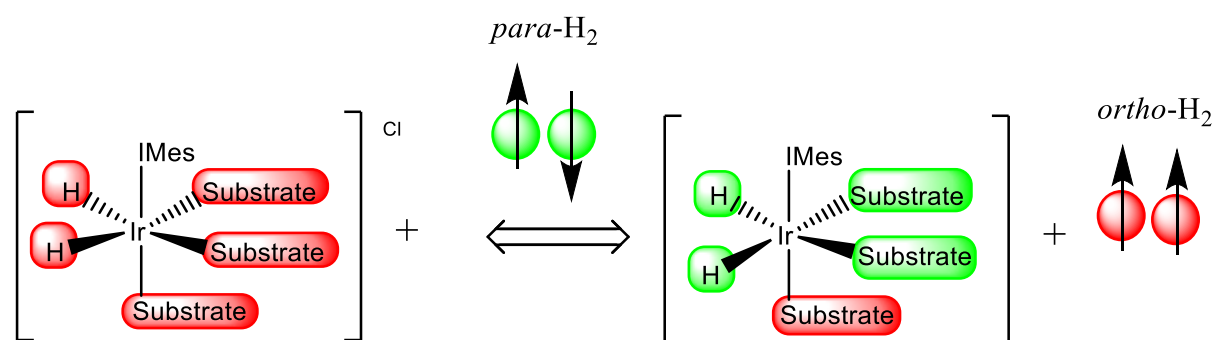
Figure 1.6: Energy levels and their representative NMR spectra with natural abundance hydrogen (a) and *para*-H₂ (b). In the upper photos, the population of each spin state is illustrated by the line thickness. Image from Duckett et al., 2012¹⁶



One variation of the PHIP effect called signal amplification by reversible exchange (SABRE) was introduced in 2009.⁵⁸ As a PHIP technique, it utilises *para*-H₂ to hyperpolarise a substrate molecule, however, this time it is not incorporated into the product. Instead, *para*-H₂ now adds reversibly to the magnetisation transfer catalyst which also coordinates the substrate to be hyperpolarised (Figure 1.7). This allows the substrate to become hyperpolarised if there is a transfer of the original polarisation in *para*-H₂ through the spin-coupling network of the magnetisation transfer catalyst. It is the reversibility of the binding steps that allows a substrate to come transiently into contact with *para*-H₂ that is key to this processes success as it allows the build-up of hyperpolarised product in a way that is directly analogous to the creation of a classical reaction product.⁵⁸

Polarisation of a target substrate is achieved by using *para*-H₂ spin-order. The atoms of hydrogen in *para*-H₂ are magnetically symmetric, hence it has no magnetic moment and is NMR silent. Once the *para*-H₂ symmetry is broken through a suitable chemical change the spin-order can be transfer hyperpolarisation to substrate ligands if they are coordinated to a SABRE catalyst.⁵⁹

Figure 1.7: Schematic representation of SABRE hyperpolarisation transfer mechanism. Green colour represents hyperpolarised state and red represents thermal state.



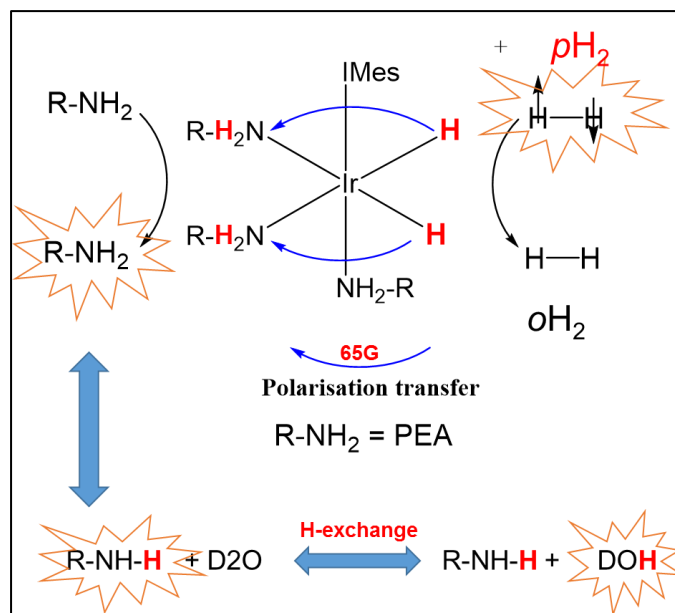
The protons of a substrate that are in spin-spin contact with the hydrides in the catalyst become hyperpolarised first, and then the rest of substrate protons become hyperpolarised via the substrate couplings network of ^1H - ^1H .⁶⁰ Though the proton is the most commonly studied nucleus using SABRE, the technique has also been applied to the hyperpolarisation of other nuclei such as: ^{13}C , ^{15}N , ^{19}F , and ^{31}P . The hyperpolarisation of these nuclei can occur either indirectly by transferring the hyperpolarisation intramolecularly from the ^1H resonances, or directly through coupling to hydrides.⁶¹ The latter is known as SABRE-SHEATH (SABRE in shield enables alignment transfer to heteronuclei) which was primarily used for hyperpolarising ^{15}N and then applied to other nuclei such as: ^{13}C ⁶² and ^{19}F .⁶³

The initial set of SABRE-hyperpolarised molecules relied on molecules that contain nitrogen such as N-heterocycles.⁶⁴ Pyridine and its derivatives are the most common utilised molecules in SABRE. Over 8000-fold enhancements of pyridine ^1H NMR signals were reported by Cowley *et al.* after optimisation of the experiment conditions. This enhancement level in pyridine was attained with a magnetic field strength of 65 gauss (G). The study utilised $[\text{IrCl}(\text{COD})(\text{IMes})]$ as the pre-catalyst,⁶⁴ and due to its consistent and strong hyperpolarisation, it continues to be the most widely utilised SABRE pre-catalyst.⁶⁵⁻⁶⁶

Recently, a new SABRE method named **SABRE-RELAY**⁶⁷ has been reported to hyperpolarise molecules that cannot bind to such a metal complex. This approach relies on them containing at least one labile proton though. SABRE-RELAY starts

with the SABRE hyperpolarisation of an amine. Subsequently, polarisation is relayed into a specified target substrate through exchange of a hyperpolarised proton from the amine, as outlined in (Figure 1.8).

Figure 1.8: SABRE-RELAY achieved by polarised proton exchange.



Several factors influence hyperpolarisation transfer efficiency these include: the temperature, the polarisation transfer field (PTF), the length of the relaxation time (T_1), and the concentration of substrate.^{66, 68-69} The effects of all these parameters are considered in this thesis.

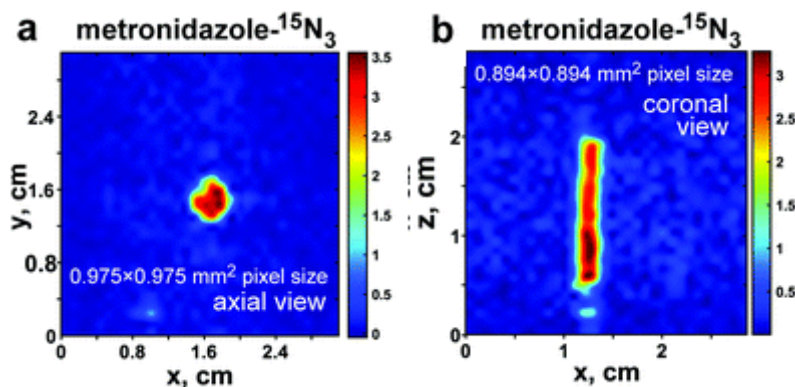
In order for magnetisation to be observed in NMR experiment, RF pulses are used (typically of 90°) to flip the net magnetisation into the xy-axis for signal detection. This is necessary to create an oscillating magnetic field, orthogonal, to the main field which can in turn induce a response in an appropriately oriented detection coil. The time it takes for 63% of spins to recover to their original orientation is known as the relaxation time T_1 ,⁷⁰ and it is an important factor in SABRE as mentioned earlier. The relaxation time determines the lifetime of a signal before it decays. In the SABRE process, the lifetime of the hyperpolarised signal is limited by the T_1 time. Once hyperpolarisation is generated by the SABRE method, the substrate quickly returns to its equilibrium state. Therefore, a long hyperpolarised time is essential to maintain a

strong signal throughout experiments. The long relaxation is required especially for imaging applications to provide sufficient time for an injected agent to reach a target site. Moreover, relaxation time of substrates can be affected by the presence of the SABRE catalyst and interactions with other molecules.⁷¹

Deuteration is a well-established strategy for increasing the lifetime and efficiency of hyperpolarisation techniques. Since deuterium and proton nuclei have distinct nuclear spins and lie far apart in frequency the T_1 relaxation of the hyperpolarised ^1H signals is often reduced.⁷² For example, the lifetime of hyperpolarised ^1H signals of methyl-4,6- d_2 -nicotinate was improved by 20% when using deuterated IMes (d_{22} -IMes).⁷¹ Other studies have also reported improvement of the hyperpolarised signals lifetime and signal enhancement levels when deuteration is utilised.⁷³⁻⁷⁴ These improvements have made SABRE more suitable for MRI and biomedical applications.

MRI of ^1H ,⁷¹ ^{13}C ,⁷⁵ and ^{15}N ⁷⁶ were successfully shown for some of the hyperpolarised-SABRE compounds. Despite the fact that nuclei such as ^{15}N have very low sensitivity (1% of ^1H sensitivity), the detection of SABRE hyperpolarised contrast agents is expected to reduce the sensitivity issue. For example, MRI of the antibiotic drug metronidazole was successfully performed (Figure 1.9) after hyperpolarisation by SABRE-SHEATH, with high polarisation level (30%) and long T_1 relaxation (~10 min), which makes it a promising agent for *in vivo*.⁷⁷

Figure 1.9: MR images of ^{15}N for hyperpolarised solution of ^{15}N -labelled metronidazole in 5 mm NMR tube. (a) axial view of the hyperpolarised metronidazole sample. (b) coronal view of the hyperpolarised metronidazole sample. Image taken from Birchall *et al.*,2020.⁷⁷



In addition, other substrates of interest in biochemical contexts have also been studied using the SABRE hyperpolarisation method. For instance, it has been shown that SABRE works for amino acids,⁷⁸ glucose, fructose,⁷⁹ and peptides.⁸⁰ The field of SABRE hyperpolarisation is rapidly evolving with new substrates and applications constantly being discovered.

The original aim of this project was to develop a new MR approach to study plants using the SABRE technique. For this purpose, the aim was to hyperpolarise an array of plant hormones. Plans to use these materials in plant imaging studies were subsequently curtailed due to COVID. Phenylethylamine was selected as the test hyperpolarisation carrier agent to start out this research.

Chapter 2: SABRE with phenylethylamine, ethanolamine, benzylamine, and ammonia.

2.1 Introduction

Chapter 1 showed that the range of substrates that can be polarised by SABRE includes the nitrogen containing heterocyclic aromatic compounds pyridine,⁸¹ pyridazine,⁸² pyrimidine,⁸³ and nicotinamide.⁸⁴ This chapter focusses on examining secondary amines, a substrate class that has only recently been polarised by SABRE.⁶⁷

Amines are organic compounds that are derived from NH_3 (ammonia). They possess a lone pair of electrons on nitrogen and are basic in nature. They are fundamental to the creation of amino acids and play a major role in growth and living systems.⁸⁵ Some types of amine are hormones that regulate physiological functions in the body.⁸⁶⁻⁸⁷ For example, histamine works as a neurotransmitter in the central nervous system (CNS).⁸⁸⁻⁸⁹ They also have an important role in defence mechanisms against pathogens.⁸⁶⁻⁸⁷ Another example is tyrosine, which works as a precursor in the synthesis of the thyroid gland hormones thyroxine (T4) and triiodothyronine (T3).⁹⁰ The two additional neurotransmitters epinephrine and norepinephrine also contain secondary amine functions.⁹¹⁻⁹²

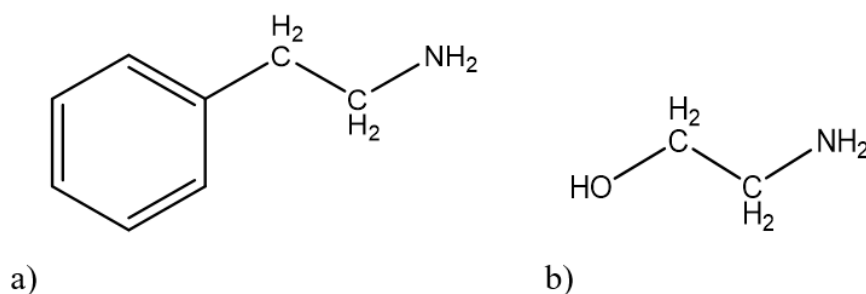
Amines are also used in the pharmaceutical industry where the product dopamine (a compound of the phenethylamine family) is a common medication used to treat low blood pressure and heart disease. It is given to a patient intravenously.⁹³⁻⁹⁵ Another example is chlorpheniramine which is a medication used for treating allergic reactions.⁹⁶ Amines are also important in other industries, for example butylamine is a common ingredient in the synthesis of some agriculture chemicals.⁹⁷ Other amines such as aniline are used in the synthesis of dyes and pigments.^{85, 97-98}

The detection and characterisation of amines is therefore important. Notably, the NH stretch is readily visible in IR spectroscopy at around 3288 cm^{-1} for a secondary amine and moves on deuteration.⁹⁹ The mass spectrometry of amines is also a very important tool in their characterisation. The nitrogen rule states that detected fragments with zero or an even number of nitrogen atoms have even mass. In contrast, molecules with odd

numbers of nitrogen atoms have odd masses. Accurate mass chemical ionisation methods are often used when examining such species as they can reveal the presence of nitrogen in complex species through the empirical formula determination. Fragmentation patterns also help with analysis. Normally, the most intense peak in the resulting mass spectrum results from cleavage of the bond β to the amine nitrogen and this leads to loss of a radical and creation of a new cation. More complex fragmentations occur depending on structure which often prove to be diagnostic.¹⁰⁰

The NMR spectra of amines are also diagnostic of their structure and their chemical shifts highly dependent on the solvent. NH resonances appear in the ^1H NMR spectrum at between δ 0.5 and 3 alongside the hydrogen substituents of an alkyl. When the substituents are aromatic, this resonance shifts position to between δ 3 and 5. The nitrogen centre also affects the chemical shift of adjacent CH_2 protons which appear in the region 1.5 – 2 ppm. Furthermore, the ^{13}C resonance of the carbon adjacent to nitrogen appears at around δ 45 when it is aliphatic in nature. The associated ^{15}N resonances are though much harder to detect and occur around zero ppm. This chapter deals with the examination of the amines: phenethylamine, ethanolamine (Figure 2.1), ammonia, and benzylamine with the SABRE technique and the studies seek to achieve the highest level of NMR signal enhancement possible.

Figure 2.1: Structure of phenethylamine (a) and ethanolamine (b).



Phenylethylamine is a trace amine that exists in a wide range of species including plants, animals, and humans. It can be found in legume plants, which is one of the largest plant families and includes trees, shrubs, herbs, and vegetables. They also find use as foods and as precursors in pharmaceutical synthesis.¹⁰¹ Phenylethylamine is also a precursor in the biosynthesis of benzenoids, the 2nd largest type of emitted plant volatile.¹⁰² In humans, phenethylamine works as a neurotransmitter and can lead to psychiatric conditions. Supplements are given to patients with phenethylamine deficiency.¹⁰³⁻¹⁰⁴

In contrast, ethanolamine is essential for the synthesis of cell membranes. It is used by plants to synthesise the two major phospholipids phosphatidylethanolamine (PE) and phosphatidylcholine (PC). In addition, PC can also be synthesised from choline which is derived from ethanolamine. The production of ethanolamine can be direct or indirect in plants, whereas in animals it is only found to be indirect.¹⁰⁵ The indirect ethanolamine production method involves a base-exchange reaction while the direct method is through the decarboxylation of serine.¹⁰⁶ All human body cells contain ethanolamine in the form of the lipid PE. Ethanolamine can also be found freely in body fluids such as blood, with a concentration range from 0 to 12 μM , while the range is expected to be much larger in the digestive tract as a result of breaking down PE coming from ingested food. Ethanolamine is an important stimulant for the growth of cells. It also provides the protection of cells as it is mandatory for the synthesis of glycosylphosphatidylinositol anchored proteins (GPI-APs). Furthermore, it has a strong anti-cancer activity.¹⁰⁷

2.2 Developing SABRE for phenylethylamine

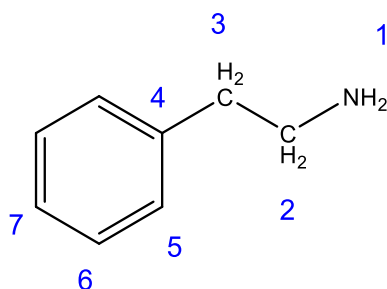
As discussed earlier, pyridine is one of the first substrates that has been examined extensively by SABRE. This was possible due to the presence of the lone pair which allows pyridine to bind to a metal centre and in this case form the active SABRE complex $[\text{Ir}(\text{H})_2(\text{IMes})(\text{pyridine})_3]\text{Cl}$. Since amines such as phenethylamine, ethanolamine and benzylamine, or indeed ammonia itself, possess a lone pair of electrons it was hypothesised that they too can bind to the metal catalyst and form active complexes which will enable them to be hyperpolarised through the SABRE approach.

As mentioned earlier, SABRE requires three main components to be present in order for it to function. These are a metal catalyst, *para*-H₂, and a substrate, in this case phenylethylamine (**1**). The most commonly used SABRE precatalyst contains the ancillary ligand 1,3-bis(2,4,6-trimethylphenyl) imidazol-2-ylidene (IMes). The resulting precatalyst is 16-electron Ir(Cl)(COD)(IMes) (**2**).⁶⁶ It is utilised in the SABRE measurements that feature throughout this thesis. It forms [Ir(H)₂(IMes)(**1**)₃]Cl (**3**) under SABRE conditions upon reaction with **1**. However, given the complexity of SABRE it is important to comprehensively understand the starting point.

2.2.1 Characterisation of phenylethylamine

Phenylethylamine was characterised by recording ¹H and ¹³C NMR spectra in dichloromethane-*d*₂ solution at 400 MHz. The resulting ¹H NMR spectrum contains signals at δ 7.33 (m, 2H), 7.23 (m, 2H), 7.22 (m, 1H), 2.95 (t, 7 Hz, 2H), 2.75 (t, 7 Hz, 2H) and 1.15 (br, 2H) for this material. Table 2.1 outlines these NMR data and the assignments for phenethylamine. The signal enhancements that these NMR signals generate will be examined utilising the SABRE techniques.

Table 2.1: NMR characterisation data for phenethylamine in dichloromethane-*d*₂ at 298 K with labelling according to the inset structure.



Resonance number	¹ H (ppm)	¹³ C (ppm)
1	1.15 (br, 2H)	-
2	2.95 (t, <i>J</i> = 7 Hz, 2H)	43.74
3	2.75 (t, <i>J</i> = 7 Hz, 2H)	40.32
4	-	140.36
5	7.23 (m, 2H)*	128.3
6	7.33 (m, 2H)	128.8
7	7.22 (m, 1H)*	125.9

*Overlap

2.2.2 T_1 relaxation time of phenethylamine

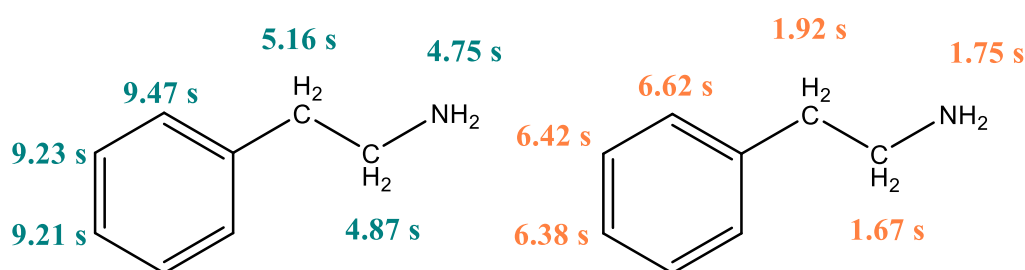
As illustrated in the introduction, it is now known that the SABRE effect is dependent on the T_1 values of the polarised nuclei. These values have been shown to change due to the presence of the active SABRE catalyst in solution.¹⁰⁸ This is not surprising as it is the catalyst that enables spin order to flow from nuclei that were in *para*-H₂ into the substrate. It is therefore important to define these effects before completing an experiment. T_1 values are determined by the inversion recovery experiment. When 2.65 mM of phenylethylamine was examined in dichloromethane-*d*₂ solution at 400 MHz and 298 K the T_1 values of Figure 2.2 were determined. Subsequently, a sample was prepared which contained phenylethylamine and [Ir(H)₂(IMes)(**1**)₃]Cl (**3**) under H₂ in dichloromethane-*d*₂ and its T_1 values were re-measured. These are also shown in Figure 2.2.

It is clear that the catalyst acts to reduce the T_1 values as expected. The reduction of T_1 for the two responses adjacent to the NH binding site is 65 %. At site 3, next to the phenyl ring, the reduction percentage was slightly reduced to 62 %. The phenyl ring, whose protons are furthest from the binding site, are the least affected and their T_1 falls by 27 %. Thus, this effect clearly reduces by moving away from the ligand binding site, a result of the interaction with the metal which reduces with distance from the binding site. It might therefore be expected to see that these groups receive less polarisation under SABRE, but as their T_1 's are higher, the signal intensity they show is likely to survive to the point of measurement more efficiently. This is something that will be tested experimentally.

Relaxation is a complex phenomenon that depends on a number of factors which are grouped together as spin-lattice and spin-spin effects. The lattice reflects spins that can be located in the same molecule or neighbouring molecules while the second effect involves two identical spins undergoing a flip-flop to invert their respective alignments. The mechanisms of relaxation acts to reorientate the macroscopic magnetisation of the sample, and when this deals with motion in the z-axis (longitudinal) the term T_1 is used while transverse changes are referred to as T_2 . Molecular motion within the lattice can create magnetic dipole fluctuations that match the Larmor resonance frequency and they interact, via a dipole-dipole coupling, with

the nuclear spins we probe. Quantitatively, these molecular motions are characterised by a correlation time which falls as the molecular size increases, temperature decreases or solvent viscosity increases. T_1 is proportional to the reciprocal of the correlation time meaning that as we increase molecular size, T_1 falls. It is for this reason that binding to the catalyst reduces T_1 .

Figure 2.2: T_1 values for the ^1H NMR signals of free phenethylamine (**1**) (green) and (**1**) in the presence of **3** and H_2 (orange), at 9.4 T (due to phenyl ring signal overlap the T_1 is for the multiplet). The concentrations used were 2.65 mM of **1** and 2 mM of iridium.

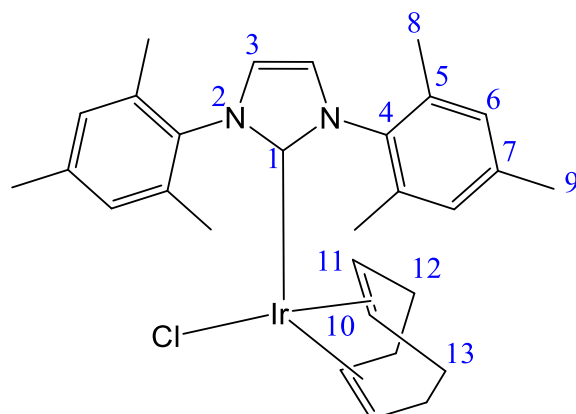


2.2.3 Reaction of phenylethylamine with $\text{Ir}(\text{Cl})(\text{COD})(\text{IMes})$ (**2**)

In order for SABRE to operate in this study, the iridium complex $\text{Ir}(\text{Cl})(\text{COD})(\text{IMes})$ (**2**) was reacted with the substrate (**1**) and hydrogen to form an active catalyst of the type $[\text{Ir}(\text{H})_2(\text{IMes})(\text{sub})_3]\text{Cl}$. To prepare such a sample, for these experiments', specific amounts of **1** and **2** are combined in an NMR solvent in an air-sensitive NMR tube supplied by J. Young. The sample is then degassed, using a high vacuum system. After this point, the sample is left to activate under H_2 , until it becomes ready for the SABRE experiments. During this time the sample is expected to become colourless.

A dichloromethane- d_2 solution of $\text{Ir}(\text{Cl})(\text{COD})(\text{IMes})$ (**2**) was therefore prepared as a control sample. This solution was analysed by ^1H NMR spectroscopy, and Table 2.2 lists the NMR data for compound **2** that is present at this stage. Diagnostic resonances for **2** appear at δ 7.01 for the imidazole rings backbone protons in the NHC ligand, IMes, and at δ 7.05 for the mesityl ring CH group. Alkene resonances for bound COD are readily seen at δ 4.07 and 3.04. Changes in the intensity of these resonances will be useful in monitoring any reactions involving this complex.

Table 2.2: NMR characterisation data for square planar IrCl(COD)(IMes) (**2**) in dichloromethane- d_2 at 298 K with resonances attributed according to the labelling of the inset structure.



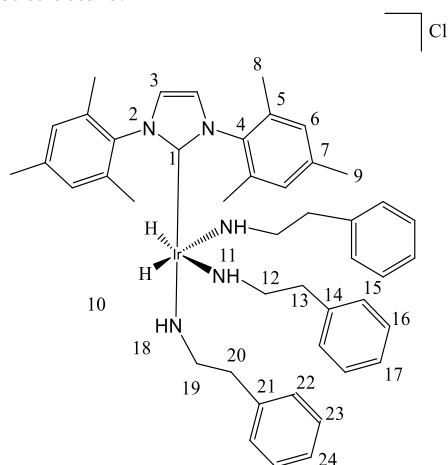
Resonance number	^1H (ppm)	^{13}C (ppm)	^{15}N (ppm)
1	-	174.61	
2	-	-	191.3
3	7.01 (s, 2H)	123.6	
4	-	-	
5	-	-	
6	7.05 (s, 4H, br)	129.2, 128.2	
7	-		
8	2.2 (s, 6H), 2.3 (s, 6H)	18.1, 19.3	
9	2.41 (6H)	20.8	
10	4.07 (2H)	82.1	
11	3.04 (2H)	51.7	
12	1.75 (2H), 1.37 (2H)	28.8	
13	1.68 (2H), 1.29 (2H)	33.4	

The yellow coloured 5 mM NMR sample containing **2** in dichloromethane- d_2 was degassed on a high vacuum system, and a 10-fold excess of **1** relative to **2** added. Hydrogen gas was then added to this sample to hydrogenate the COD ligand attached to the metal centre thereby forming cyclooctane (COA). This process allows **1** to bind to the metal centre instead of COD. For this reaction to occur the sample was left for 24 hours at 298 K before further NMR spectra were recorded. During this period the solution became colourless. The resulting ^1H NMR spectra revealed several changes when compared to the previously discussed data for the precursors **1** and **2**. The most significant of these changes was the detection of a hydride resonance at δ -24.07.

After 24 hrs only one hydride signal remains evident and hence this reaction proceeds cleanly to one product (Figure 2.3). The hydride signal at δ -23.95 is accompanied by the appearance of three other notable resonances at δ 4.42, 3.68 and 2.78. These are due to NH₂ signals of bound **1**. There are two further signals for the carbene ligand at δ 7.00 and 6.75 that are visible in the aromatic region. Moreover, the signals for the bound COD ligand in **2** at δ 3.04 and 4.07 have disappeared. Collectively these observations are indicative of the formation of [Ir(H)₂(IMes)(**1**)₃]Cl (**3**). It is apparent from these data that the resonance for the imidazole ring proton moves substantially from δ 7.01 to 6.75 on going from **2** to **3**. Full NMR data for the complex **3** is presented in Table 2.3.

The ¹H NMR resonances of phenethylamine also move on binding. The signal for the CH₂N proton resonance appears at δ 2.95 in free **1** but upon binding three more appear. Two correspond to inequivalent CH resonances for a ligand *trans* to hydride, at δ 2.41 and 3.30. For the ligand *trans* to IMes, the CH₂N protons remain equivalent and a single peak is seen at δ 2.78. The positions of these four resonances are critical for the SABRE analysis of **1** in solution. Based on the reported literature, ligands *trans* to hydride should undergo rapid exchange with those in solution.⁶⁹ Therefore SABRE is expected to result in enhanced signals at δ 2.95 in **1** and at δ 2.41 and 3.30 for the bound amine ligand in **3**, with only limited if any signal gain for the signal at δ 2.78.

Table 2.3: NMR characterisation data for octahedral $[\text{Ir}(\text{H})_2(\text{IMes})(\mathbf{1})_3]\text{Cl}$ (**3**) that forms when phenylethylamine (**1**) and H_2 react with $\text{Ir}(\text{Cl})(\text{COD})(\text{IMes})$ (**2**) in dichloromethane- d_2 at 298 K with the labels according to the inset structure.



Resonance number	^1H (ppm)	^{13}C (ppm)	^{15}N (ppm)
1		153.8	
2			192.21
3	6.75	121.73	
4		138.14	
5		135.06	
6	7.0	129.4	
7		138.64	
8	2.17	18.30	
9	2.21	21.10	
10	-23.95		
11	4.42 (t, $J_{\text{HH}} = 11$ Hz, 2H) * $J_{\text{15NH}} = 68$ Hz 2.11 (br, t, $J_{\text{HH}} = 11$ Hz, 2H) * $J_{\text{15NH}} = 68$ Hz		-7.2
12	2.41 (dt, $J_{\text{HH}} = 9$ and 11 Hz, 2 H) 3.30 (2H, overlap)	50.7	
13			
14		141.8	
15	7.32 (dd, $J_{\text{HH}} = 7$ Hz)	128.33	
16	7.25 (t, $J_{\text{HH}} = 7$ Hz)	126.88	
17	~7.28 - overlap	-	
18	3.685 (t, $J_{\text{HH}} = 5.9$ Hz, 2H) * $J_{\text{15NH}} = 69$ Hz		-16.2
19	2.78 (t, $J_{\text{HH}} = 6.15$ Hz, 2H)	53.9	
20		-	
21	7.32	128.33	
22	~7.2 - overlap	-	
23	~7.12 - overlap	-	

* ^{15}N coupling determined via 2D NMR spectrum on unlabelled sample

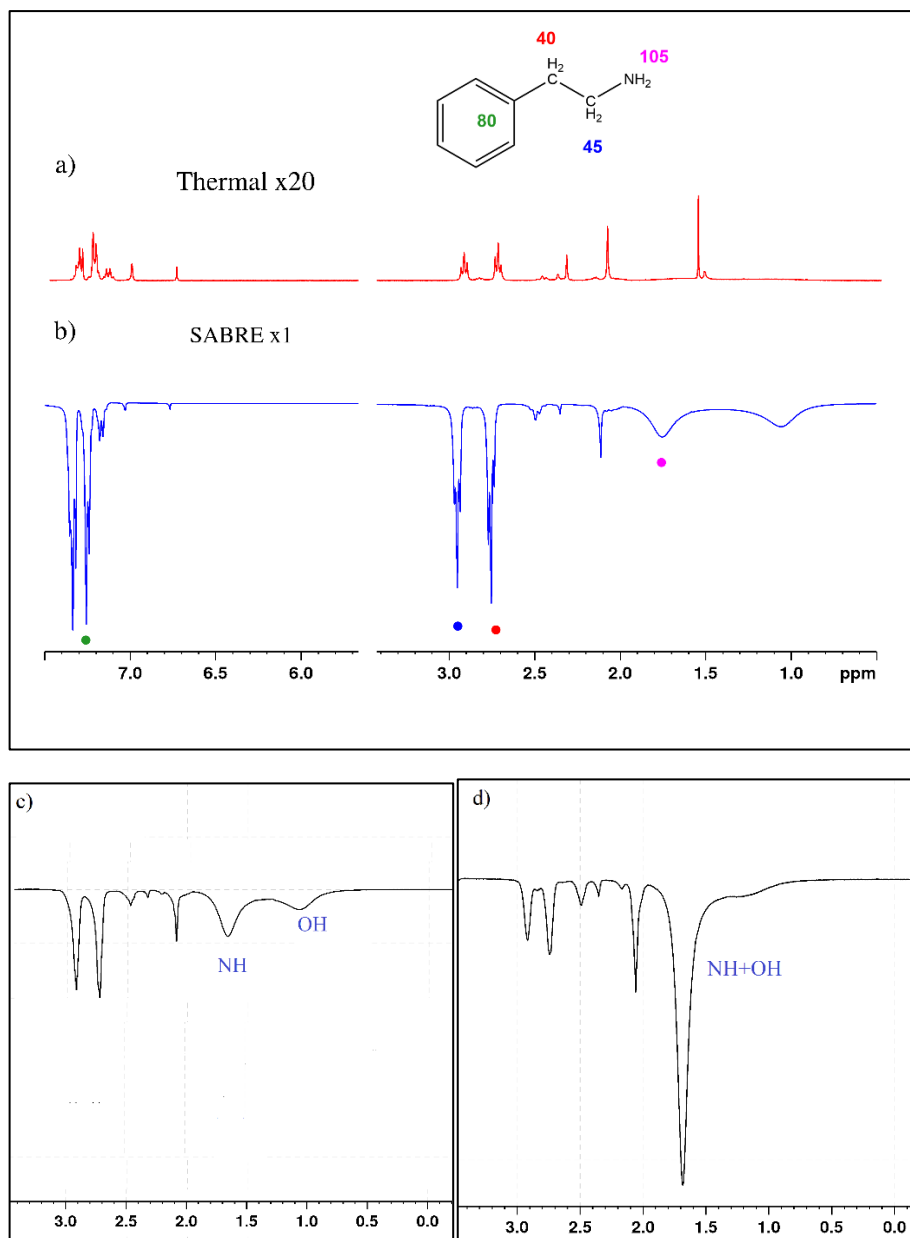
2.2.4 SABRE of **1** achieved by the catalyst $[\text{Ir}(\text{H})_2(\text{IMes})(\mathbf{1})_3]\text{Cl}$ (**3**)

The SABRE sample for **1** was prepared, and placed in a 400 MHz (9.4T) NMR for a single thermal scan which will be used as a reference for enhancement levels calculations. Then, 3 atmospheres of *para*-H₂ were added to the sample with an initial 10-fold excess of **1** to hyperpolarise it by the SABRE technique. The sample was then vigorously shaken at ~60 G in the stray field around the NMR magnet for a duration of 10 seconds. It was then dropped quickly into the NMR magnet to record the resultant NMR spectrum. The measurements were repeated 3 times after refilling with *para*-H₂ for each measurement for statistical purposes.

These data showed that the ¹H NMR resonances of free phenylethylamine exhibited signal enhancement as illustrated in Figure 2.3. It is immediately apparent that the CH₂N signal for free **1** at δ 2.95 shows the strongest aliphatic proton signal gain (45-fold per proton) even though these protons have the shortest T_1 . Interestingly, the overlapping aromatic protons yield an average ¹H resonance signal gain of 80-fold which given their distance from the binding site, and hence in-efficient hyperpolarization, must be due to the T_1 effects described above.

Strong signals are seen at δ 1.35 for the NH resonance of **1** in these NMR spectra, which when compared to the position in other samples has moved slightly due to the presence of the catalyst. The sample involved in this study used an initial 10-fold excess of **1** relative to **2**. Upon expanding the spectral region, weak hyperpolarized signals for bound **1** *trans* to hydride were evident as expected at δ 2.41 and 3.30. The intensity ratio for enhanced signals of bound CH₂N at δ 2.41 and 3.30 to the free signal at δ 2.95 (per proton) were 1 : 1: 25 which confirm that there is rapid ligand exchange between the species giving rise to these signals. It can be concluded from these data that **1** can be hyperpolarised by the SABRE method via **3**.

Figure 2.3: ^1H NMR spectra showing the effect of SABRE on the ^1H NMR response of phenethylamine (**1**). (b) single scan control spectrum, (a) single scan SABRE NMR spectrum. The SABRE precatalyst was $\text{Ir}(\text{Cl})(\text{COD})(\text{IMes})$ (**2**) (5mM), **1** concentration was 5.3mM, *para*- H_2 was present at 3 bar and transfer undertaken at 60 G. (c) a two broad peaks of NH and OH when precautions were taken to eliminate water contamination. (d) the two peaks of NH and OH are coalescing into a single broad peak due to limited water contamination.



It was observed that when precautions were taken to exclude water, the NH resonance of **1** shows significant signal gain at δ 1.75 as detailed in Figure 2.4 c, and a broad peak appears at δ 0.95. The later signal is due to OH protons. When a normal sample was used, there was limited water contamination, and exchange between the NH and

OH groups. This results in the coalescence of these two peaks into a single broad peak close to the peak at δ 1.67. This is shown in Figure 2.3 d. Hence the chemical shifts of the NH resonances are prone to move as a function of the sample.

2.3 SABRE Optimisation

To fully exploit the advantages of the SABRE technique in MRI and NMR applications, optimisation of SABRE is required to get the highest possible signal gain. There are several known factors that can affect the signal gain produced through the SABRE technique. Firstly, the relaxation time of the substrate as demonstrated in section 2.2.2. Secondly, the magnetic field where polarisation transfer takes place. Thirdly, SABRE kinetics which deals with the exchange rates of a substrate and *para*-H₂ on the catalyst. These are affected by the substrate to catalyst ratio alongside their absolute concentrations, and the temperature at which polarisation transfer occur.^{64, 82, 109} This is a reflection of the fact that the lifetime of the SABRE catalyst is important because the rate of transfer of polarisation from *para*-H₂ to the substrate depends on the size of the spin-spin couplings that connect them. In addition, it is the spin order of the catalysts hydride ligands that form from *para*-H₂ which provides the net signal amplification. Hence the rate of *para*-H₂ exchange is of critical importance. It is important to realise that once the catalyst breaks down, under ligand exchange, any magnetic states that are associated with spins whose coupling is lost in this process are destroyed. This means that polarisation that is associated only with resonances in the free substrate will be detected upon dissociation. The effect of these factors will be examined in the following sections.

2.3.1 Effect of substrate loading on the ¹H polarisation level in **2** when its concentration is kept constant.

In theory, a lower substrate loading relative to catalyst will act to increase the proportion of polarised molecules, as this increases their chance to be repolarised. Upon increasing the substrate excess, the proportion of substrate molecules that experience SABRE might therefore be expected to fall. However, this effect is complicated by the kinetics of ligand exchange. Substrate loss from the catalyst is dissociative. Thus, the intermediate $[\text{Ir}(\text{H})_2(\text{IMes})(\mathbf{1})_2]\text{Cl}$ that forms from

$[\text{Ir}(\text{H})_2(\text{IMes})(\mathbf{1})_3]\text{Cl}$ does so at a rate which is independent on the catalysts concentration. However, $[\text{Ir}(\text{H})_2(\text{IMes})(\mathbf{1})_2]\text{Cl}$ reacts with *para*- H_2 and $\mathbf{1}$. The former leading to hydride polarisation replenishment and the latter the reformation of $[\text{Ir}(\text{H})_2(\text{IMes})(\mathbf{1})_3]\text{Cl}$. Consequently, too high a concentration of $\mathbf{1}$, against a set *para*- H_2 concentration can act to reduce the net *para*- H_2 exchange rate and lead to lower polarisation levels. It is therefore important that these effects are examined.

To do this, a fresh 5 mM NMR sample of $\mathbf{1}$ and $\text{Ir}(\text{COD})(\text{IMes})\text{Cl}$ ($\mathbf{2}$) in dichloromethane- d_2 was prepared. This sample contained an initial 5:1 ratio of substrate relative to iridium. H_2 was again added over-night to form $\mathbf{3}$. A series of SABRE measurements were then undertaken on this sample. SABRE was again evident for signals of $\mathbf{1}$ which appear at δ 7.32, 7.24, 2.95 and 1.21 in this sample. Signals for bound $\mathbf{1}$ *trans* to hydride at δ 2.41 and 3.30 were also enhanced. The intensity ratio for the enhanced bound signal at δ 2.41 relative to the free signal at δ 2.95 and 3.30 (per proton) in $\mathbf{1}$ changed to 1 : 30 on starting with a 5:1 ratio instead of the 1 : 25 as seen for the 10:1 ratio. This supports the idea that the proportion of $\mathbf{1}$ which is polarised increases as the excess falls. It can also be seen that it is only the signals for $\mathbf{1}$ that lie *trans* to hydride in $\mathbf{3}$ that show appreciable signal amplification. It can therefore be concluded that when $\mathbf{1}$ lies *trans* to IMes any ligand exchange must be slow as its signals shown very minimal signal gain. Furthermore, the overall enhancement levels seen for ^1H NMR NH signals of $\mathbf{1}$ have increased from those measured with a 10-fold excess (Table 2.4).

Table 2.4: ^1H NMR SABRE enhancements, per proton for the indicated groups of $\mathbf{1}$ for 5 and 10-fold excesses relative to $\mathbf{2}$, based on 3 averages.

Position (see Table 2.1)	Signal enhancements level	
	5:1 loading	10:1 loading
Sites 4-7 (5H)	85.3 ± 4.7	80.9 ± 3.4
Site 3 (2H)	40.4 ± 2.2	40.1 ± 1.9
Site 2 (2H)	44.6 ± 2.7	43.1 ± 2.1
Site 1 (2H)	110.2 ± 4.5	104.6 ± 3.8

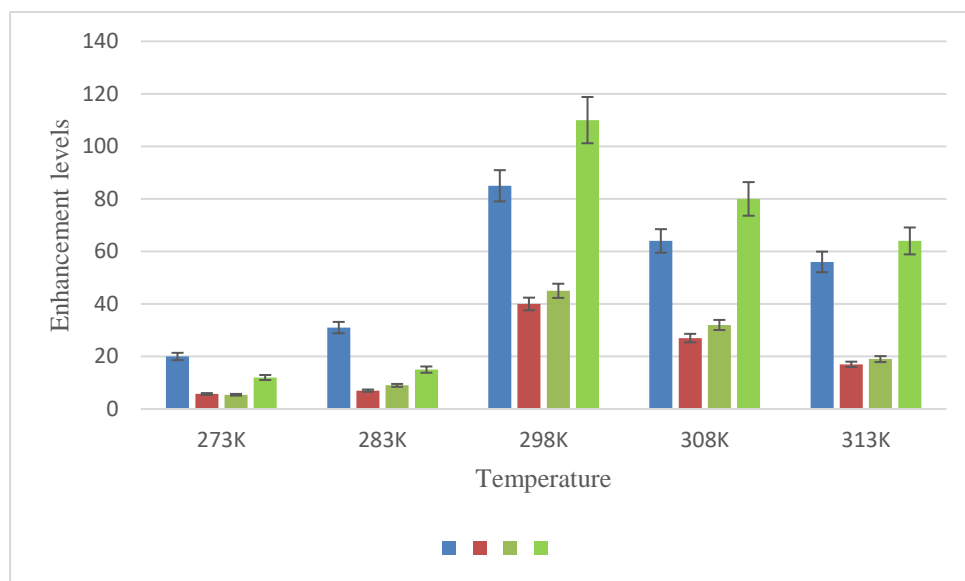
A slightly more promising NMR signal enhancement level was achieved with the lower substrate loading of 5:1, for **1** which is consistent with theory as *para*-H₂ is the limiting reagent. However, the scale of these relative signal gains is surprisingly low. This would suggest that the effect of the excess of **1** is low and hence the ligand exchange rates are slow. The T_1 values for **1** in the presence of **3** for a 5:1 initial excess are detailed in Figure 2.2 and follow the trend site 1 ~ site 2 < site 3 < site 4-7. It is clear that the aromatic protons, with long T_1 s, gain in intensity from this concentration effect whilst those of sites 2 and 3 are essentially unaffected.

2.3.2 Temperature effect on polarisation

Theoretically, the higher the temperature the faster ligand exchange. In order to explore the effect of temperature on polarisation transfer to **1** under SABRE a 5mM NMR sample of **2** with 2.65 mM of **1** in dichloromethane-*d*₂ was prepared. SABRE was performed at room temperature (298 K) and then at the temperatures 313, 308, 283 and 273 K. The results are summarised in Figure 2.4 and reveal that the best enhancement levels for the free material are obtained at room temperature. There is a clear decline in this enhancement level at lower temperatures, which is due to slower exchange, and this is evident in all of the resonances of **1**. There is also a slight decrease in the signal enhancement at higher temperatures, which suggests that the ligand exchange rates now become too fast for efficient polarisation transfer.

The aromatic protons, having the longest T_1 retain their hyperpolarization for the longest time period and therefore are a good indicator of the efficiency of the slower polarisation transfer step. As temperature increases, the rate of ligand exchange reaches the point where there is optimum polarisation transfer to the NH, which cascades to the other nuclei. Beyond that point the enhancement levels fall.

Figure 2.4: SABRE enhancement levels for the indicated (see inset structure) ^1H NMR resonances of free phenethylamine (**1**) after polarisation transfer at 273, 283, 298, 303, and 313 K.

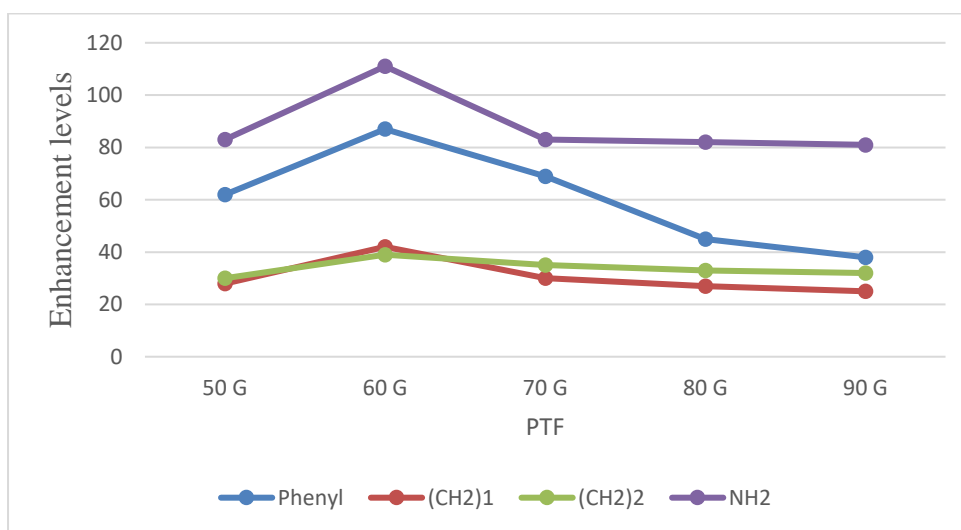


2.3.3 SABRE at variable magnetic field strengths

The sample undergoing SABRE will experience a background magnetic field during the polarisation transfer step. The strength of this magnetic field controls the efficiency of the SABRE as a consequence of the need to match the interacting nuclei's chemical shift difference with $^2J_{\text{HH}}$, the hydride-hydride coupling, in the catalyst. At 65 G, this difference becomes minimal.⁵⁸ Therefore, this field is used throughout this thesis. However, as each substrate might be different, it was decided to explore the effect of range of fields around 65 G in order to define which field led to optimal transfer.

The effect of this PTF is usually explored using a flow system as it is more reproducible than the shake and drop method. However, the solvent in these studies is dichloromethane- d_2 which has a low boiling point of 313 K. Thus, the solvent will evaporate when exposed to *para*- H_2 in the flow system. Hence for these measurements a 5-fold excess sample of **1** relative **2** was prepared and the sample shaken in fields of value 50, 60, 70, 80, and 90 G and the result quantified at 9.4 T. These data are shown in Figure 2.5. The SABRE enhancement seen at 60-70 G proved to be the highest, which is consistent with literature.^{64, 110-111}

Figure 2.5: ^1H NMR SABRE enhancement levels for **1** (resonances indicated) at 50, 60, 70, 80, and 90 G.

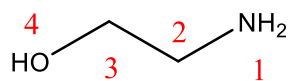


In summary, it can be concluded that the SABRE polarisation of **1** is feasible and that is optimal when completed using catalyst **3** in a PFT of 65 G when the ratio of **1:3** is 2:1. Under these conditions the enhancement of ^1H was 110-fold for NH_2 , 45-fold for NHCH_2 , 40-fold for CHCH_2 , and 85-fold for the phenyl ring.

2.4 Developing SABRE for Ethanolamine

After a successful polarisation of **1**, ethanolamine was next to be examined. This was completed in order to expand the range of amines that can be polarised with SABRE. Ethanolamine was dissolved in dichloromethane- d_2 to record ^1H and ^{13}C NMR spectra at 400 MHz. The resulting ^1H NMR spectrum contains signals at δ 1.98 (br, 3H), 2.84 (t, 6.82 Hz, 2H), 3.58 and (t, 7 Hz, 2H) for this material. Table 2.5 outlines these NMR data and the assignments for ethanolamine.

Table 2.5: NMR characterisation data for ethanolamine in dichloromethane- d_2 at 298 K with labelling according to the inset structure.



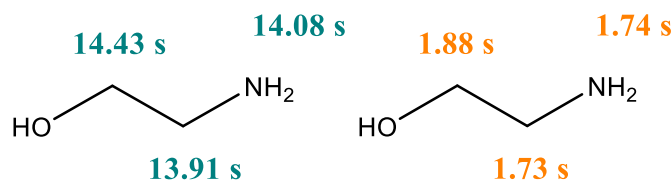
Resonance number	^1H (ppm)	^{13}C (ppm)
1	1.98 (3H, averaged chemical shift)*	-
2	2.84 (t, $J = 6.82$ Hz, 2H)	63.74
3	3.58 (t, $J = 6.82$ Hz, 2H)	43.82

*1 overlap with 4

2.4.1 T_1 relaxation time of ethanolamine

When ethanolamine alone was examined in dichloromethane- d_2 solution at 400 MHz the T_1 values of Figure 2.6 were determined. Subsequently, a sample was prepared which contained ethanolamine and **4** under H_2 in dichloromethane- d_2 and the T_1 values were re-measured. These are also shown in Figure 2.6. It is clear that the catalyst acts to reduce the T_1 values again as expected. The T_1 for the two methyl groups were similarly reduced by ~88%. However, both of these resonances are far more affected than those of phenylethylamine which fell by ca 67%. This could be indicative of faster ligand exchange.

Figure 2.6: T_1 values for the ^1H NMR signals of free ethanolamine (green labelled), and ethanolamine in the presence of H_2 (orange labelled), at 9.4 T. The concentrations used were 2.35 mM of ethanolamine and 2 mM loading of IMes (**2**).

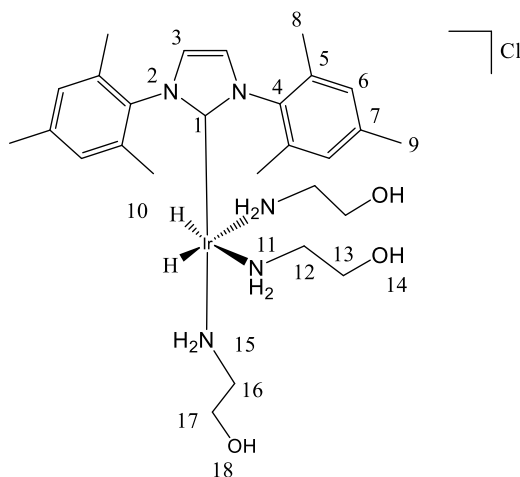


2.4.2 Reaction of ethanolamine with $\text{Ir}(\text{Cl})(\text{COD})(\text{IMes})$ (**2**)

In order to examine ethanolamine under SABRE a 5 mM NMR sample containing ethanolamine was prepared (Figure 2.1b) with a 5 fold excess relative to (**2**) (5mM) in 0.6 ml of dichloromethane- d_2 . The sample was reacted with H_2 and the expected

complex $[\text{Ir}(\text{H})_2(\text{ethanolamine})_3(\text{IMes})]\text{Cl}$ (**4**) formed. The ^1H and ^{13}C NMR chemical shifts for this product in dichloromethane- d_2 are presented in Table 2.6.

Table 2.6: NMR characterisation data for $[\text{Ir}(\text{H})_2(\text{ethanolamine})_3(\text{IMes})]\text{Cl}$ (**4**) in dichloromethane- d_2 at 253 K alongside the labelled structure.



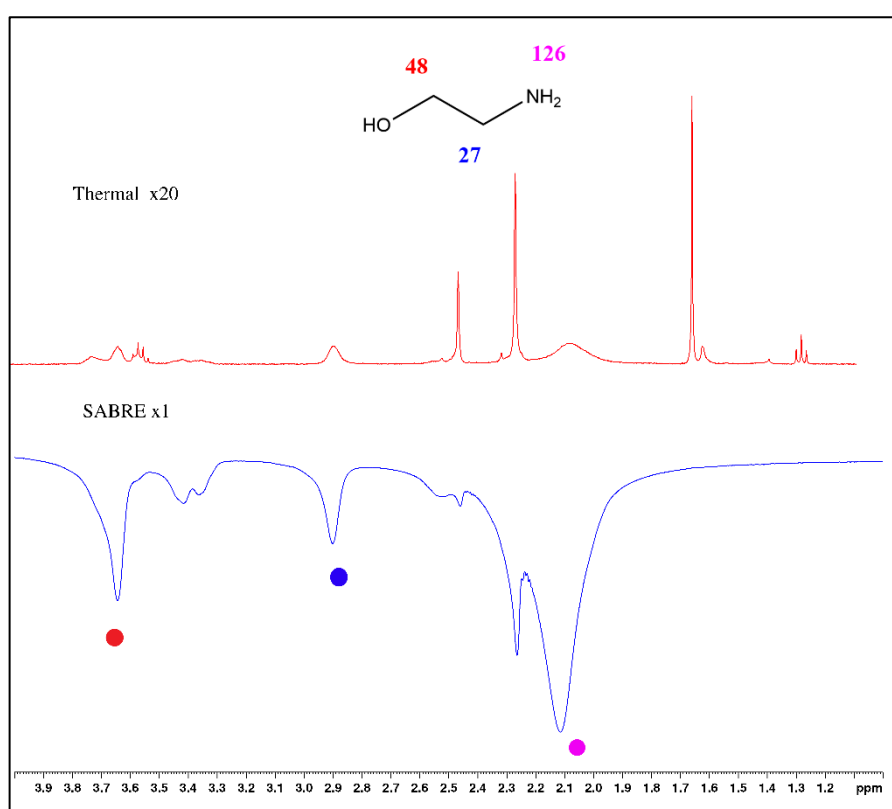
Resonance number	^1H (ppm)	^{13}C (ppm)	^{15}N (ppm)
1	-	152.76	-
2	-	-	191.7
3	6.80 (2H)	121.75	-
4	-	137.6	-
5	-	135.81	-
6	7.04 (4H)	129.19	-
7	-	138.73	-
8	2.15 (12H)	18.2	-
9	2.33 (6H)	20.8	-
10	-23.91		-
11	3.36 (2H), 2.18 (2H)	-	-16.8
12	2.34 (2H), 1.68 (2H)	50.82	-
13	3.27 (2H), 3.16 (2H)	63.83	-
14	*	-	-
15	3.51 (2H)	-	-23.5
16	2.74 (2H)	54.43	-
17	3.42 (2H)	62.98	-
18	*	-	

- Not attributed due to exchange with residual water

4 yields a hydride signal at δ -23.91. Three other resonances were also noticeable at δ 3.51, 3.36, and 1.68 for the bound NH_2 of ethanolamine. There are two further signals for the carbene ligand at δ 7.04 and 6.80 that are visible in the aromatic region. The signals for COD ligand of **2** at δ 4.07 and 3.04 have disappeared in accordance with this reaction. These data are therefore indicative of the formation of **4**. It is apparent

from these data that the resonance for the imidazole ring proton moves substantially from δ 7.01 to 6.82 on going from **2** to **4**. Subsequently this sample was examined with *para*-H₂ and the resulting SABRE ¹H NMR enhancement levels are shown in Figure 2.7. The resonances are broad because the OH and NH of ethanolamine are in dynamic exchange.

Figure 2.7: ¹H NMR spectra showing the effect of SABRE on the ¹H NMR response of phenethylamine, signal scan control (top) spectrum, single scan SABRE NMR (bottom) spectrum. The SABRE precatalyst was Ir(Cl)(COD)(IMes) (5mM), the ligand was present in a 5 fold excess, *para*-H₂ was present at 3 bar and polarisation transfer undertaken at 60 G. The affected resonances are indicated in the structure.



2.5 SABRE Optimisation of Ethanolamine

2.5.1 Effect of ethanolamine concentration on the ¹H NMR based polarisation level when the concentration of precatalyst **2** is kept constant

To investigate the effect of ethanolamine concentration on the degree of polarisation transfer, two 5 mm NMR samples containing ethanolamine in a 5 and 10 fold excess relative to IMes (5mM) were prepared in 0.6 ml of dichloromethane-*d*₂. Table 2.7

highlights the resulting SABRE signal enhancements levels achieved after polarisation transfer from a 60 G seconds of exposure to *para*-H₂.

Table 2.7: ¹H NMR SABRE enhancement levels for ethanolamine obtained from 5 mM IMes samples with 10- and 20-fold excess of ethanolamine, three measurements were taken.

Resonance number (see Table 2.6)	5 mM IMes	
	¹ H NMR signal enhancement level	
	5:1 loading	10:1 loading
1	126.2 ± 4.1	86.5 ± 4.9
2	27.1 ± 2.0	25.3 ± 1.9
3	47.6 ± 5.3	47.1 ± 3.5

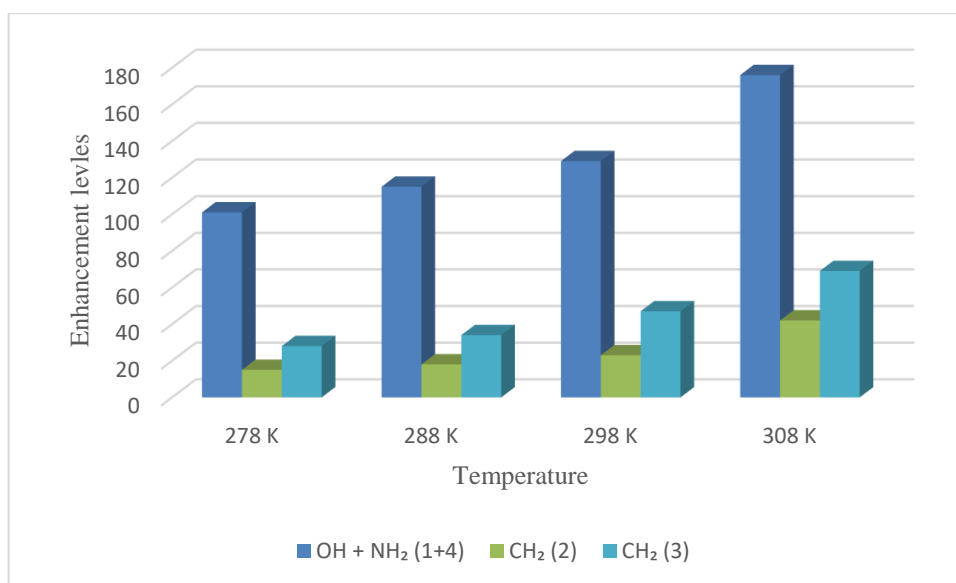
It is clear that when comparing the thermally polarised ¹H NMR signals observed from these measurements, that the enhancement levels are larger for the NH site 1 than the adjacent CH site 2. The site next to the OH, site 3 provides a larger signal than that for the CH next to the NH group. From an HN perspective, the lower loading gives rise to a very significant NH signal gain. This is reflective of the excess of *para*-H₂ which as a limiting reagent is shared with few protons at the lower loading and therefore results in a larger signal gain. However, the fact the site 2 and 3 signals then have similar enhancements suggest that the NH signal gain does not transfer efficiently to them. This would be consistent with a shorter *T*₁ which would act to offset the expected gain and reduce the size of these signals. The fact that the signals for site 3 are larger than those for site 2 is however surprising giving these sites similar *T*₁ values (Figure 2.6). It would therefore seem sensible to suggest that SABRE-Relay acts to enhance the intensity of resonance for site 3 alongside SABRE via the NH site. This effect will reduce with increase in the concentration of the OH protons as their presence will promote faster proton exchange which is detrimental to later SABRE-Relay.

2.5.2 SABRE under low and high temperature experiments

An NMR sample of ethanolamine with a 5-fold excess relative to **2** was prepared to examine the effect of temperature on the signal enhancement level. SABRE was performed at room temperature (298 K) and after cooling the sample to the following temperatures: 288 K, and 278 K (Figure 2.8). This showed a decline in enhancement

levels at lower temperatures. After that, the sample was tested at 298 K and 308 K. The highest enhancement levels were seen in the experiments at 308 K. This is consistent with an increase in the rate of ethanolamine exchange.

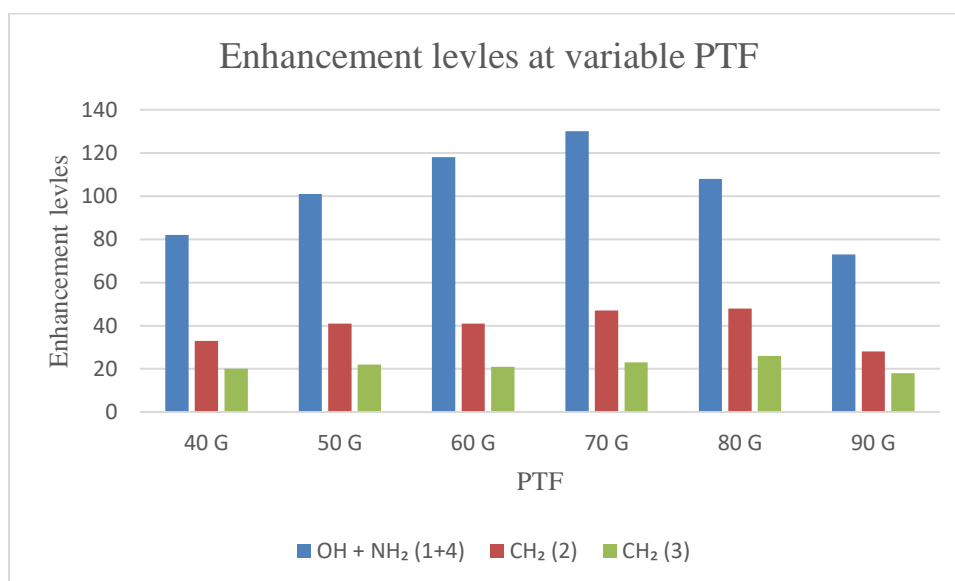
Figure 2.8: ^1H NMR signal enhancement levels for the indicated resonances of ethanolamine under SABRE at 278, 288, 298, and 308 K respectively.



2.5.3 SABRE at variable magnetic field strengths

Another sample of ethanolamine containing a 5 fold excess relative to 2 mg of **2** in 0.6 ml dichloromethane- d_2 was prepared. This sample was used to explore the effect of magnetic field strength on the transfer polarisation level. The sample was shaken at the field strengths: 40, 50, 60, 70, 80, and 90 G as the results are shown in Figure 2.9. These values were achieved by using the stray field of magnet used to make the NMR measurements. The best SABRE enhancement was achieved using a 60-70 G field.

Figure 2.9: ^1H NMR enhancement levels for the indicated resonances of ethanolamine using SABRE at: 40, 50, 60, 70, 80, and 90 G.



2.6 Developing SABRE for benzylamine and ammonia

After testing the efficiency of the SABRE polarisation of phenethylamine and ethanolamine, the molecules ammonia (NH_3) and benzylamine were examined. Thus, a SABRE sample containing **2** and a 6-fold excess of NH_3 was prepared. This reacts to form the SABRE complex $[\text{Ir}(\text{H})_2(\text{IMes})(\mathbf{2}\text{-NH}_3)_3]\text{Cl}$ (**5**). The resulting ^1H NMR spectrum showed a hydride resonance at $\delta -23.61$, with a broad resonance for free NH_3 at $\delta 0.49$. The signal for bound NH_3 ligand equatorial to hydride appears at $\delta 2.21$ while the axial ligand appears at $\delta 2.84$, and their corresponding ^{15}N signals were located by ^1H - ^{15}N HMQC measurements to be at $\delta -34.9$ and -46.5 respectively. The full characterisation data of **5** is illustrated in Table 2.8. After that, 3 bar pressure of *para*- H_2 was added and shook the sample for 10 s at 65 G and 298 K before dropping it into 9.4 T NMR for measurement. The ^1H NMR spectrum showed a 154-fold enhanced signal for free NH_3 when compared to its thermally polarised signal, while the equatorial NH_3 ligand was enhanced by 77-fold (Figure 2.10). Therefore, these results confirm that **2-NH₃** underwent SABRE catalysis. When water was present in the sample, the enhancement of free NH_3 was reduced by 40-fold. This reduction is reflected by the enhanced water peak at $\delta 1.86$ showing 75-fold signal enhancement.

The ratio of 2- NH_3 : NH_3 : H_2O for this sample was 1 : 17.5 : 5. When the T_1 relaxation time for free NH_3 was measured by inversion recovery, it was found to be 5.5 s.

Figure 2.10: (a) Thermally polarised ^1H NMR spectra of (5) scaled by x32 (b) Hyperpolarised ^1H NMR spectra of 4 (single scan) showing polarised free and bound NH_3 , and residual water signal indicated.

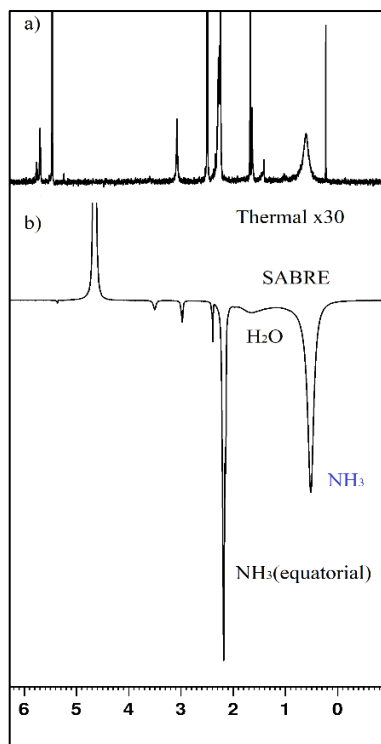
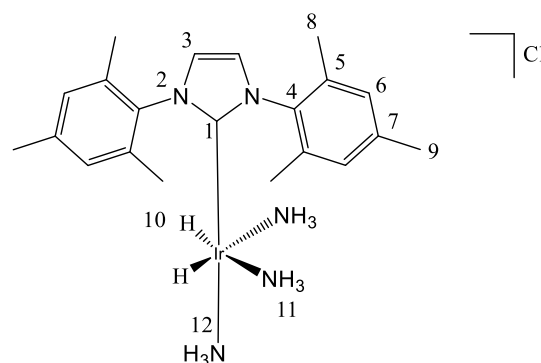


Table 2.8: NMR characterisation data of $[\text{Ir}(\text{H})_2(\text{IMes})(\text{BnNH}_2)_3]\text{Cl}$ (**5**) in dichloromethane- d_2 at 298 K with resonances attributed according to the labelling of the inset structure.



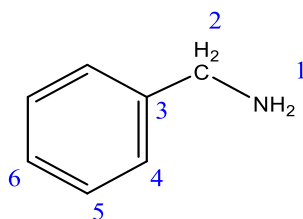
Resonance number	^1H (ppm)	^{13}C (ppm)	^{15}N (ppm)
1		153.8	
2			190.83
3	6.80	121.5	
4		138.11	
5		135.25	
6	7.00	129.00	
7		138.64	
8	2.10	18.30	
9	2.35	20.78	
10	-23.61		
11	2.21 (br, s) * $J_{\text{NH}} = 67$ Hz		-34.9
12	2.84 (br, s) * $J_{\text{NH}} = 69$ Hz		-46.5

* ^{15}N coupling determined via 2D NMR spectrum on unlabelled sample

To examine benzylamine (BnNH_2), it was first characterised by recording ^1H and ^{13}C NMR spectra in dichloromethane- d_2 solution at 400 MHz (Table 2.9). After that, a sample with 5 mM of **2** and a 10-fold excess of BnNH_2 relative to **2** was prepared which was dissolved in 0.6 ml solution of dichloromethane- d_2 , and exposed to a 3-bar pressure of H_2 . When this was examined by NMR spectroscopy, the ^1H NMR spectrum contained several changes relative to that before H_2 addition. The most significant of these changes was the formation of a hydride resonance at $\delta -23.95$ similar to those of **3** and **4** above. Moreover, the signals for the COD ligand of **2** at $\delta 4.07$ and 3.04 had disappeared. The NH_2 protons signals of the bound BnNH_2 ligand *trans* to hydride were split into two inequivalent resonances at $\delta 5.00$ and 2.30 . Two signals at $\delta 3.65$ and 3.30 were seen for the NCH_2 protons. Conversely, the axial ligand which is *trans* to the NHC gives rise to single equivalent resonances at $\delta 4.25$ for the corresponding NH_2 protons and at $\delta 3.85$ for the NCH_2 protons. Comprehensively, these results are

indicative of the formation of $[\text{Ir}(\text{H})_2(\text{IMes})(\mathbf{2}\text{-BnNH}_2)_3]\text{Cl}$ (**6**). Full characterisation data for this complex is presented in Table 2.10. The rate constant for BnNH_2 ligand loss from **2-BnNH₂** was determined by Rayner through EXSY methods and found to be 3.33 s^{-1} while the corresponding rate for H_2 loss was 2.83 s^{-1} , both at 298 K. In contrast, the rate of dissociation of NH_3 in **2-NH₃** is 0.32 s^{-1} , which is ~ 10 times lower than that of BnNH_2 .¹⁰⁸

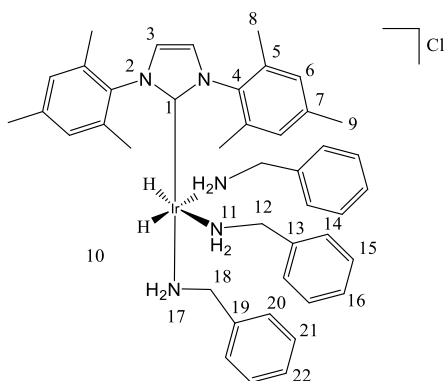
Table 2.9: NMR characterisation data for benzylamine in dichloromethane-*d*₂ at 298 K.



Resonance number	¹ H (ppm)	¹³ C (ppm)
1	1.51 (br, 2H)	-
2	3.84 (s, 2H)	46.37
3	-	143.36
4	7.28 (m, 2H)	126.92
5	7.31 (m, 2H)*	128.34
6	7.32 (m, 1H)*	128.91

*Overlap

Table 2.10: NMR characterisation data for $[\text{Ir}(\text{H})_2(\text{IMes})(\text{BnNH}_2)_3]\text{Cl}$ (**6**) in dichloromethane- d_2 at 298 K with the labels according to the inset structure.



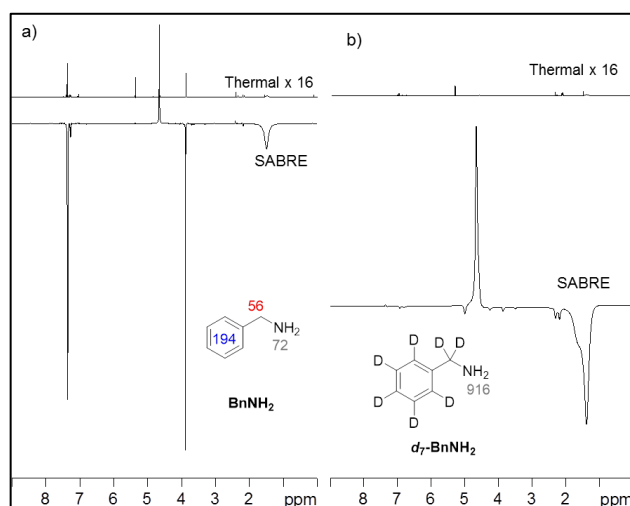
Resonance number	^1H (ppm)	^{13}C (ppm)	^{15}N (ppm)
1		153.8	
2			192.83
3	6.80	121.73	
4		138.11	
5		135.25	
6	6.90	129.29	
7		138.64	
8	2.17	18.30	
9	2.21	20.78	
10	-23.95		
11	5.00 (br, dt, $J_{\text{HH}} = 5$ and 11 Hz, 2H) * $J_{15\text{NH}} = 68$ Hz 2.30 (br, t, $J_{\text{HH}} = 11$ Hz, 2H) * $J_{15\text{NH}} = 68$ Hz		-6.4
12	3.65 (dt, $J_{\text{HH}} = 5$ and 15 Hz, 2H), 3.30 (ddd, $J_{\text{HH}} = 3, 12$ and 15 Hz, 2H)	53.14	
13		141.8	
14	7.35 (d, $J_{\text{HH}} = 5$ Hz)	128.33	
15	7.25 (t, $J_{\text{HH}} = 5$ Hz)	126.88	
16	~7.28 - overlap	-	
17	4.25 (t, $J_{\text{HH}} = 7$ Hz, 2H) * $J_{15\text{NH}} = 69$ Hz		-13.4
18	3.85 (t, $J_{\text{HH}} = 7$ Hz, 2H)	57.26	
19		-	
20	7.30	128.35	
21	~7.28 - overlap	-	
22	~7.28 - overlap	-	

* ^{15}N coupling determined via 2D NMR spectrum on unlabelled sample

In order to hyperpolarise this sample, *para*- H_2 was added, and a series of shake and drop measurements performed at 65 G which resulted in the detection of NMR signals that were enhanced by 72, 56, 194-fold per proton for the NH_2 , CH_2 , and Ph groups respectively as demonstrated in Figure 2.11a. In contrast, when $\text{BnNH}_2\text{-}d_7$ was used instead of BnNH_2 , the polarisation was focused on just the NH_2 protons which led to

their signals showing a significant signal enhancement increase, by 367 %, when compared to the undeuterated sample (Figure 2.11b).

Figure 2.11: (a) ^1H NMR spectra of BnNH_2 hyperpolarised (bottom) and thermal polarised (top) (b) ^1H NMR spectra of $\text{BnNH}_2\text{-}d_7$ hyperpolarised (bottom) and thermal polarised (top).¹⁰⁸



To examine the effect of T_1 on the polarisation level, the values for BnNH_2 and $\text{BnNH}_2\text{-}d_7$ with and without the active complex were measured. For BnNH_2 , the value of T_1 for the NH_2 protons was 1.1 s, and it was 4.7 s for the CH_2 protons at 9.4 T. The corresponding value for the NH_2 group of $\text{BnNH}_2\text{-}d_7$ was 1.1 s. in the presence of the active complex. This means the effect of T_1 is minimal and the higher NH_2 signal enhancement seen for the NH_2 signal of $\text{BnNH}_2\text{-}d_7$ must be due to a decline in spin dilution which can improve the efficiency of SABRE polarisation transfer. In the absence of the catalyst, the T_1 values of BnNH_2 become 9.0 s for (NH_2) and 11.0 s for (CH_2), while the T_1 value of the NH_2 group of $\text{BnNH}_2\text{-}d_7$ is now 10.1 s. The T_1 relaxation values of BnNH_2 and BnNH_2 are slower when measured without the active complex, as expected.

The fact that the NH_2 protons T_1 in the absence of a catalyst increases slightly with ^2H labelling of the residual protons in the amine is expected. However, it was surprising to find that in the presence of the catalyst both sets of protons exhibit similar T_1 values of 1.1 s. Hence the reduction in T_1 observed was over 90%, and consequently the accuracy of the data precluded seeing what can be estimated as a 0.1 s difference. Repeating these measurements with a much larger excess of amine would be expected

to move the T_1 values towards those of the pure free amine and thereby make any difference easier to visualise.

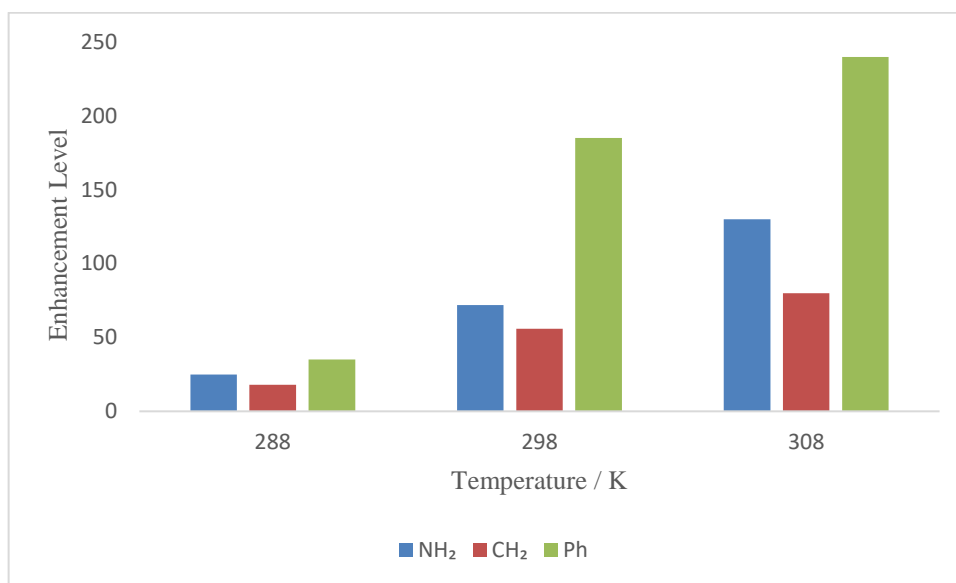
2.6.1 Effect on SABRE polarisation by substrate-catalyst ratio

As seen in previous results, the SABRE polarisation is dependent on substrate-catalyst ratio. Thus, this effect was examined by using different ratios of BnNH_2 which ranged from 4 to 20-fold excess relative to **2** in a set of measurements under the same conditions, of a 65 G polarisation transfer field and 298 K. The results showed similar total enhancement levels for these samples. Therefore, these results show that the obtained signal enhancements from these measurements are effectively independent of the BnNH_2 excess which suggests that the maximum polarisation level is restricted by the catalysts fast relaxation time and slow ligand exchange.

2.6.2 Effect on SABRE polarisation by temperature

The temperature can affect SABRE polarisation transfer as a result of changes in catalyst lifetime. It was found that cooling a sample containing **5** to 288 K resulted in a reduced signal enhancement level compared to that performed at 298 K, as shown in Figure 2.12. In contrast, warming the sample to 308 K increased the total signal enhancement level by ~40%. The dissociation rate constant for BnNH_2 increased to 9.85 s^{-1} at 308 K. Thus, it was concluded that this improvement in signal gain is due to the faster exchange rate of BnNH_2 ligands and a shorter lifetime of the catalyst. For NH_3 , the observed signal enhancement became 251-fold at 308 K, while it was enhanced by 154-fold at 298 K. This fits with the observed dissociation rate constant increase for NH_3 loss which rises from 1.64 s^{-1} at 298 K to 10.42 s^{-1} at 308 K.¹⁰⁸

Figure 2.12: Temperature effect on SABRE polarisation of 2-BnNH₂ adapted from lali *et al.*¹⁰⁸



2.7 Summary

The amines tested in this chapter can form SABRE active complexes. Enhancement by SABRE was achieved for all these amines through their active complexes. The ¹H signal enhancement of NH₂ response for ethanolamine was 126-fold, which is higher than that of PEA (110-fold) and BnNH₂(72-fold). For the CH₂ response of NCH₂, BnNH₂ showed the highest enhancement with 56-fold, while it was 50 and 24-fold for PEA and ethanolamine respectively. Using a ratio of 5-fold excess relative to **2** showed the highest signal gain for most of these amines, and 65G is the optimum field for polarisation transfer. For total enhancement per molecule, the highest ¹H signal was for BnNH₂-d₇ (916-fold), while PEA, NH₃, and ethanolamine were 280, 350, and 200-fold respectively.

The *T*₁ relaxation time of (NH₂) in the presence of the active complex was similar for free PEA and ethanolamine (1.75 s), while it was 1.1 s for BnNH₂. Whilst the *T*₁ value for the protons of free NH₃ were 5.5 s. Moreover, the *T*₁ value of the CH₂ group in BnNH₂ was longer than that of the analogous group in ethanolamine and PEA.

2.8 Conclusion

Initially, the focus was on the hyperpolarisation of the amines: phenethylamine, ethanolamine, benzylamine, and NH_3 . Then, focus was on the optimisation of the enhancement levels. All tested amines formed suitable active complexes and were hyperpolarised by SABRE technique, which gave NMR signal enhancement levels of between 200-916 fold. The highest enhancement levels were acquired using a 5-mM sample with a 5-fold excess of substrate relative to **2** catalyst. This result was obtained at 298 K using a transfer field of 65 G. The associated proton resonances of phenethylamine and benzylamine proved to have a longer signal lifetime than ethanolamine due to the presence of the phenyl group.

Interestingly, in some experiments the solvent used was not completely dry and this led to the polarisation of water through proton exchange with the hyperpolarised amines. Therefore, this can allow hyperpolarisation of water and other molecules that contain OH such as alcohols which cannot be directly polarised by SABRE since they cannot bind to the iridium centre.

Therefore, the intention is to use these amines as polarisation transfer agents for hyperpolarisation of plants' natural products (essential oils), which are basically plant alcohols.

Chapter 3: Hyperpolarisation of essential oils

In this chapter the focus is on examining the important plant derived oils geraniol, nerol and citronellol. Geraniol is actually an acyclic monoterpene derived alcohol that is commonly found in aromatic plants. It has a chemical formula of $C_{10}H_{18}O$, and therefore one heteroatom substituent and a molecular weight is 154.25 grams per mol. It therefore counts as a small molecule whose NMR characterisation should be straightforward.

Geraniol was originally extracted from palmarosa oil, but is now known to be the main constituent of the oils rose oil, citronella oil, and palmarosa oil. Geraniol is a liquid, and has a rose-like odour. It is widely used in the industry of perfumes and food flavouring. Additionally, geraniol has an anti-microbial and antioxidant effects, and can also be used as natural repellent against insect.¹¹² Nerol is also monoterpene and found in many aromatic plants, but it was originally obtained from neroli oil. Nerol has the same empirical formula and molecular weight as geraniol, but differs according to the geometric arrangement of the double bond. It can be found in the oils of lemon grass and hops, and is often accompanied by geraniol. It too is a colourless liquid with a similar fresh rose-like scent that is used in the industry of perfumes and food flavouring.¹¹²⁻¹¹³

Citronellol is another important acyclic monoterpene. It is again one of the main components of many plant oils such as basil, citrus, citronella, cymbopogon (lemongrass) and roses. It gives the plant an aromatic fragrance and is widely used in the cosmetics industry. It also has an anti-bacterial effect and can work as a deterrent against some insects.¹¹⁴⁻¹¹⁵

The aim of the first part of this chapter is to utilise SABRE-RELAY for the examination of these three natural oils. The aim is to obtain an optimal NMR signal gain in order to demonstrate that they can be characterised by NMR spectroscopy at low loadings. This reflects an analytical development that will improve the utility of NMR spectroscopy for the examination of alcohols more generally. The effects of SABRE-RELAY as a function of the structure of these oils are also sought to be probed. One key question is whether the hyperpolarisation will transfer across the

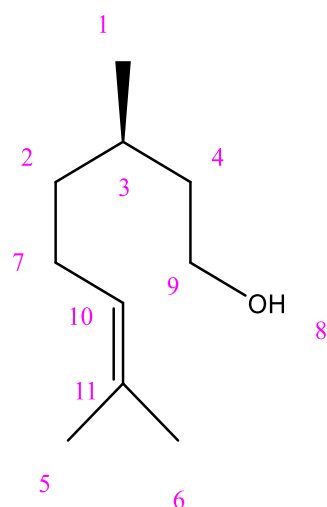
whole molecule? This will involve assessing how a secondary carbon centre impacts on progress across the molecule. Furthermore, the presence of an alkene function will be examined to see if it can be beneficial to the process. These results will be linked to the relaxation times of the detected protons. The research will also examine if the outcome is influenced by the identity of the amine. Addition testing to see if SABRE-RELAY can be improved by using a ^2H -labelled carrier, or whether it is possible to detect the ^{13}C signals of these materials is detailed.

3.1 Results and Discussion

3.1.1 NMR Characterisation of Citronellol through SABRE-RELAY

In order to start this process, citronellol first needs characterising by NMR. To achieve this, citronellol was dissolved in dichloromethane- d_2 . The solvent dichloromethane- d_2 was selected because it is aprotic and therefore will not contribute to hydrogen transfer between the NH and OH of the target substrate. Furthermore, it is of low viscosity and exhibits lower toxicity than the alternative chloroform. The resulting ^1H NMR spectrum contains signals at δ 0.94 ($\text{CH}_3\text{-H}_1$), 1.22 ($\text{CH}_2\text{-H}_2$), 1.39 ($\text{CH}_2\text{-H}_4$), 1.59 (CH-H_3), 1.65 ($\text{CH}_3\text{-H}_5$), 1.72 ($\text{CH}_3\text{-H}_6$), 2.03 ($\text{CH}_2\text{-H}_7$), 2.14 (OH-H_8), 3.65 ($\text{CH}_2\text{-H}_9$), and 5.14 (CH-H_{10}) as listed and attributed in Table 3.1. The resonance at δ 3.65 is due to the $\text{CH}_2\text{-H}_9$ group that is adjacent to the OH and its appearance should reflect a key marker for the success of SABRE-RELAY. Since SABRE-RELAY depends on an amine for the transfer of polarisation, this process was initially examined with the sensitizers that were hyperpolarised in Chapter 2: ethanolamine, phenylethylamine and ammonia. These measurements are now summarised alongside the necessary characterisation data.

Table 3.1: NMR characterisation data for citronellol in dichloromethane- d_2 at 298 K.



Resonance number	^1H (ppm)	^{13}C (ppm)
1	0.94 (d 6.6 Hz, 3H)	19.2 (q, 123 Hz)
2	1.22 (m, 1H), 1.38 (m, 1H)	37.2 (t, 126 Hz)
3	1.59 (m, 1H)	29.2 (d, 125 Hz)
4	1.39 (m, 1H), 1.64 (m, 1H)	39.9 (t, 124 Hz)
5	1.65 (s, 3H)	17.3 (q, 119 Hz)
6	1.72 (s, 3H)	25.4 (t, 123 Hz)
7	2.03 (m, 1H), 1.67 (m, 1H)	25.4 (t, 126 Hz)
8	2.14 (1H)	-
9	3.65 (m, 2H)	60.9 (t, 139 Hz)
10	5.14 (m, 1H)	124.6 (d, 149 Hz)
11	-	131.1 (s)

3.1.2 SABRE-RELAY of Citronellol with the sensitizer Phenethylamine

An NMR sample for SABRE was prepared using a 5-fold excess of phenethylamine relative to iridium that contained 2 mg (5 mM) of Ir(IMes)(COD)Cl (**2**) as the precatalyst in a 0.6 ml solution of dichloromethane- d_2 . 3 bars of normal hydrogen gas were then added to the sample, and it was left to activate overnight. The sample was then checked by recording ^1H NMR spectra at 9.4 T. These NMR spectra showed a hydride signal at δ -23.95, alongside resonances δ 4.42, 3.68 and 2.78 signals for bound phenethylamine (**1**). These observations indicate the successful formation **3**. At this stage, 3 μl (27 mM) of citronellol was added, reflecting a 5-fold excess based on iridium and a series of shake and drop experiments undertaken. The resulting hyperpolarised ^1H NMR spectra showed signal enhancements for all of the proton

responses of citronellol (Figure 3.1b) that were previously listed in Table 3.1, with the total signal enhancement for the 19 protons of the carbon scaffold being just 244-fold, which is reflective of an average signal gain of 13 per proton. As expected, the highest signal gain, of 43 per proton, was seen for the δ 3.65 (CH₂-H₉) resonance, which reflects the closest protons to the OH group. The enhancement level for the alkenic proton (CH-H₁₀) response was only 6-fold. It would therefore appear that phenethylamine is a disappointing co-catalyst for the hyperpolarisation of citronellol; improvements with deuterated phenethylamine will be discussed in section 3.1.5.

3.1.3 SABRE-RELAY of citronellol with the sensitizer ethanolamine

In order to test whether the hyperpolarisation level seen with phenethylamine could be improved the amine was varied, first examining ethanolamine. The ratio of amine to catalyst (**2**) was retained at 5:1 as in the previous experiment. The sample was again left overnight under a hydrogen atmosphere to activate it; this led to the formation of (**4**). 3 μ l of citronellol (27 mM) was then added and a series of shake and drop measurements performed. These measurements showed enhancement of the citronellol ¹H NMR responses as expected. However, it was now difficult to precisely estimate the level of enhancement for citronellol due to overlap with ethanolamine signals in the region δ 1.20 to δ 2.30. Consequently, ethanolamine may not be suitable for this purpose. Nonetheless, the CH₂O (CH₂-H₉) response now proved to be enhanced by 87-fold, which was twice the size of that achieved with phenethylamine. However, the enhancement level for the (CH-H₁₀) response was only 7-fold which was similar to that obtained with phenethylamine.

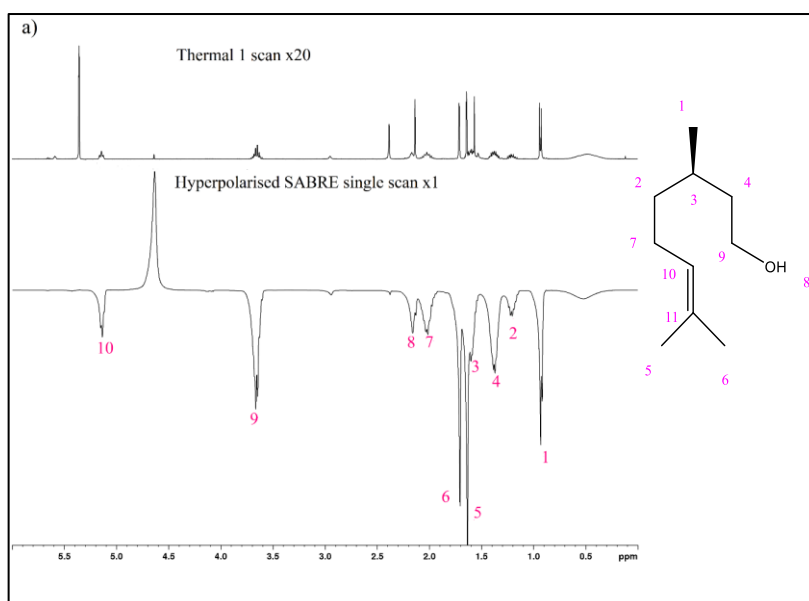
3.1.4 SABRE-RELAY with the sensitizer ammonia

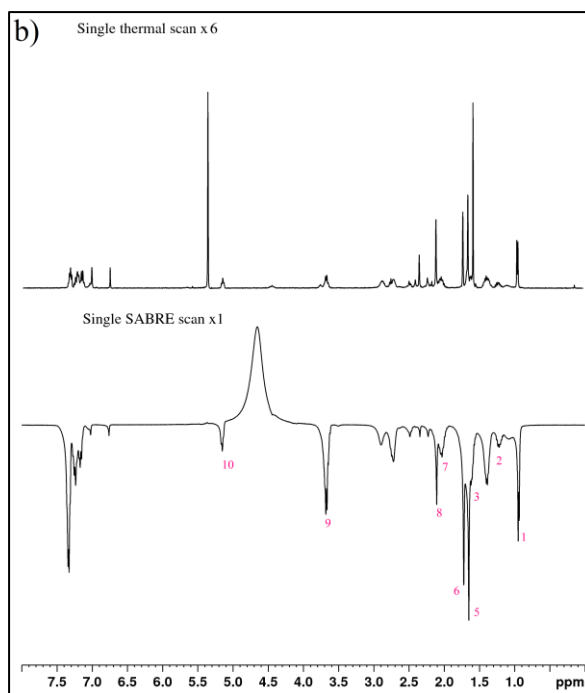
Another potential agent for transferring hyperpolarization is NH₃. A SABRE-RELAY sample was therefore prepared using ammonia in 0.6 ml of dichloromethane-*d*₂ with 2 mg of (**2**). The sample was degassed and ammonia added using a high vacuum line. After adding 3 bars of hydrogen and leaving the sample overnight, it became activated. Then the sample was checked by recording a ¹H NMR spectrum. This showed a hydride resonance at δ -23.61 with other resonances at δ 2.21 and 2.84 for the bound NH₃ ligand and a broad resonance at δ 0.47 for the free NH₃. Based on the integrals

of these signals, it can be concluded that the initial excess of NH_3 relative to iridium was 8-fold. This led to the successful formation of **5**.

After that, 5 equivalents of citronellol relative to (**5**) were added. Measurements were then undertaken, which showed significant enhancement levels for all of the ^1H NMR responses of citronellol (Figure 3.1a). The enhancement levels obtained with ammonia were significantly higher than those obtained with PEA and ethanolamine. This is reflected in the fact that the total signal gain was now 2935-fold rather than the 244-fold of phenethylamine which reflects a 1103% improvement. Additionally, the CH_2O ($\text{CH}_2\text{-H}_9$) resonance showed a 300-fold per proton gain rather than the 43-fold seen with phenethylamine. Thus, this resonance has improved by 598%. The resonance (CH-H_{10}) was enhanced by 65-fold which is 983% larger than that with phenethylamine, which is comparable to the overall gain.

Figure 3.1: a) ^1H NMR spectra to illustrate the enhancement of citronellol's ^1H responses achieved with SABRE-RELAY using NH_3 as the carrier. Thermally polarised NMR spectrum (upper) alongside single scan SABRE-RELAY response (lower). The inset structure can be used to link these resonances to their origin in Citronellol. b) The enhancement of citronellol's ^1H responses achieved using SABRE-RELAY with **1** as the carrier is demonstrated through ^1H NMR spectra. The upper spectrum represents the thermally polarized NMR response, while the lower spectrum shows the result of a single scan using SABRE-RELAY. The inset structure at (a) provides a means to correlate these resonances with their corresponding positions in citronellol.





3.1.5 SABRE-RELAY with deuterated phenethylamine (PEA- d_4)

SABRE-RELAY was performed with normal PEA which showed a relatively weak enhancement level compared to those achieved with ammonia. Consequently, another series of measurements were performed using PEA- d_4 (the aliphatic protons are deuterated) to see whether the presence of the ^2H label could improve on the observed enhancement levels. Thus, a sample was prepared with PEA- d_4 using the same concentrations of reagents as utilised in Section 3.1.1. A series of shake and drop measurements were then performed. The results showed that higher levels of signal enhancement were achieved for the citronellol response. Now the total signal enhancement level was 771-fold, which is three times larger than that with normal PEA and the resulting average per proton gain increases to 40-fold. Moreover, the resonances seen for CH- H_1 to CH $_2$ - H_9 increased in size by between three and four times the values found with proteo PEA.

It should be noted from these data that the signal gains are no longer proportional to the number of protons within the group. This is a consequence of the fact that polarisation transfer radiates out across the molecule in a nonlinear fashion, whilst being further attenuated by relaxation. The enhancement levels are reproducible so

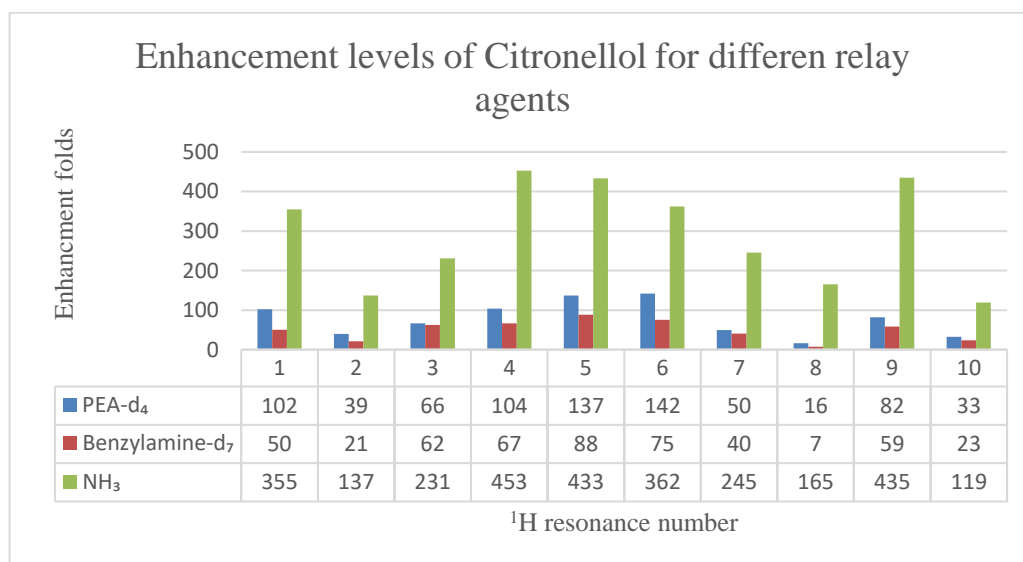
calibration is possible, alongside quantification. In this context, however, the main focus was to magnify the response to the highest level.

3.1.6 SABRE-RELAY with deuterated benzylamine- d_7

A commercial source of deuterated benzylamine- d_7 , where the NH_2 group retains a ^1H label is also available. A sample containing a 5-fold excess of this amine and a 5 excess of the substrate relative to iridium was prepared. The total enhancement level attained through the shake and drop experiment was now 492, which was lower than that achieved with $\text{PEA}-d_4$. Hence, again NH_3 reflects the better agent.

Figure 3.2 reflects a chart that shows the difference in signal enhancement levels per proton for the best three agents used across the resonances of citronellol. Interestingly, the signals for (CH_3-H_5) and (CH_3-H_6) are relatively stronger with $\text{PEA}-d_4$ and benzylamine- d_7 even though they are located furthest from the OH. This may again be a result of relaxation changes and will be assessed in due course.

Figure 3.2: Comparison of citronellol signal enhancements per proton for the three SABRE-RELAY carriers $\text{PEA}-d_4$, Benzlammine- d_7 , and NH_3 samples.



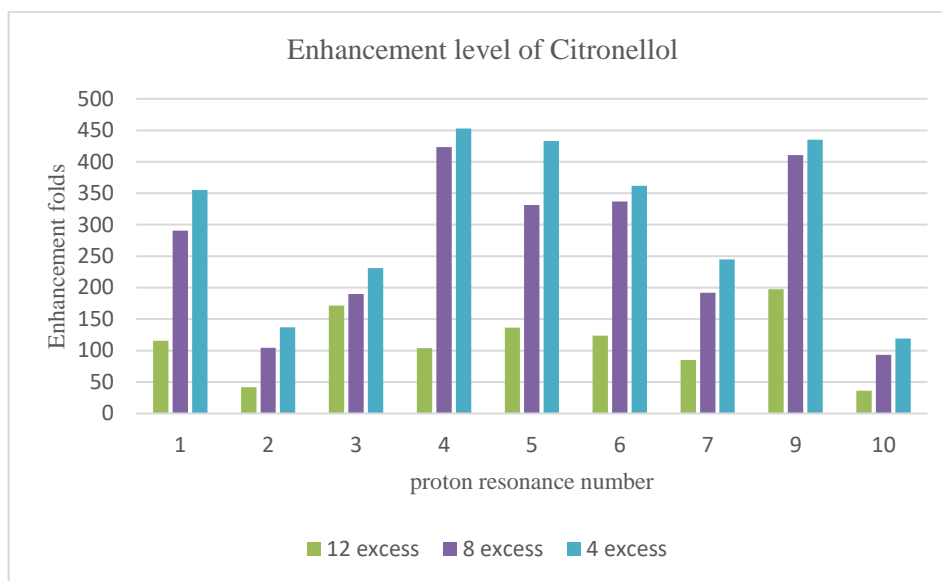
3.1.7 Effect of the concentration of transfer agent and substrate on the enhancement level of SABRE-RELAY

3.1.7.1 SABRE Relay with different concentrations of ammonia

Since the level of signal enhancement should be related to concentration, the effect of using different concentrations of these species was studied to find the optimum concentration where the enhancement level is maximised. First, a SABRE-RELAY sample was prepared using the same method as in the previous experiment. The amount of ammonia used at the start now reflected a 12 excess relative to **5**. The shake and drop technique was performed and ^1H NMR spectra were recorded. These measurements were then repeated after reducing the ammonia level to 8 and 4 fold excesses respectively by bubbling nitrogen gas through the sample. The amount of citronellol was retained at a 5-fold excess relative to **5** throughout.

The total signal enhancement level found for the sample when ammonia was in a 12 excess was 1141-fold. After reducing that excess to 8 fold the signal gain increased to 2587-fold. Further reduction of ammonia to a 4-fold excess improved the enhancement level to 2935 fold. These values are all obtained by comparison with the corresponding thermally polarised NMR spectrum. Figure 3.3 highlights the corresponding changes in enhancement level per proton observed in these three samples.

Figure 3.3: ^1H NMR signal enhancement level for the indicated Citronellol protons (per proton) achieved with the excesses of NH_3 relative to **5** being 12, 8 and 4 fold as indicated.



These measurements confirm that the CH_2O group ($\text{CH}_2\text{-H}_9$) always yields a strong signal gain. The CH_2 group next to this is ($\text{CH}_2\text{-H}_4$) yields a response almost as strong as that of ($\text{CH}_2\text{-H}_9$). The next group is the (CH-H_3) for which the responses of all three samples are much closer in relative size, albeit smaller than those of ($\text{CH}_2\text{-H}_4$) and ($\text{CH}_2\text{-H}_9$) across the series. It is particularly noteworthy that the resonances for ($\text{CH}_3\text{-H}_5$) and ($\text{CH}_3\text{-H}_6$) which correspond to the remote Me groups are strong. The CH and CH_2 groups ($\text{CH}_2\text{-H}_2$) and (CH-H_{10}) are weak.

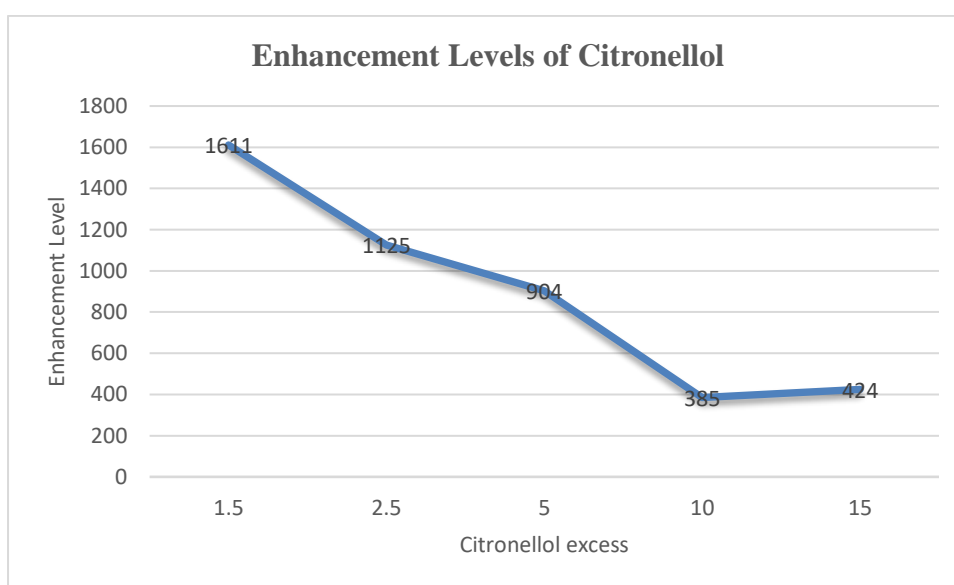
These data confirm that hyperpolarisation transfer across the whole spin system is possible. Given the intensity variations they also suggest that another effect is important in controlling their relative sizes. This is likely to be relaxation and will be discussed later.

3.1.7.2 SABRE-RELAY with different loadings of citronellol

In order to examine the effect of different substrate excess levels relative to catalyst on the level of signal enhancement, 5 samples were prepared from a stock solution that contained 3 ml of dichloromethane- d_2 and 10 mg of (**2**) and a 10-fold excess of NH_3 . This solution was degassed and put under 3 bar hydrogen pressure until activated. Then, it was divided into 5 samples so each contained 0.6 ml

dichloromethane- d_2 , 2 mg of (1), and a fold 10 excess of NH_3 . After that, different excesses of citronellol were added to each sample, these were 1.5, 2.5, 5, 10 and 15 excesses in a glovebox. Then, *para*- H_2 was added and the samples were shaken for 10 seconds prior to recording hyperpolarised ^1H NMR spectra. The highest enhancement level was obtained with the 1.5-fold excess of citronellol, which was the smallest excess used in this experiment. Then, the enhancement level became smaller with every addition of citronellol used (Figure 3.4).

Figure 3.4: ^1H NMR signal enhancements seen for citronellol with 1.5, 2.5, 5, 10 and 15 equivalents relative to (2).



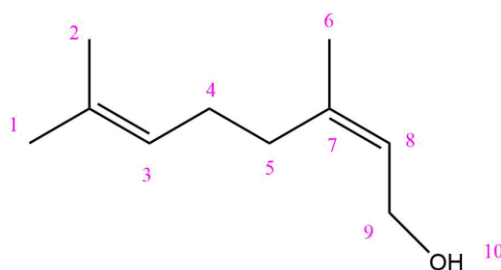
These data are self-consistent. It is also interesting to note that Figure 3.4 reveals essentially linear behaviour. This would be consistent with a chemical process involving an inverse first order dependence on the corresponding reagent that is being changed. Hence the signal enhancement level can be thought to be inversely proportional to the excess of citronellol relative to ammonia.

Additionally, this indicates that a smaller sub stoichiometric excess of citronellol relative to the amine can improve the enhancement level, which could allow easier detection of citronellol ^1H resonances and similar plant alcohols even if they are present in a very small quantity. However, by using a small amount of the substrate, such as 1.5 excess ($\sim 1\mu\text{l}$), the ability to detect ^{13}C resonances is reduced (see later).

3.1.8 NMR Characterisation of nerol through SABRE-RELAY

Having established that citronellol can be polarised well by SABRE-RELAY, the examination of the plant alcohol nerol was then undertaken. First, characterisation of this substrate is needed. Upon dissolving nerol in dichloromethane- d_2 the resulting ^1H NMR spectrum contained signals at δ 1.65 ($\text{CH}_3\text{-H}_1$), 1.78 ($\text{CH}_3\text{-H}_2$), 5.16 (CH-H_3), 2.18 ($\text{CH}_2\text{-H}_4$), 1.72 ($\text{CH}_3\text{-H}_6$), 5.45 (CH-H_8), 4.11 ($\text{CH}_2\text{-H}_9$) and 1.57 (OH-H_{10}) as detailed in Table 3.2. To examine the hyperpolarisation of this substrate, the new SABRE-RELAY technique was used again.

Table 3.2: NMR characterisation data for nerol in dichloromethane- d_2 at 298 K.



Resonance number	^1H (ppm)	^{13}C (ppm)
1	1.65 (s, 3H)	17.39
2	1.78 (s, 3H)	23.06
	-	132.19
3	5.16 (m, 1H)	123.94
4	2.18 (d, 2H)	26.54
5	2.18 (d, 2H)	31.91
6	1.72 (s, 3H)	25.44
7	-	139.55
8	5.45 (t, 1H)	124.54
9	4.11 (d, 2H)	58.84
10	1.57 (br, 1H)	-

The initial measurements were performed using phenylethylamine in the first instance. Thus, a sample containing complex **3** was prepared as in 3.1.1.1. After that, a 5-fold excess of nerol relative to **2** (5 mM) was added. *para*- H_2 was then added and a series of SABRE measurements performed. The corresponding ^1H NMR signal enhancements were recorded. The resulting NMR spectra showed that nerol ^1H resonances can successfully be polarised by the SABRE-RELAY technique. The total

signal enhancement of nerol ^1H by PEA was 173-fold, which is again weak, and so phenylethylamine is a disappointing co-catalyst for hyperpolarisation of nerol as well.

To improve on the previous measurement, PEA was replaced with PEA- d_4 .^{108, 116} Then, shake and drop measurements were performed after adding *para*- H_2 and recorded appropriate NMR spectra. The total signal enhancement of nerol was now 643-fold compared to 173-fold with normal PEA, which is an improvement by 272 %. Additionally, the CH_2O ($\text{CH}_2\text{-H}_9$) resonance signal gain has improved from 48-fold to 145-fold per proton which is an improvement by 202 %.

3.1.9 SABRE-RELAY with ammonia

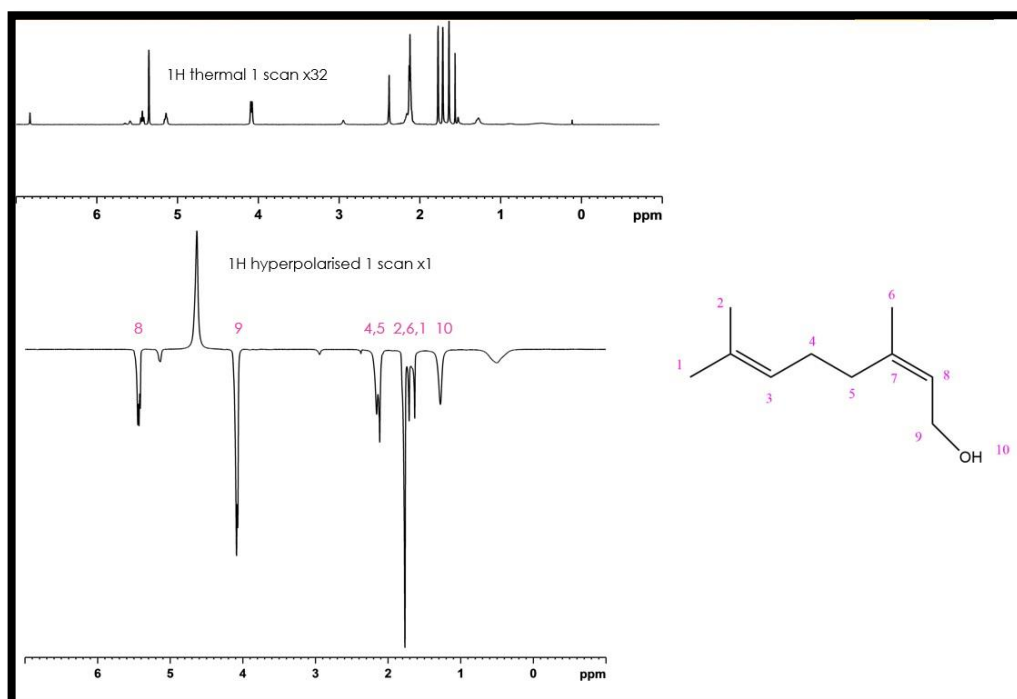
Another SABRE-RELAY sample was prepared using ammonia. The sample was prepared in 0.6 ml of dichloromethane- d_2 and 2 mg of IrIMes. After degassing the sample by the high vacuum line, ammonia was added. Then, normal hydrogen was added, and the sample was left overnight to activate, which led to the formation of (4). 3 μl of nerol was then added. Then *para*- H_2 was added to the sample.

Measurements were then undertaken, which showed high signal enhancements for nerol ^1H NMR responses as illustrated in Figure 3.5, and Table 3.3. The signal enhancement levels obtained with ammonia were significantly higher than that obtained with PEA. This is reflected in the fact that the total signal gain was now 2544-fold rather than the 173-fold of phenethylamine which reflects a 1371 % improvement. Additionally, the CH_2O resonance showed a 856-fold gain rather than the 48-fold seen with phenethylamine, which is higher by 1683 %.

Table 3.3: ^1H NMR enhancement levels for nerol using ammonia after a delay time of 3.5 s and the corresponding values after correction for T_1 without this delay.

Resonance number	Number of protons in the group	Enhancement (fold) for the ^1H signals per proton	Enhancement T_1 corrected
1	3	160	222
2	3	366	667
3	1	56	111
4	2	550	611
5	2	overlap	-
6	3	195	257
7	0	--	-
8	1	361	838
9	2	856	1373
10	--	--	-
Total signal gain		2544	4079

Figure 3.5: Typical ^1H NMR spectra of Nerol under SABRE-RELAY.



3.1.10 SABRE-RELAY of nerol with deuterated benzylamine- d_7

The effect of using benzylamine- d_7 as the polarisation carrier was also examined. This sample contained a 5-fold excess of the amine and a 5 excess of the substrate relative to the IrIMes catalyst. The total enhancement level produced in nerol was now 982-fold. Although this enhancement was higher than that obtained with PEA- d_4 under similar conditions (643-fold) it was lower than that obtained with ammonia (2544-fold).

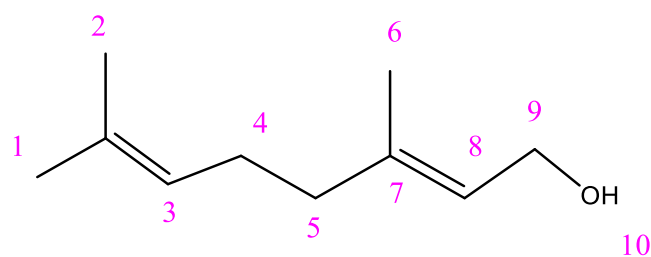
Hence, it can be seen that for citronellol excluding NH_3 , PEA- d_4 is the optimum carrier while for nerol it is benzylamine- d_7 . This difference in behaviour suggests that the amines pK_a must play a complex role in optimisation of the polarisation transfer process alongside the steric bulk of the substrate. Interestingly in all cases so far, NH_3 has proved optimal.

3.1.11 NMR Characterisation of Geraniol through SABRE-RELAY

Although geraniol has the same chemical formula and molecular weight as nerol, it exists in a different geometric form. Nerol was examined to see if this change in structure had any effect on the enhancement level output by SABRE.

When geraniol is dissolved in dichloromethane- d_2 the resulting ^1H NMR spectrum contained signals at δ 1.65 (H_1), 1.72 (H_2), 5.15 (H_3), 2.17 (H_4), 2.08 (H_5), 1.70 (H_6), 5.42 (H_8), 4.14 (H_9), and 1.57 (H_{10}) (Table 3.4). The amines used in this study were benzylamine- d_7 , PEA- d_4 and ammonia, which were the best agents used with citronellol and nerol.

Table 3.4 : NMR characterisation data for geraniol in dichloromethane- d_2 at 298 K.



Resonance number	^1H (ppm)	^{13}C (ppm)
1	1.65 (s, 3H)	25.4
2	1.72 (s, 3H)	17.5
	-	131.6
3	5.15 (m, 1H)	124.0
4	2.17 (d, 2H)	26.5
5	2.08 (d, 2H)	39.5
6	1.70 (s, 3H)	16.0
7	-	139.3
8	5.42 (t, 1H)	123.7
9	4.14 (d, 2H)	59.3
10	1.57 (br, 1H)	-
11	-	

3.1.12 SABRE-RELAY with deuterated benzylamine- d_7

A SABRE sample was prepared using a 5-fold excess of benzylamine- d_7 relative to 2 mg of **2** and 0.6 ml of dichloromethane- d_2 . The sample was then exposed to a 3 bar pressure of normal hydrogen and left to activate overnight. After that, a 5-fold excess of the substrate geraniol was added under nitrogen, and 3 bar of *para*- H_2 . A series of shake and drop measurements were then made at 9.4 T. These results showed that the total ^1H NMR signal enhancement for the 17 protons of geraniol was 1011-fold.

3.1.13 SABRE-RELAY with deuterated phenethylamine (PEA- d_4)

An analogous SABRE-RELAY sample was then prepared using the deuterated amine, PEA- d_4 . The sample contained 5-fold excess of PEA- d_4 and geraniol relative to 2 mg of pre-catalyst **2**, and was activated under H_2 overnight. The geraniol proton responses, after adding *para*- H_2 , showed a total ^1H NMR signal enhancement level of 820-fold which is 19% worse than that achieved with benzylamine- d_7 .

3.1.14 SABRE-RELAY with ammonia

2 mg of pre-catalyst **2**, was then placed in a SABRE-RELAY sample that contained a 5-fold excess of geraniol, and a 5-fold excess of ammonia. The samples were activated following the same method as the previous experiments. The total signal gain for the ^1H resonances of geraniol now proved to be 2746-fold under analogous conditions. This was the highest enhancement level achieved in comparison to other amines used (Table 3.5) and confirms the benefit of using NH_3 is widespread.

Table 3.5: Comparison of the ^1H NMR signal enhancement levels achieved for the protons in geraniol as a function of resonance according to the relay substrate NH_3 , $\text{PEA-}d_4$ and $\text{Benzylamine-}d_7$.

resonance number	^1H NMR signal enhancement (fold)		
	NH_3	$\text{Benzylamine-}d_7$	$\text{PEA-}d_4$
1	296	213	84
2	1081	284	332
3	101	27	17
4	200	55	Overlap total 140
5	434	83	
6	overlap with 2	overlap with 2	overlap with 2
7	-	-	-
8	189	107	78
9	446	242	169
total	2746	1011	820

While average enhancement delivers insightful information about a specific element. Total enhancement provides a more comprehensive view by accounting for the cumulative enhancement attained over the entire sample which ensures a full appreciation of the hyperpolarisation level achieved by the entire molecule. Therefore, it is a sensible and efficient metric in discussing these data.

3.2 ^{13}C NMR signal enhancements for Citronellol, Nerol and Geraniol

After enhancing the ^1H NMR resonances in citronellol, nerol and geraniol, their ^{13}C NMR resonances were investigated to see if it was possible to detect them as

hyperpolarised signals. The aim of this study was to demonstrate that these oils can be fully characterised through SABRE-RELAY. However, the detection of a ^{13}C NMR resonance is very challenging compared to ^1H since its natural abundance is just 1%. Furthermore, the magnetogyric ratio is $\frac{1}{4}$ of that of a proton and so overall, the ^{13}C signals are 6,400 times harder to detect than those of ^1H . For the detection and measurement of ^{13}C NMR resonances with SABRE-RELAY and the optimised conditions for hyperpolarising ^1H nuclei in the previous measurements were utilised.

First, citronellol was tested for the detection of its ^{13}C resonances, the results of which are listed in Table 3.1. The enhanced ^{13}C NMR responses are illustrated pictorially in Figures 3.6 and 3.7. These NMR spectra show strong signal enhancements for the OCH_2 group (185-fold) and the CH_2 next to this (175-fold), but the CH next to that is actually the strongest signal (230-fold). The enhancements seen for the ^{13}C resonances associated with sites 2 and 7 are much less (73, 54 fold respectively). Interestingly, the ^{13}C response for the next site (number 10, the alkenic CH group) also showed a strong enhancement of 230 -fold, making the signal similar in size to that of the OCH_2 group. The final $\text{C}(\text{Me})_2$ signal proved to be weakly enhanced. It is therefore clear that all of the carbon back-bone in citronellol are amplified under SABRE-Relay with the enhancement levels varying from signals 230 to 30 fold. As signal to noise scales with the square root of the number of observations, it can be predicted that it would take between 0.75 hrs and 44 hrs for a normal measurement to achieve the same signal to noise level if 3 seconds were left between scans. Hence these enhancements reflect a significant improvement in scan time.

It should be clear from the appearance of these NMR spectra that simple Zeeman magnetisation is not involved here. The antiphase character of the signals conveys that they result from a heteronuclear longitudinal two-spin order term. This observation is consistent with other SABRE derived heteronuclear data and demonstrates that the hyperpolarisation is transferred via the ^1H domain. It is for this reason that the ^{13}C NMR measurements were made when the best ^1H NMR signal gains were obtained, and no decoupling was employed. The best ^{13}C NMR signals are seen though for the two CH groups, with the OCH_2 and OCH_2CH_2 groups following. It would therefore appear that the ^1H polarisation level of the attached proton does not link explicitly

through to the ^{13}C enhancement level; the corresponding ^1H enhancement levels were 231, 119, 435 and 453 for these four resonances respectively.

This could indicate that the relaxation times of either the protons or ^{13}C signals are important, and these will be discussed in the next section. The signal enhancements seen for the ^{13}C resonance of the two methyl groups, at sites 5 and 6 respectively, were lower as expected due to their remote location from the initial OH entry site. They are also expected to have relatively short relaxation times. In conclusion, all the carbon signals in citronellol were hyperpolarised, which allows it to be detected (and characterised) in a single NMR scan even though the amount of material present in this 0.6 ml sample was just 0.027 moles.

However, the ability of the ^{13}C NMR responses of nerol and geraniol (listed in Tables 3.2 and 3.4) to be detected through SABRE-RELAY relative to citronellol is reduced. For nerol, the OCH_2 , OCH_2CH and $\text{OCH}_2\text{CH}=\text{C}$ signals are seen with gains of 328, 367 and 57 –fold respectively. The first two values are larger than those seen for any of the ^{13}C NMR resonances in citronellol described earlier. No ^{13}C NMR signal gains were observed for the carbon back-bone beyond this point. Consequently, the SABRE-Relay enhancement seems to stop at the carbon centre with no protons directly bound to it. Furthermore, the CH_2 signal gain is now 90% of the CH gain which makes the two signals far closer in intensity than was seen for citronellol, but their relative order is reversed.

The corresponding ^1H NMR signal gains for citronellol totalled 2935-fold whilst those for nerol totalled 2544-fold. Hence the overall ^1H levels of these materials are 14% higher for citronellol. For geraniol, the detected ^{13}C responses followed a similar trend of that of nerol. The OCH_2 , OCH_2CH and $\text{OCH}_2\text{CH}=\text{C}$ signals gains were 297, 305, and 65 –fold respectively, which were slightly lower than that seen for nerol. There was also no carbon signal detected after these sites.

Insensitive nuclei enhancement by polarisation transfer (INEPT) is a method used to transfer the spin population imbalance from ^1H to ^{13}C to improve the ability to detect ^{13}C .¹¹⁷ Furthermore, the resulting ^{13}C NMR spectrum can now be measured with ^1H decoupling. It proved possible to use the INEPT protocol to detect all of the ^{13}C

resonances in citronellol. Some typical data are shown in Figure 3.6. The OCH₂ resonance appears with a S/R ratio of 43:1 in this single scan ¹³C{¹H}-INEPT measurement which compares to a value of 7.5 for the equivalent resonance in the directly detected ¹³C measurement (this is a 1:2:1 triplet which means with decoupling a S/N of 15 would be seen). It is therefore clear that utilisation of the ¹H transfer sequence is more efficient than simple SABRE-Relay at 60 G when ¹³C is probed.

When a ¹³C{¹H}-INEPT spectrum is recorded for nerol, the first three resonances are again amplified. The OCH₂ signal now again appears with the strongest signal strength and has a S/N value of 36:1, while that for the CH 27:1. These values exceed those in the direct ¹³C NMR measurement which were 10:1 and 8.6 respectively. This trend also applies to geraniol, as the S/N values after INEPT for the OCH₂ and CH resonances were 43:1 and 25:1, while that of direct ¹³C measurement were 27:1 and 12:1 respectively. These data again demonstrate the benefits of INEPT transfer to SABRE-RELAY when the aim is simply to detect a diagnostic response with maximum S/N.

Figure 3.6: ^{13}C NMR responses for citronellol. Top, 2048 scan spectrum, middle single scan hyperpolarised spectrum and bottom hyperpolarised single scan refocused and decoupled INEPT spectrum using a cnst2 of 122 Hz.

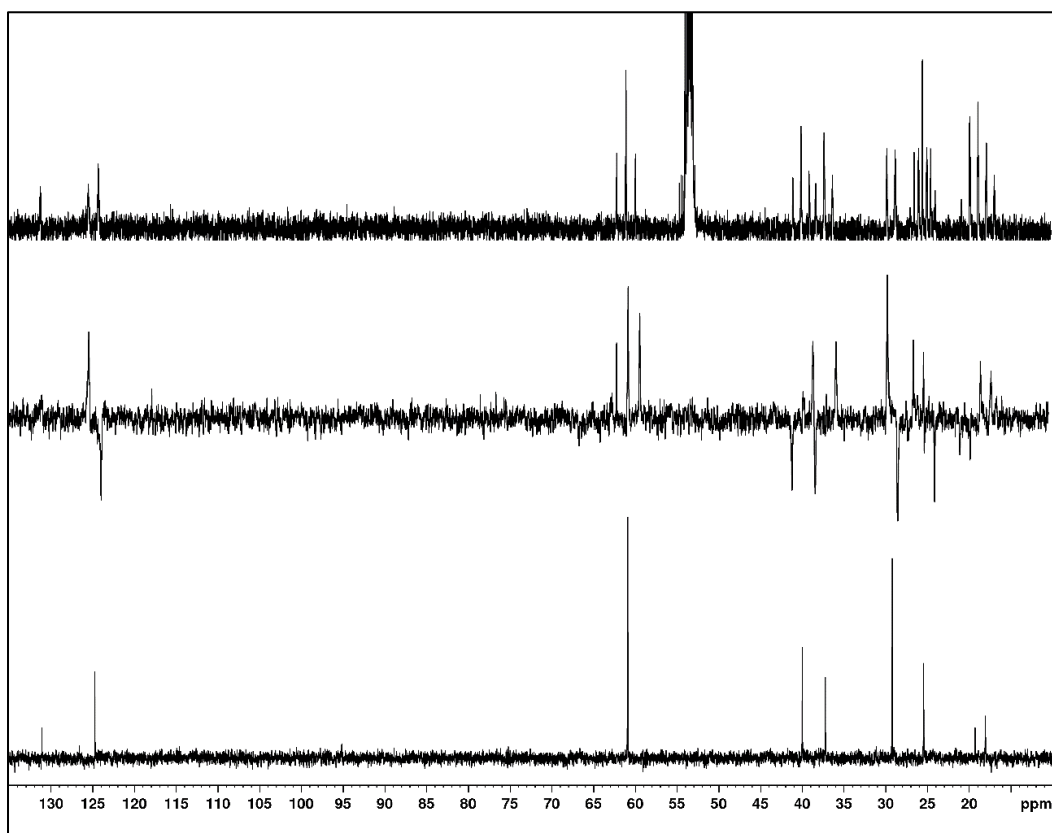
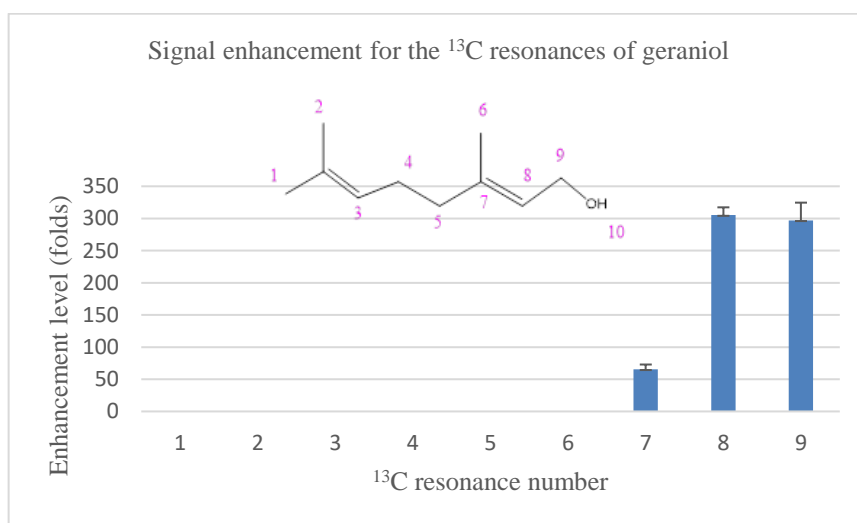
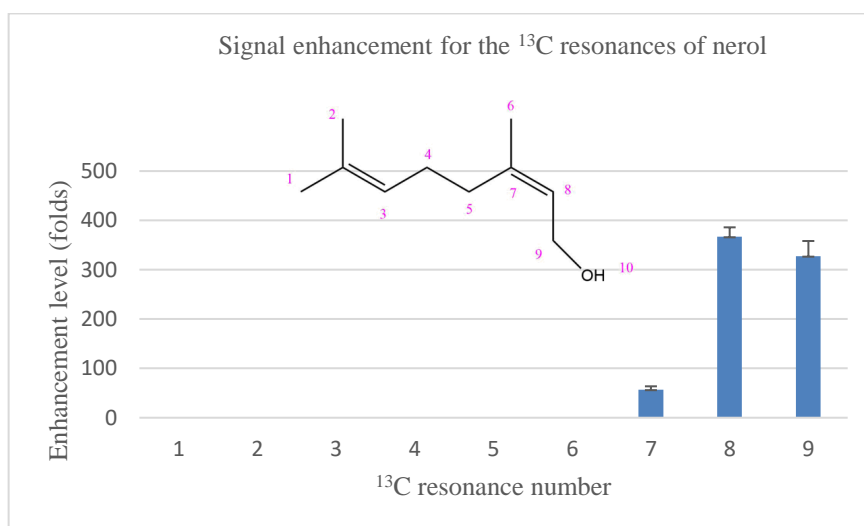
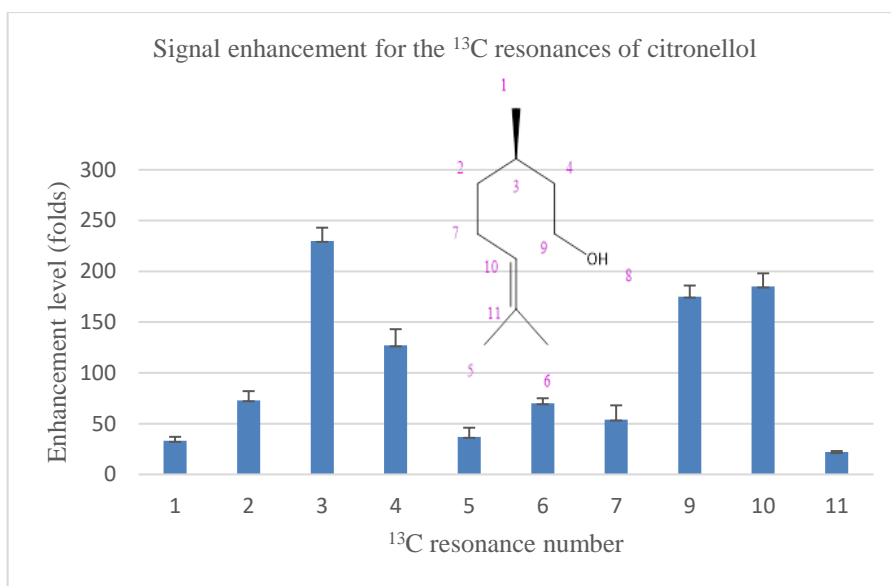


Figure 3.7: Comparison of the average signal enhancement levels for ^{13}C of citronellol, nerol, and geraniol.

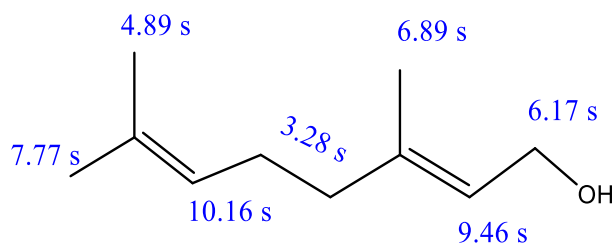


3.3 Effect of T_1 relaxation

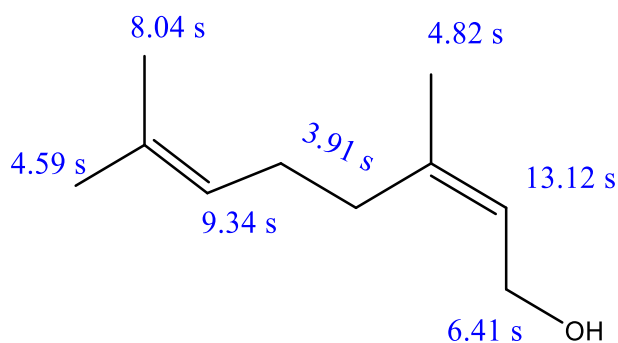
It must be remembered that these measurements take place in the high field NMR magnet of the spectrometer, while the SABRE-RELAY process takes place at low field outside the scanner. Hence there is a time delay between the two activities. This reflects a period of between 3 and 4 seconds. As this process is completed manually, there is an element of variability here.

In NMR, the relaxation time of a signal is measured as a characteristic of the molecule. Such values were determined here using an inversion recovery measurement. These measurements were carried out at 9.4 T. The values that result from analysis of these data are detailed below in Figure 3.8.

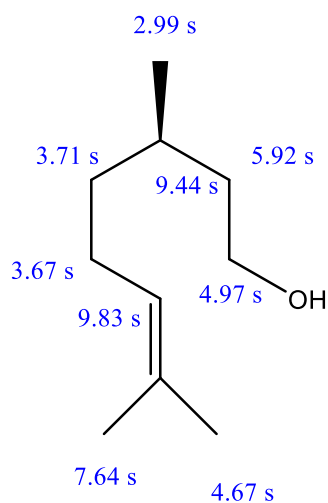
Figure 3.8: T_1 relaxation times, at 9.4 T, for the indicated ^1H NMR groups in citronellol, nerol and geraniol.



Geraniol



Nerol



Citronellol

The value T_1 actually reflects the time taken for 63% of the signal to vanish. Hence for citronellol, the CH_2O resonance should decay by 63% in 4.97 seconds while for geraniol and nerol the corresponding times are 6.17 and 6.41 seconds respectively. Hence if it is assumed it takes 3 seconds for a measurement to be made, and these

values correspond to the relaxation times during the process of transfer it is possible to back calculate the initial enhancement. Thus, if each group were to be enhanced initially by 100-fold, the signal seen at the point of measurement would be 54-fold for the citronellol CH₂O group and 61.5 and 62.6 for the other two samples respectively. This effect clearly needs to be taken into account when comparing their performance under SABRE-RELAY.

The best levels of signal gain seen for these three groups from these data are 432, 446, and 856. Upon reversing this calculation, and measuring the ¹H enhancement after transfer allowing for *T*₁ decay, values of 790, 725 and 1373 are obtained. Hence the raw CH₂O hyperpolarisation level is still best for nerol, even though the best overall detected performance is seen for citronellol. Consequently, as citronellol is more easily seen, it can be concluded that it's OH hyperpolarisation is shared more efficiently across all spins with the result that although any individual signal enhancement level is attenuated, overall, it stills wins out over relaxation.

Indeed, when the whole of the molecule is taken into account, for citronellol the total enhancement value is 2935 after the 3 second transfer time. Hence the real enhancement value before transfer becomes ~5177-fold. In contrast, for geraniol the recorded value is 2746 which becomes ~4916, while for nerol they are 2544 and 4079 respectively.

It becomes clear therefore that all of these agents actually polarise to similar extents and that the differences seen are a result of *T*₁ and the efficiency of sharing within any spin system. This result is somewhat unexpected. with citronellol providing a C-H coupling route to all spins within the molecule. In contrast, this route is stopped at the alkene quaternary carbon centre in both nerol and geraniol. Hence the ¹³C signal enhancements of resonances beyond this point fails. Consequently, the ¹³C signal

gains are focussed into fewer resonances and a much stronger overall signal gain results.

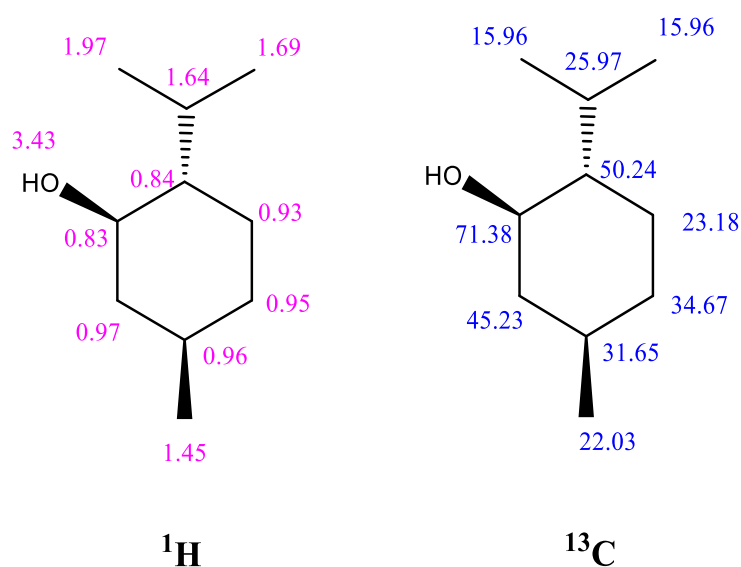
3.4 Increasing the substrate range

In order to further explore these results, the number of alcohols and essential oils components that were polarised by SABRE-RELAY was further increased by examining the substrates menthol, verbenol, and rhodinol.

3.4.1 SABRE-RELAY of Menthol

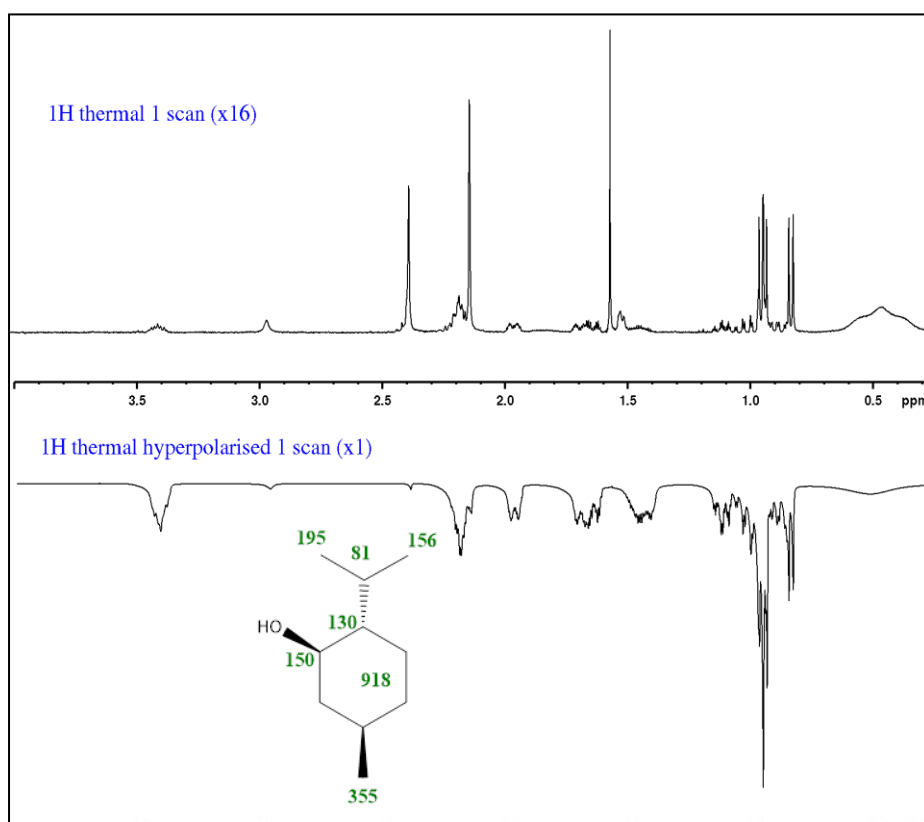
The characterisation data for menthol in dichloromethane- d_2 is detailed in Figure 3.9. These resonances are diagnostic of this compound and the signal at δ 0.83 (H^1) which is adjacent to the OH will be a key marker through which to judge the success of SABRE-RELAY. This is because menthol is an alcohol and when it is hyperpolarised by the SABRE-RELAY technique, hyperpolarisation enters the substrate from this point. Furthermore, C-H couplings exist across the spin system which means that as with citronellol, it was hypothesised that all its ^{13}C resonances will become hyperpolarised.

Figure 3.9: NMR responses of menthol when dissolved in dichloromethane- d_2 at 298 K.



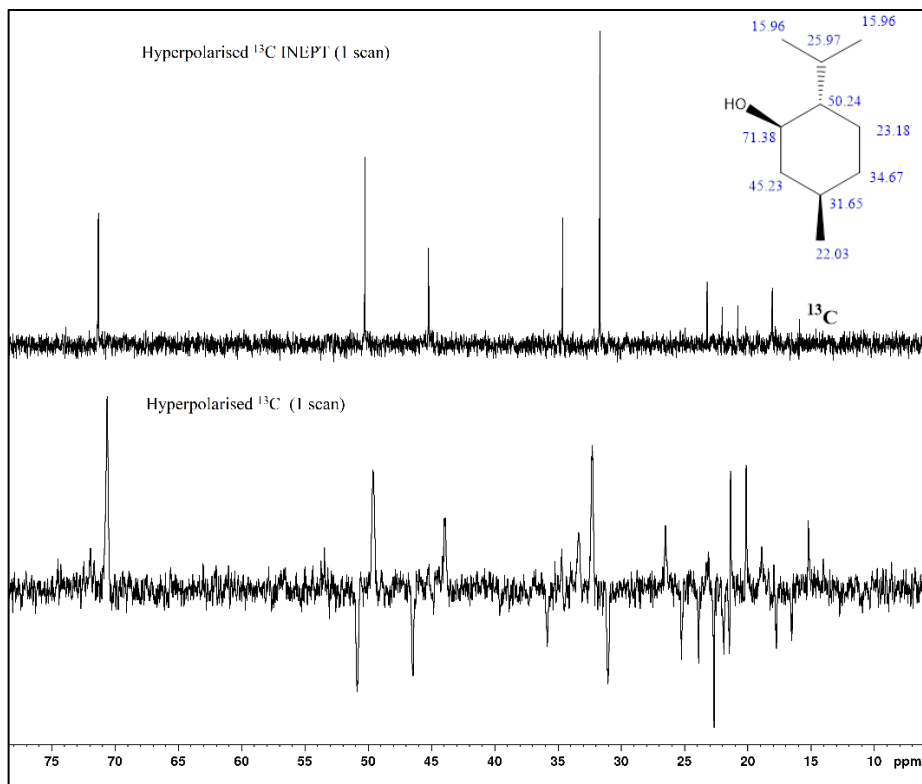
For hyperpolarising menthol with SABRE-RELAY, the optimised conditions were used for citronellol (5mM of **2**, using ammonia as a transfer agent, using 5 equivalents of both the substrate and ammonia, PTF at 65 G). Thus, a SABRE-RELAY sample was prepared under these conditions. Measurements were then undertaken, which showed significant enhancement levels for all the ^1H NMR responses of menthol (Figure 3.10). The ^1H signal enhancement for OCH_2 resonance of menthol was 150-fold, while that of citronellol was 435-fold, which is larger by 97%. However, the total enhancement levels obtained for menthol was 2244-fold which is only 24% lower than that seen with citronellol.

Figure 3.10: Enhancement of menthol ^1H responses with SABRE-RELAY.



Shake and drop measurements were then taken to probe the ^{13}C NMR responses of menthol using INEPT and thermal hyperpolarised pulse programs (Figure 3.11).

Figure 3.11: Single scan hyperpolarised ^{13}C responses of menthol using refocussed INEPT with a cnst2 of 122 Hz, top spectrum, and SABRE-RELAY bottom spectrum.

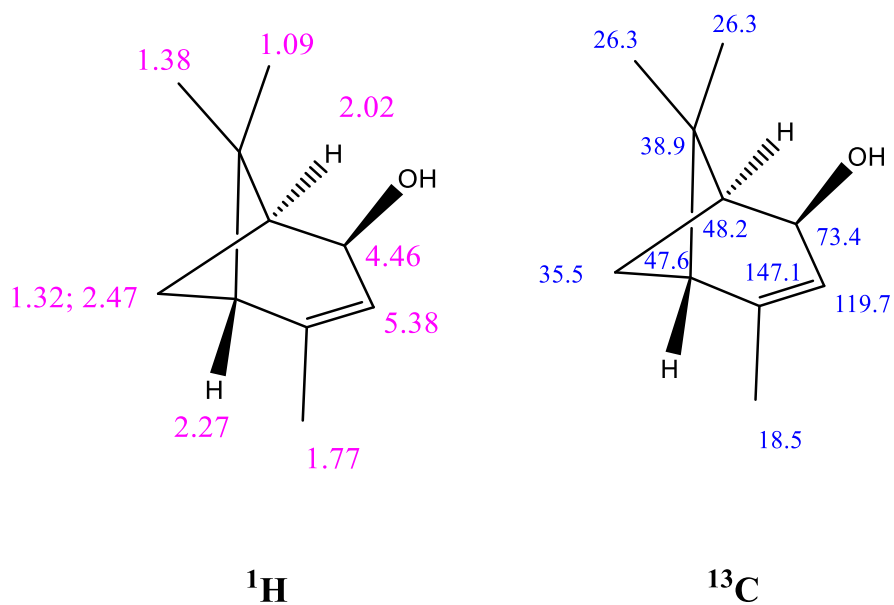


As expected, these data confirm that hyperpolarisation transfer takes place across the whole spin system menthol, and although the raw signal enhancements range from 71 – 16-fold and are therefore less than those seen for citronellol, all of its resonances are visible.

3.4.2 SABRE-RELAY of Verbenol

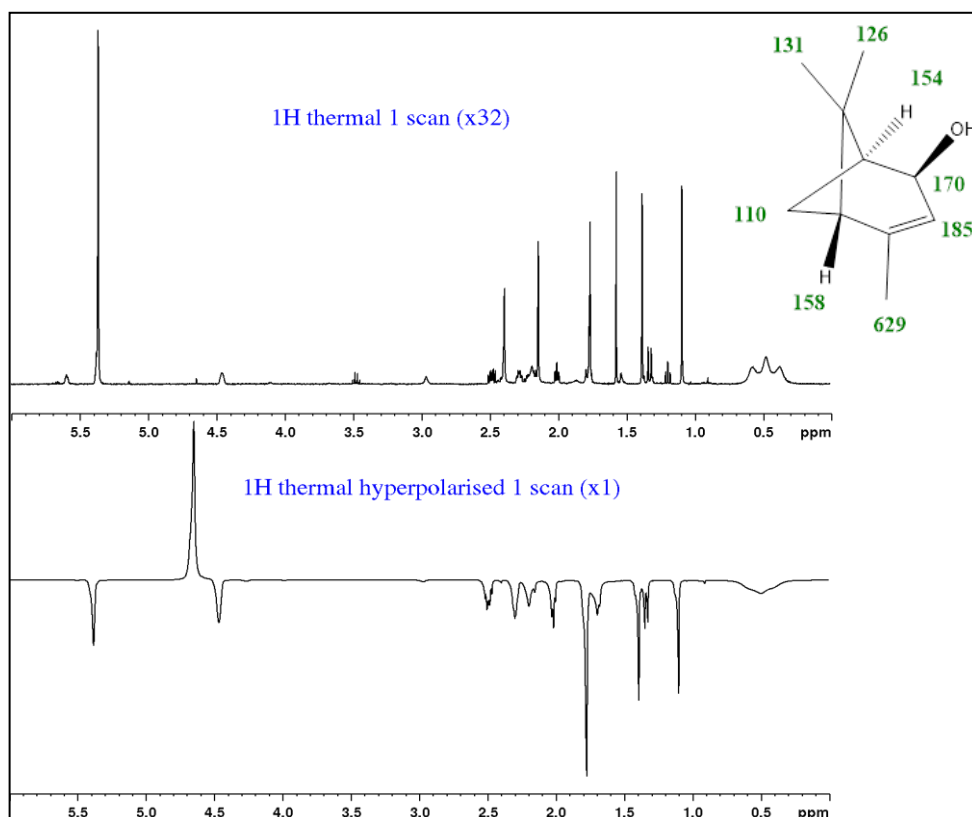
Having established that menthol can be polarised well by SABRE-RELAY, verbenol were subsequently examined. The characterisation data for verbenol in dichloromethane- d_2 is highlighted in Figure 3.12. To hyperpolarise verbenol, the optimised SABRE-RELAY conditions of hyperpolarising citronellol were used again. The aim was again to maximise the signal gain and detect appropriate responses for verbenol.

Figure 3.12: NMR responses of verbenol when dissolved in dichloromethane- d_2 at 298 K.



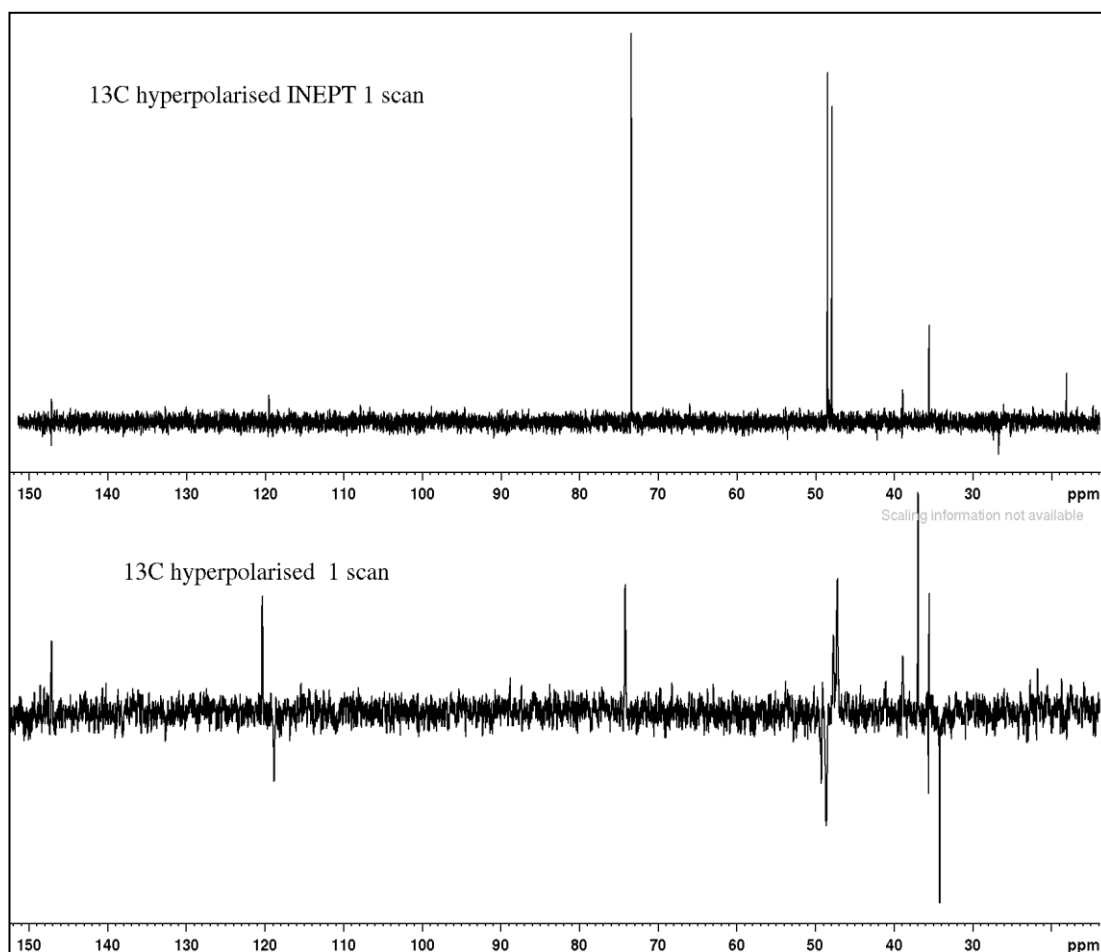
Measurements were then undertaken, which showed high signal enhancement results for verbenol ^1H NMR responses (Figure 3.13). The total enhancement level obtained was 1773-fold and all its ^1H NMR the signals are amplified.

Figure 3.13: ^1H NMR spectra of verbenol with SABRE-RELAY showing enhancement level of ^1H responses.



After all the ^1H resonances were successfully hyperpolarised, shake and drop measurements were then taken to probe the ^{13}C responses of verbenol using multiple pulse programs (Figure 3.14). As expected, all the ^{13}C responses in verbenol were hyperpolarised apart from the two methyl groups at δ 26.3, which are the furthest responses from binding site and exhibit no three bond coupling to a CCH group.

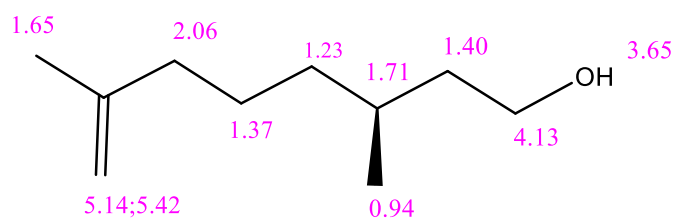
Figure 3.14: Single scan ^{13}C NMR spectra of verbenol with SABRE-RELAY (bottom) and refocused INEPT (top).



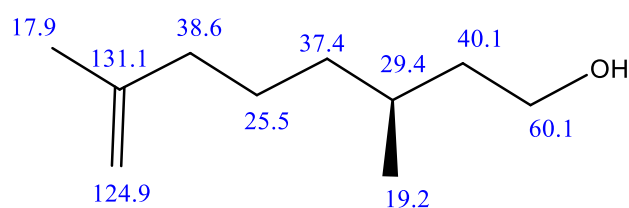
3.4.3 SABRE-RELAY of Rhodinol

Rhodinol is another interesting agent that is widely used in perfumes and cosmetics products due to its rosy scent.¹¹⁸ The structure of rhodinol is very similar to that of citronellol as shown below. The NMR responses of rhodinol when dissolved in dichloromethane- d_2 are illustrated in Figure 3.15 and these again are similar to citronellol. Again, as in the previous SABRE-RELAY measurements, the optimised conditions for citronellol were utilised for these measurements.

Figure 3.15: NMR responses of rhodinol when dissolved in dichloromethane- d_2 at 298 K.



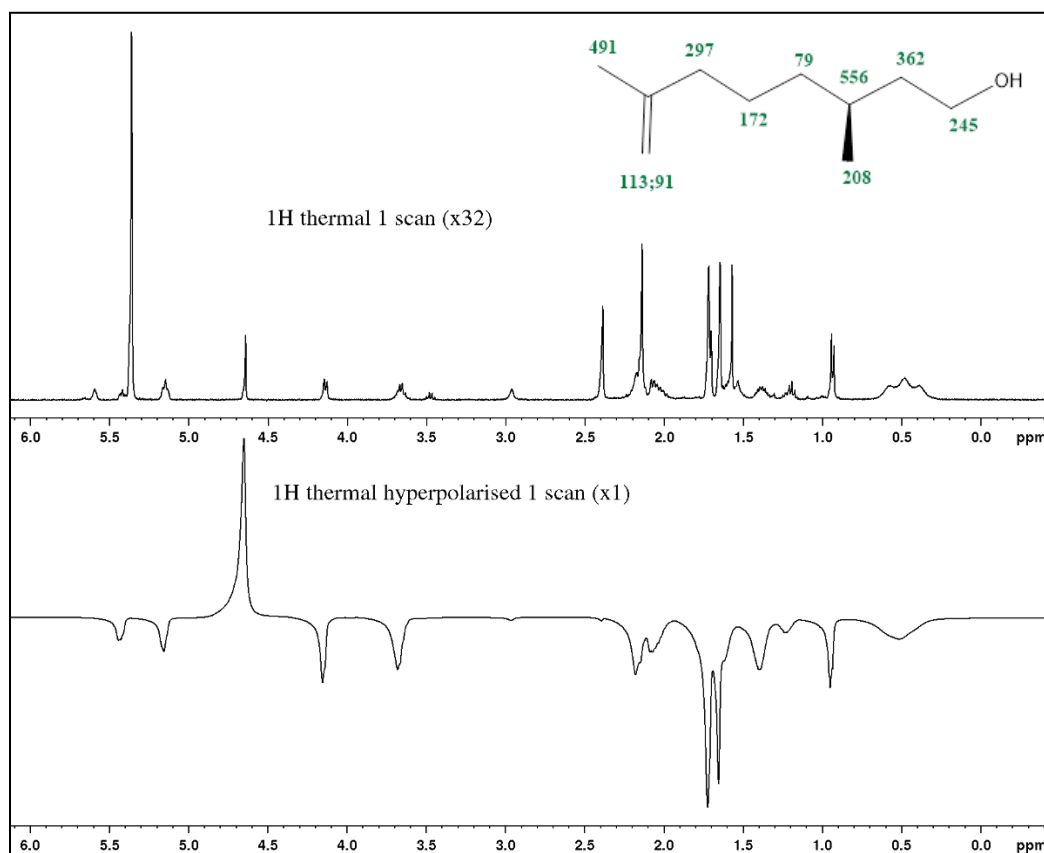
^1H



^{13}C

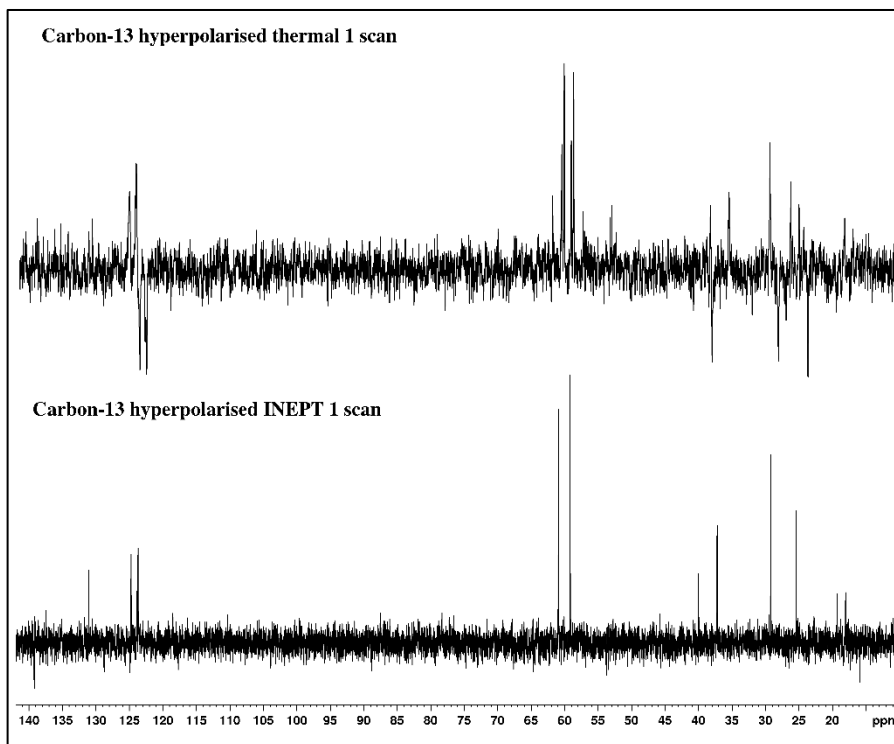
Measurements were then undertaken, which showed significant enhancement levels for all of the ^1H NMR responses of rhodinol (Figure 3.16). The total enhancement level for ^1H responses was 2614-fold, which is 12% lower than that achieved with citronellol.

Figure 3.16: ^1H NMR spectra of rhodinol with SABRE-RELAY showing enhancement level of ^1H responses.



Shake and drop measurements were also undertaken for ^{13}C responses of rhodinol (Figure 3.17). Hyperpolarisation was successfully transferred through the whole spin system of rhodinol.

Figure 3.17: Single scan hyperpolarised ^{13}C responses of rhodinol obtained in 1 second (top) and through refocussed INEPT (bottom).



3.5 Conclusions and Perspective

Interestingly, the polarisation of the plant based natural products (essential oils) citronellol, nerol and geraniol through SABRE RELAY was successfully demonstrated. A strong enhancement for many of the ^1H and ^{13}C signals of these substrates can be observed by NMR. The amine substrates (PEA, PEA- d_4 , ethanolamine, Benzylamine- d_7 , and NH_3) were used to hyperpolarise these materials.

The amine ammonia proved to consistently out-perform the other amines tested. The enhancement levels proved to maximise when the excess of amine is low relative to the target substrate. Furthermore, when water is present as a contaminant in the system a much reduced polarisation level results. Therefore, the data illustrated was from dried samples. There is therefore a need to reduce the rate of OH exchange as this maximises the lifetime of the OH group which in turn maximises the level of polarisation transfer that is possible. By recording the T_1 values of the protons in these agents it was shown that citronellol was the best of the group. It is clear that those resonances with a short T_1 are disproportionately reduced at the point of measurement.

The spin systems of the three agents citronellol, rhodinol and verbenol can be crossed through a network of $^3J_{\text{HH}}$ couplings until the alkene function is reached. This arrangement enables most of the ^1H and ^{13}C nuclei in these molecules to receive polarisation through SABRE Relay. However, for nerol and geraniol this was not the case. Nerol showed weak ^1H NMR signal gains for all its resonances, whilst geraniol showed gains for just the $\text{MeC}=\text{CHCH}_2\text{OH}$ signals. This change is a result of the new coupling network. When there is a larger trans $\text{RC}=\text{CH}$ spin-spin coupling, weak polarisation propagation across the double bond proves to be possible and the whole molecule is enhanced. For geraniol, the *cis* coupling is smaller and consequently polarisation remains locked on the OH side of the alkene. This allows very high signal enhancements to result for the $\text{C}=\text{CHCH}_2\text{OH}$ group.¹¹⁹

In the corresponding ^1H NMR spectra there is considerable overlap of peaks, and it would therefore be impossible to examine a mixture of these materials. In contrast, the ^{13}C signals are distinctive and separate. Hence a simple SABRE RELAY or INEPT measurement could be used to not only rapidly identify one of these materials but also to distinguish them in a mixture. The data for menthol, verbenol, and rhodinol also show that their full ^1H NMR spectrum can be signal enhanced through SABRE. However peak overlap again would be an issue if a mixture was examined. Diagnostic ^{13}C signals can however be readily produced. These measurements therefore confirm the benefit of SABRE as a tool to examine OH containing natural oils.

Chapter 4: Hyperpolarisation of Water with SABRE

4.1 Introduction

Water is indispensable and a source for life in all plants. It works as a solvent in which nutrients are dissolved, and subsequently plants can absorb them. Moreover, it is a key component in the photosynthesis process, through which plants can produce their foods. It works as a carrier for the food and nutrients to the different plant parts. It also acts as a solvent for all biochemical reactions that take place within plants. Water also helps plants to regulate their temperature, and maintain their rigidity and form.¹²⁰⁻¹²² These examples show how significant the role of water is for plant growth and survival. A better understanding of plant-water relations is therefore desirable.

MRI and NMR are two powerful tools that can be used for this purpose, but there are some challenges that limit their efficiency. First, is the absence of contrast between moving and stationary water. Secondly, there is the inherent issue of low sensitivity which has already been discussed.¹²³⁻¹²⁴ One effective approach that can be used to overcome this is by using hyperpolarisation techniques such as DNP⁴⁶ and SABRE, as also discussed earlier.⁵⁸

Water has been hyperpolarized using the DNP technique before.¹²⁵⁻¹²⁷ However, the hyperpolarization of water by the SABRE technique was not reported at the start of this work, due to the fact that SABRE catalysts commonly exhibit very low solubility in this medium. Fortunately, a new SABRE method which is named SABRE-RELAY⁶⁷ has been reported as a new approach to hyperpolarise molecules that fail to readily bind to the iridium centre of the SABRE catalyst but have at least one labile proton, such as water. In this case, SABRE-RELAY starts with the hyperpolarisation of an amine. Subsequently, polarisation is relayed into a specified target substrate through proton exchange, as illustrated in (Figure 1.6).

The aim of this study was to achieve the maximum hyperpolarization of water by SABRE-RELAY whilst seeking to extend its relaxation time in order to enable future plant studies by MRI. Over the last six years, there has been a growing interest in the

hyperpolarisation of water, using the DNP technique.¹²⁵⁻¹³⁰ In fact, it has already been shown that hyperpolarised water can be used as a contrast for perfusion and angiography imaging on animal models.¹²⁸⁻¹³⁰ In this work, the short T_1 value of water $\sim 3.5\text{s}$ ¹³¹, was overcome by the introduction of deuterium and DMSO which extended the T_1 value of the remaining protons to $\sim 30\text{s}$.^{127-128, 132}

The aim of this chapter was to use SABRE-RELAY to hyperpolarise water. The hypothesis to be examined is whether an agent like benzylamine or NH_3 can produce strongly hyperpolarised water signals via proton exchange. The importance of the effect of ^2H labelling under SABRE will be probed in order to extend the relaxation times of the hyperpolarised product in accordance with the methods of DNP.

One complication associated with this work will be the use of dichloromethane as the primary solvent. H_2O has limited solubility in dichloromethane and dissolved water, metastable water clusters and bulk water have been proposed to exist in this medium. The former gives signals at around 1.5 ppm whilst the bulk water signal appears around 4.8 ppm. Hence, it is expected to see a change in resonance position with water composition and this situation could be complicated by exchange between the two environments and the fact of using hyperpolarisation which acts to amplify any response. Studies in CCl_4 , C_6D_6 and CDCl_3 have been described.¹³³ It might also be reasonable to expect the relaxation times of these environments to also differ, but this situation will be complicated by any exchange weighted averaging that takes place if protons move between the different water pools.

4.2 Results and discussion

4.2.1 Control NMR Spectra

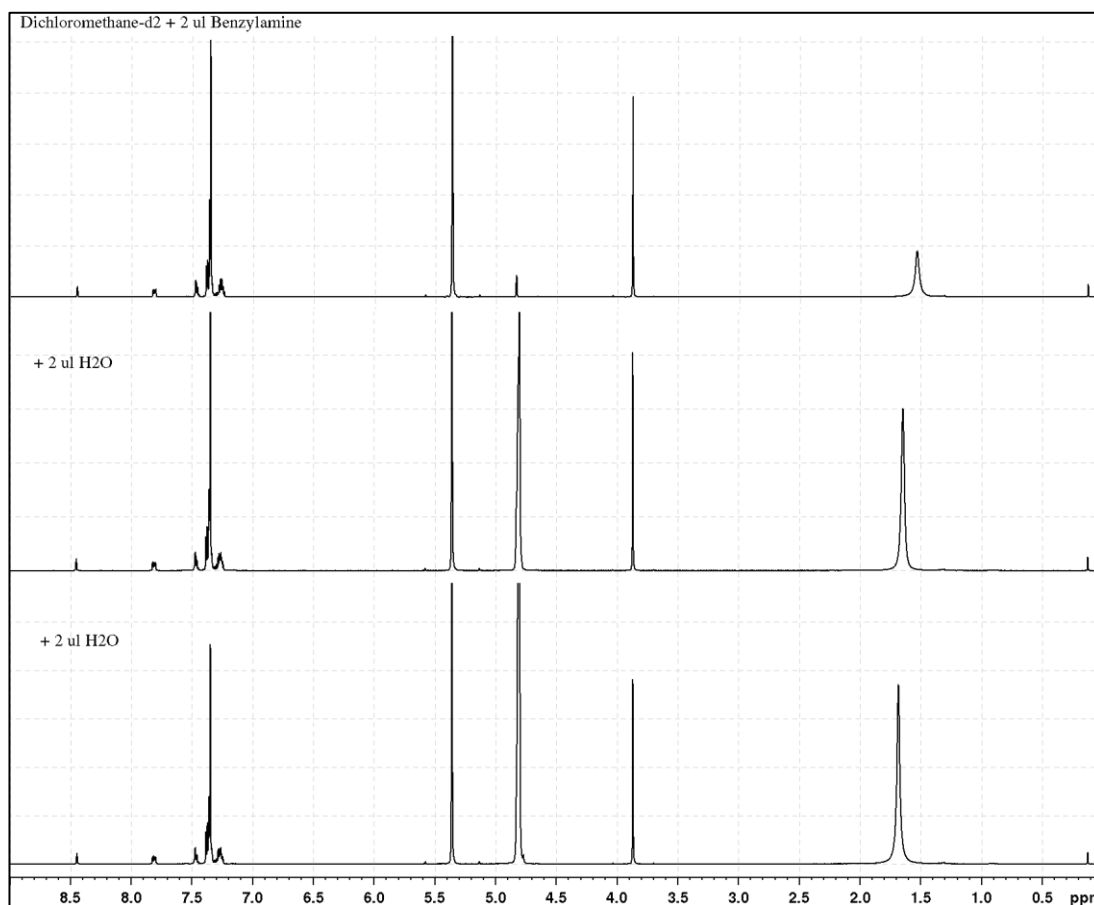
In order to study the effect of adding D_2O plays on the SABRE hyperpolarisation of BnNH_2 a number of control NMR spectra were first collected to probe the various water pools that have been suggested to exist in such solvents. These measurements started out by taking a fresh sample of dichloromethane- d_2 , which yields a 1:1:1 triplet at δ 5.36 for residual CHDCl_2 , and adding 2 μl of H_2O to it. A signal at δ 1.59 is

immediately apparent for the added H₂O that is indicative of what has been referred to as dissolved water.

In contrast, when a similar sample is prepared but BnNH₂ added, instead of H₂O, signals are readily apparent at δ 4.83, 3.84 and 1.54 alongside a broad multiplet at 7.36. The CH₂ resonance of BnNH₂ appears at 3.84 ppm and has intensity of 2 relative to the 4.83 and 1.54 signals which have strength 0.4 and 4.8 respectively. It therefore appears that H₂O is also present and exchange effects complicate the spectrum with the predicted NH₂ signal intensity being mainly focused at δ 1.54 where the dissolved water peak sits. It is concluded from this data that there is an approximate 2.8 fold excess of H₂O present in this sample relative to BnNH₂ due to water contamination.

The addition of a further 2 μ l of H₂O to this sample changed these integrals values further to 2 : 10.58 : 10.58 thereby confirming the addition of a net 9.5-fold excess of H₂O. It is clearly impossible for there to be more than 2 NH protons and hence these nominal NH and OH peak positions actually reflect exchange average positions, both of which now have high levels of OH contribution. Consistent with this, they move towards each other, from δ 4.83 to δ 4.80 and from δ 1.54 to δ 1.64. The addition of a further 2 μ l of H₂O to this sample changes these peaks again (Figure 4.1), with the resulting NMR signals now appearing at δ 4.80 and δ 1.68 and having relative areas of 19.3 and 13.4 relative to 2 for the CH₂ signal of BnNH₂ respectively. Therefore, the impact of exchange between dissolved water to bulk water and water pooling can both be seen.

Figure 4.1: Effect of the addition of H₂O on the appearance of the ¹H NMR spectra of three different samples of benzylamine in dichloromethane-*d*₂.



This is reflective in the fact that the signals no longer exhibit the same exchange weighted intensity they did in the first measurement. The addition of a further 10 μ l of H₂O changes their position again, to δ 4.82 and δ 1.69, with intensities now 126 and 14 respectively. Hence, it can be concluded that there are effectively two peak positions for protons in exchange with water in this sample which depend on loading, one at around δ ~4.80 and the other at δ ~1.6. Under these conditions it is not believed that a pure signal for the NH₂ protons of benzylamine is observed. Instead, an exchange weighted signal is clearly observed.

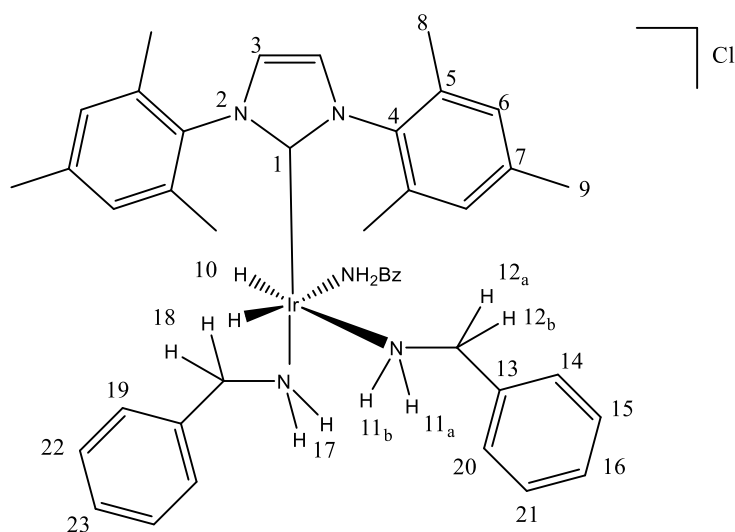
4.2.2 Characterisation of [Ir(H)₂(IMes)(BnNH₂)₃]Cl

In order to assess the hyperpolarisation of H₂O by BnNH₂ a sample of Ir(IMes)(COD)Cl was first prepared that contained a 5 mM loading of the iridium

complex. In addition, a 5-fold excess of BnNH_2 was added relative to iridium. This process was completed in dichloromethane- d_2 as the solvent. The solution was then activated with *para*hydrogen over 5 minutes at 298 K and a ^1H NMR spectrum recorded.

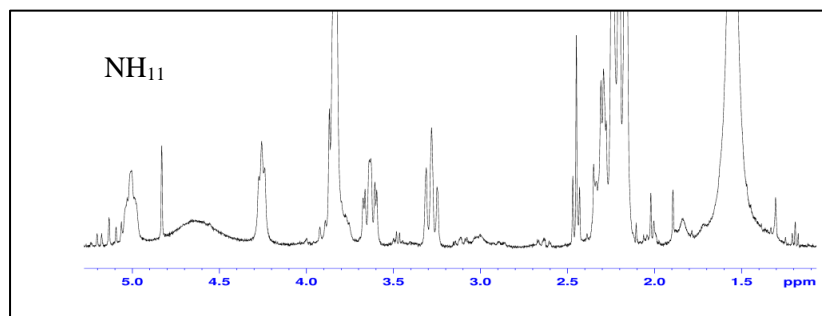
This NMR spectrum contained key ^1H NMR resonances at $\delta -23.95$ (singlet) for the hydride signal of the SABRE catalyst $[\text{Ir}(\text{H})_2(\text{IMes})(\text{BnNH}_2)_3]\text{Cl}$ and hence, it can be confirmed that the desired complex has formed. Its structure is shown below (Figure 4.2) and the number of expected resonances for the two amine ligands depend on whether they are *cis* or *trans* to hydride. In the case of the *trans* ligand, the NH and CH protons are inequivalent and will therefore lead to two signals.

Figure 4.2: 3-dimensional representation of the structure of 2-BnNH_2 , with numbering according to Table 4.1.



The resulting ^1H NMR spectrum in the region between 1 and 5 ppm is shown in Figure 4.3 and is therefore highly complex as expected.

Figure 4.3: ^1H NMR spectrum of $[\text{Ir}(\text{H})_2(\text{IMes})(\text{BnNH}_2)_3]\text{Cl}$ complex alongside resonance assignments (below).



The signals are fully attributed in Table 4.1. The NH signals and the corresponding ^{15}N - ^1H couplings were used to locate the corresponding ^{15}N resonances via a 2D ^1H - ^{15}N HMQC measurement. Furthermore, as a consequence of this connection it was possible to attribute the signals giving rise to the NH groups on the BnNH_2 ligand. Informed by this information, and the resulting COSY data, the remaining ^1H resonances in these ligands and their coupling patterns were assigned. These data confirmed that two inequivalent CH resonances were observed for the protons of the CH_2 group of the equatorial BnNH_2 ligand, which share a common 12 Hz coupling and smaller, ca 5 Hz, couplings to the two NH protons respectively (Figure 4.3).

In contrast, the ligand $\text{NH}_2\text{-CH}_2\text{-Ph}$, which is *cis* to hydride, undergoes free rotation and this allows the corresponding resonances for both the NH and CH protons to become equivalent. Consequently, there are now just one CH and one NH signal even though there are two protons in each group.

Once these assignments had been defined a sample of $\text{NH}_2\text{-CH}_2\text{-Ph}$ and $\text{Ir}(\text{COD})(\text{IMes})(\text{Cl})$ was examined under SABRE. A resonance at δ 4.64 appeared as a broad response in the resulting spectrum that showed a 266-fold enhancement (Figure 4.4). Additional hyperpolarised signals were seen at δ 5.00 for $\text{NH}_{11\text{a}}$, δ 2.30 for $\text{NH}_{11\text{b}}$, δ 3.65 for $\text{CH}_{12\text{a}}$ and δ 3.30 for $\text{CH}_{12\text{b}}$ of the $\text{NH}_2\text{-CH}_2\text{-Ph}$ ligand that lies *trans* to hydride. The corresponding signals for the ligand lying *cis* to hydride proved to be weak, are not labelled and showed little in any enhancement. This is consistent with their location *cis* to the hydride, which should, due to symmetry considerations, not polarise them.

Table 4.1: Characterization data for [Ir(H)₂(IMes)(BnNH₂)₃]Cl, 2-BnNH₂.

Resonance number	¹ H (ppm)	¹³ C (ppm)	¹⁵ N (ppm)
1	--	153.8	--
2	--	--	192.83
3	6.80	121.73	--
4	--	138.11	--
5	--	135.25	--
6	6.90	129.29	--
7	--	138.64	--
8	2.17	18.30	--
9	2.21	20.78	--
10	-23.95	--	--
11	5.00 (br, dt, J _{HH} = 5 and 11 Hz, 2H) *J _{15NH} = 68 Hz 2.30 (br, t, J _{HH} = 11 Hz, 2H) *J _{15NH} = 68 Hz	--	-6.4
12	3.65 (dt, J _{HH} = 5 and 15 Hz, 2 H), 3.30 (ddd, J _{HH} = 3, 12 and 15 Hz, 2H)	53.14	--
13	--	141.8	--
14	7.35 (d, J _{HH} = 5 Hz)	128.33	--
15	7.25 (t, J _{HH} = 5 Hz)	126.88	--
16	~7.28 - overlap	-	--
17	4.25 (t, J _{HH} = 7 Hz, 2H) * J _{15NH} = 69 Hz	--	-13.4
18	3.85 (t, J _{HH} = 7 Hz, 2H)	57.26	--
19	--	--	--
20	7.30	128.35	--
21, 22, 23	~7.28 - overlap	--	--

*¹⁵N coupling determined via 2D NMR spectrum on unlabelled sample

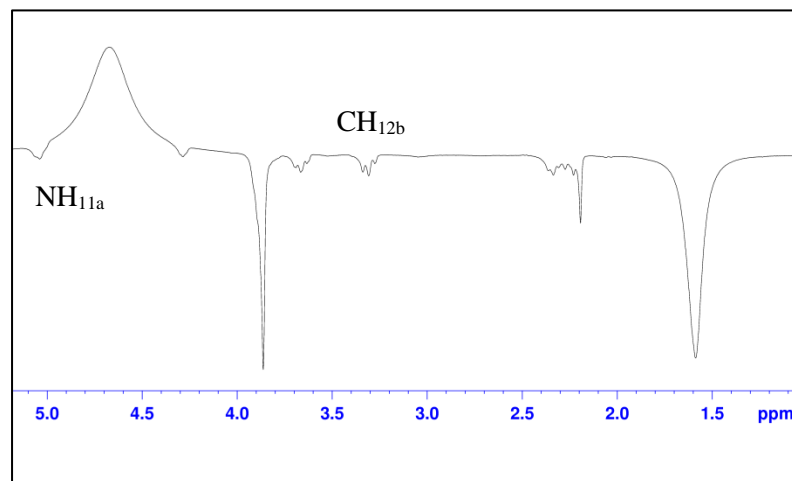
A signal for hyperpolarised, dissolved water, is also detected at $\delta \sim 1.6$ that is likely to be undergoing exchange with the protons of the NH group of free BnNH₂. The signal gain for this signal was estimated to be 32-fold.

It can be concluded from these data that it is possible to hyperpolarise the protons of H₂O through exchange and SABRE-RELAY.

1 μ l of D₂O was then added to this sample and it re-examined. This led to a change in the NMR spectrum as the corresponding resonances that were at δ 5.00 and δ 2.30 proceeded to broaden and move 22 Hz to high field. This is indicative of chemical exchange and the limited replacement of NH with ND. In contrast, the CH protons peaks at δ 3.65 and δ 3.30 retained the same area, but also became broader. In this case, it is expected to lose the NH coupling and ultimately retain the mutual CH coupling due to their diastereotopic arrangement. The corresponding SABRE RELAY

measurement yielded broadly similar signal gains for the bound BnNH₂ signals and the bulk water response at $\delta \sim 4.64$, however, the dissolved water signal at $\delta \sim 1.64$ proved to be approximately 4 times larger, moving now to $\delta \sim 1.64$. It can therefore be concluded that there is an effect of D₂O concentration on these signals.

Figure 4.4: Hyperpolarised ¹H NMR signals seen when a sample of BnNH₂ and Ir(COD)(IMes)(Cl) are examined under SABRE conditions.



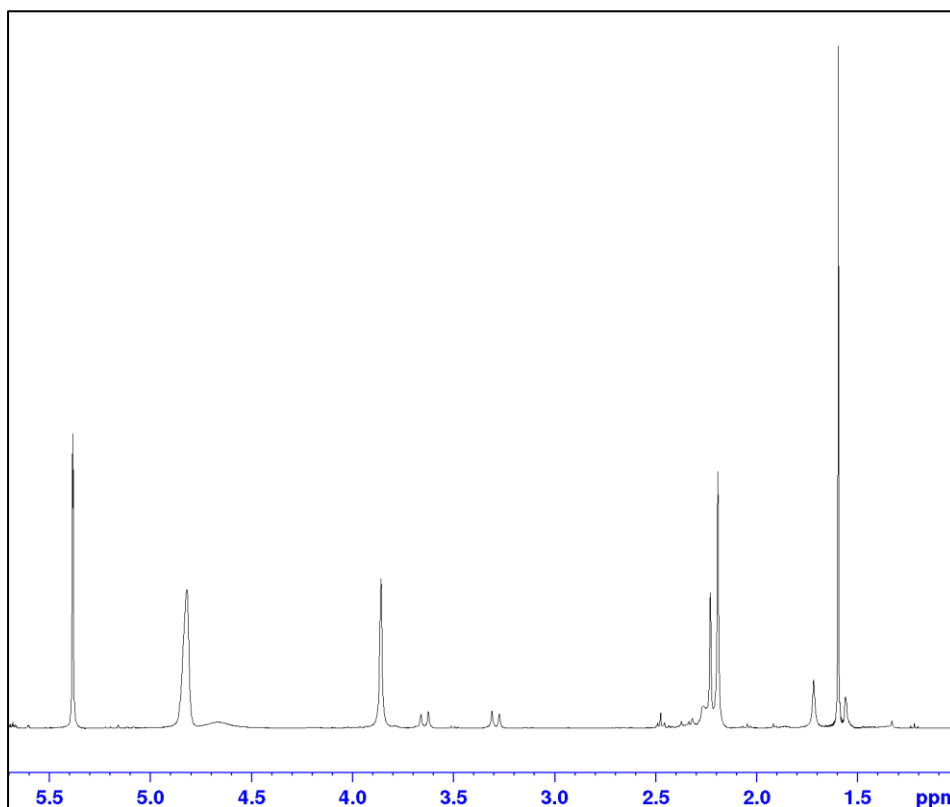
4.2.3 Effect of added D₂O on the appearance of the SABRE-RELAY polarisation derived from BnNH₂.

In order to explore this, a further 20 μ l of D₂O was added to this sample. Now the pair of NH resonances seen for the equatorial ligand of [Ir(H)₂(IMes)(BnNH₂)₃]Cl disappear. Furthermore, the very broad signal at δ 4.64 is now clearly visible. The axial NH ligand resonances also disappear. Consequently, the signals for the CH₂ groups of the ligand NH₂-CH₂-Ph also change in appearance as a consequence of the replacement of the NH protons by ND which results in a 6.4 fold reduction in any couplings they share. This means any ND couplings are hidden, and the signals at δ 3.65 for CH_{12a} and δ 3.30 for CH_{12b} now appear as simple 14.8 Hz doublets (see Figure 4.5).

This effect arises because the NH protons in BnNH₂ undergo H/D exchange with the solvent and both BnNH₂D and BnND₂ will form. These changes should therefore be compounded by a growth in the HOD and H₂O signal. Examination of these NMR spectra reveal that the signal which shows this growth lies at δ 4.80 and has a chemical

shift that is dependent on the amount of D₂O added. Therefore, an exchange weighted average for the chemical shift of the residual NH/OH signal is being seen. This is consistent with the early deductions.

Figure 4.5: The signals at δ 3.65 for CH_{12a} and δ 3.30 for CH_{12b} due to [Ir(H)₂(IMes)(BnNH₂)₃]Cl simplify into doublets after replacement of the NH proton by ND.

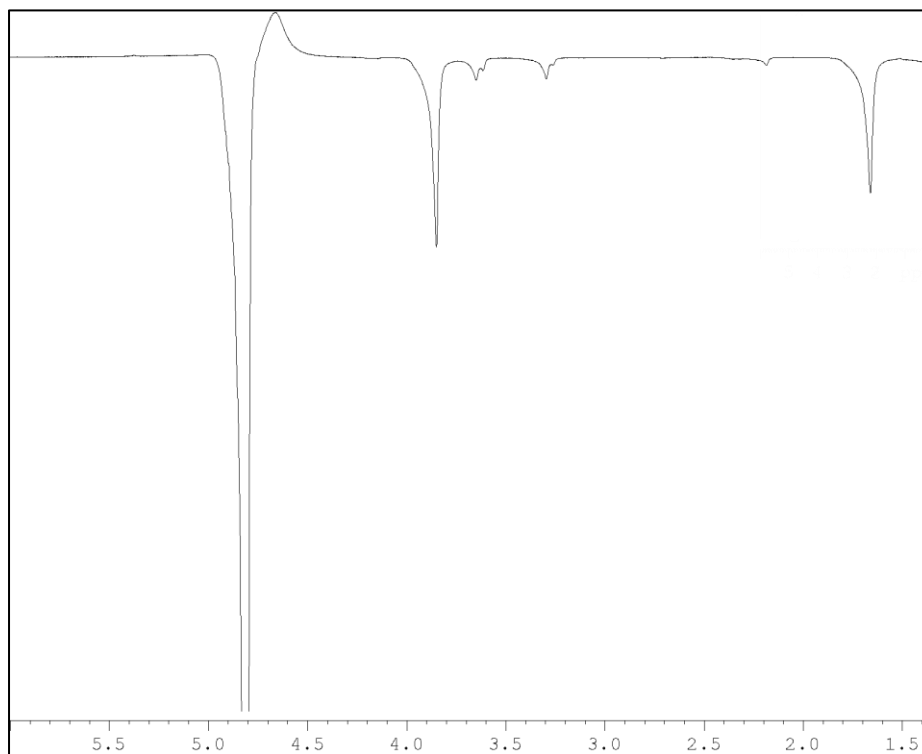


When SABRE is undertaken on the new sample, the signals for the broad NH resonance at δ 4.64 and a signal at δ 4.80 are enhanced. This measurement was made by examining an NMR sample with *para*-H₂ after shaking the NMR tube in a 60 G field for 10 seconds before completing a ¹H measurement. The signals for the bound CH₂ group protons were enhanced by a factor of 8. The signal with position very close to that of bulk water shows a signal gain of 66-fold per proton. This signal for dissolved water at δ 1.66 was enhanced by 31-fold (Figure 4.6).

It is possible to assess the effect of ²H labelling through a *T*₁ assessment. This process involves exciting the enhanced signal at δ 4.80 through a series of low tip angle measurements which are separated in time by a variable delay. The resulting signal will consequently reduce according to the low tip angle value and the time delay which

encodes relaxation. For this sample with 20 μl of D_2O , a T_1 value of 17.6 seconds was obtained for the bulk water peak at δ 4.80 peak while the dissolved water peak at δ 1.66 had a T_1 value of 22.2 seconds.

Figure 4.6: ^1H NMR signals at δ 4.80, 4.64 and δ 1.66 which correspond to the water and NH resonances that are hyperpolarised when a solution of $[\text{Ir}(\text{H})_2(\text{IMes})(\text{BnNH}_2)_3]\text{Cl}$ containing a 265-fold excess of D_2O and a 5-fold excess of BnNH_2 is examined under SABRE.



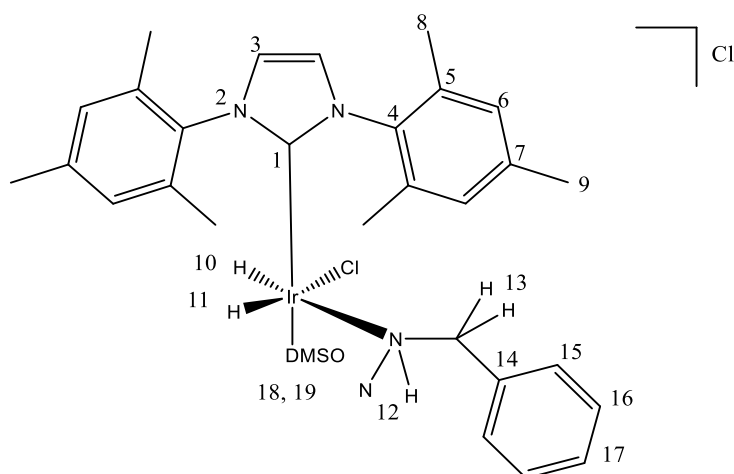
A further 0.7 μl of H_2O was then added to this sample. The result of this process was a small increase in the size of the δ 4.80 signal alongside further movement of the broad δ 4.64 peak to δ 4.66. Under SABRE, the signals at δ 4.80 and 1.66 again become enhanced but now by values of 234 and 42-fold respectively. The corresponding T_1 value for the response at δ 4.80 was now 16.38 seconds while that for the δ 1.66 peak was 20.86 seconds. Both have therefore been reduced by the addition of H_2O which means protons act to reduce the T_1 of water. It should be clear from these data that the H_2O signal also shows an enhancement value that is dependent on the amount of both the ^2H and ^1H labels present in the sample and that this effect needs studying in more detail (see later). Importantly, there is a visible decrease in signal lifetime on the addition of more H_2O which will be avoided.

4.2.4 Utilisation of DMSO as a co-ligand with benzylamine for the hyperpolarisation of H₂O

In order to evaluate and optimise this process, a further catalyst was examined. This was formed by adding DMSO to [Ir(H)₂(IMes)(BnNH₂)₃]Cl. This process results in the formation of [Ir(H)₂(IMes)(BnNH₂)₂(DMSO)]Cl which was characterised by NMR spectroscopy. The reason for adding DMSO to the solvent was to increase the solubility of water and potentially its polarisation level.

The addition of 3 μ l of *d*₆-DMSO to [Ir(H)₂(IMes)(BnNH₂)₃]Cl proved to result in an immediate change in the hydride region of the resulting ¹H NMR spectrum. It now yields two sets of coupled hydride signals as δ -23.22 and -23.86 that appear as doublets of 7.48 Hz. They are accompanied by single peaks at δ -23.18 and -23.82 that are due to the HD forms of this product which result from H-D exchange. The HD coupling is not visible in these spectra as the hydride signals relax relatively quickly, which when coupled with their dynamic behaviour leads to line broadening that prevents detection of the expected 1 Hz ²J_{HD} coupling. These data suggest that [Ir(H)₂(IMes)(BnNH₂)(DMSO)]Cl forms as expected. The resulting NH resonance for its BnNH₂ ligand that lies *trans* to hydride appear at δ 2.28 and 2.16. Full characterisation data is presented in Table 4.2.

Table 4.2: Characterization of $[\text{Ir}(\text{H})_2(\text{IMes})(\text{BnNH}_2)_2(\text{DMSO})]\text{Cl}$ complex.



Resonance number	^1H (ppm)	^{13}C (ppm)	^{15}N (ppm)
1		161.25	--
2			192.83
3	6.94	122.02	--
4		137.75	--
5		136.0, 135.82	--
6	6.93, 6.97	128.77	--
7		137.76	--
8	2.17	17.96	--
9	2.26	20.69	--
10	-23.22, d $J_{\text{HH}} = 8.5$ Hz	--	--
11	-23.86, d $J_{\text{HH}} = 8.5$ Hz	--	-6.4
12	2.28, 2.16		--
13	3.77, 3.30	51.9	--
14			--
15			--
16			--
17			-13.4
18	3.11	46.20	--
19	3.17	58.38	--

4.2.4.1 SABRE Relay using $\text{Ir}(\text{IMes})(\text{COD})\text{Cl}$, BnNH_2 , DMSO and H_2O .

A sample containing $\text{Ir}(\text{IMes})(\text{COD})\text{Cl}$, BnNH_2 , DMSO and H_2O was examined under SABRE and several effects were immediately apparent. These are reflected in a drop in the OH signal gain at δ 4.80. However, signals for the CH_2 group of $\text{BnNH}_2/\text{BnNHD}/\text{BnND}_2$ now appear with an improved signal enhancement level of 12.2-fold, while the phenyl group of this amine exhibits a total intensity gain of 9.5-fold. In addition to these signals, there are new signals at δ 3.12 that are reflective of

free DMSO and at 6.94 due to the imidazole ring in $[\text{Ir}(\text{H})_2(\text{IMes})(\text{BnNH}_2)_2(\text{DMSO})]\text{Cl}$ that are enhanced.

In order to improve on the earlier results, a sample of BnNH_2 (5-fold excess relative to iridium) with $\text{Ir}(\text{IMes})(\text{COD})\text{Cl}$ and d_6 -DMSO (14-fold excess relative to iridium) was prepared that contained a 5 mM loading of the initial iridium complex. This process was also completed in dichloromethane- d_2 as a solvent. The solution was activated with *para*- H_2 over 5 minutes at 298 K and a ^1H NMR spectrum recorded. This contained key ^1H NMR resonances at δ -23.22 and -23.86 (both doublets of 8.5 Hz) for the hydride signals of the SABRE catalyst $\text{Ir}(\text{H})_2(\text{IMes})(\text{BnNH}_2)(\text{DMSO})\text{Cl}$ alongside δ 3.17 and 3.11 signals for the inequivalent Me resonances of the bound DMSO ligand, and NH_2 proton resonances for an equatorially bound BnNH_2 ligand at δ 2.28 and 2.16 alongside a second pair of doublets at δ 3.77 and 3.30 ($J_{\text{HH}} = 14.25$ Hz) for the CH_2 group protons (Table 4.2).

A related NMR sample containing 10 μl of D_2O and d_6 -DMSO was then examined with *para*- H_2 . This involved shaking the NMR tube in a 60 G field for 10 seconds before completing a ^1H measurement. The corresponding signals for the CH_2 resonance of free BnNH_2 proved to be ~60-fold enhanced, while those of the bound ligand were over 200-fold enhanced. Surprisingly, now strong signals for bound DMSO at δ 3.17 and 3.11 also appeared in these NMR spectra despite the fact that d_6 -DMSO had been used. The corresponding OH signal at δ 1.79 for dissolved water also proved to be strongly enhanced. This suggests that DMSO can itself undergo rapid exchange with the SABRE catalyst and thereby enhance the corresponding proton signals.

A signal with a position very close to that of the free amine was visible at δ 4.81 for bulk water which showed a signal gain of 118-fold per proton.

A further result of this process is that PHIP enhanced hydride ligand signals are seen for $[\text{Ir}(\text{H})_2(d_6\text{-DMSO})(\text{IMes})(\text{BnNH}_2)_2]\text{Cl}$ at δ -23.22 and -23.86 which confirm the J_{HH} coupling is negative.

When the results for H_2O enhancement of $[\text{Ir}(\text{H})_2(\text{IMes})(\text{BnNH}_2)_3]\text{Cl}$ and for $[\text{Ir}(\text{H})_2(d_6\text{-DMSO})(\text{IMes})(\text{BnNH}_2)_2]\text{Cl}$ with 20 μl of D_2O are compared, it is noted that

the signal enhancement for bulk H₂O is 340-fold, which is 8% higher than that of the sample with *d*₆-DMSO. However, the dissolved H₂O signal enhancement for the sample with *d*₆-DMSO was 64-fold which is two times larger than that without *d*₆-DMSO. This suggests that the presence of DMSO changes both the exchange and *T*₁ characteristics of bulk and dissolved water.

When the results for H₂O enhancement for [Ir(H)₂(IMes)(BnNH₂)₃]Cl and for [Ir(H)₂(*d*₆-DMSO)(IMes)(BnNH₂)₂]Cl with 20 μl of D₂O are compared, it is noted that the signal enhancement for bulk H₂O is 340-fold, which is 8% higher than that of the sample with *d*₆-DMSO.

4.2.5 Effect of D₂O on the level of H₂O signal gain and *T*₁

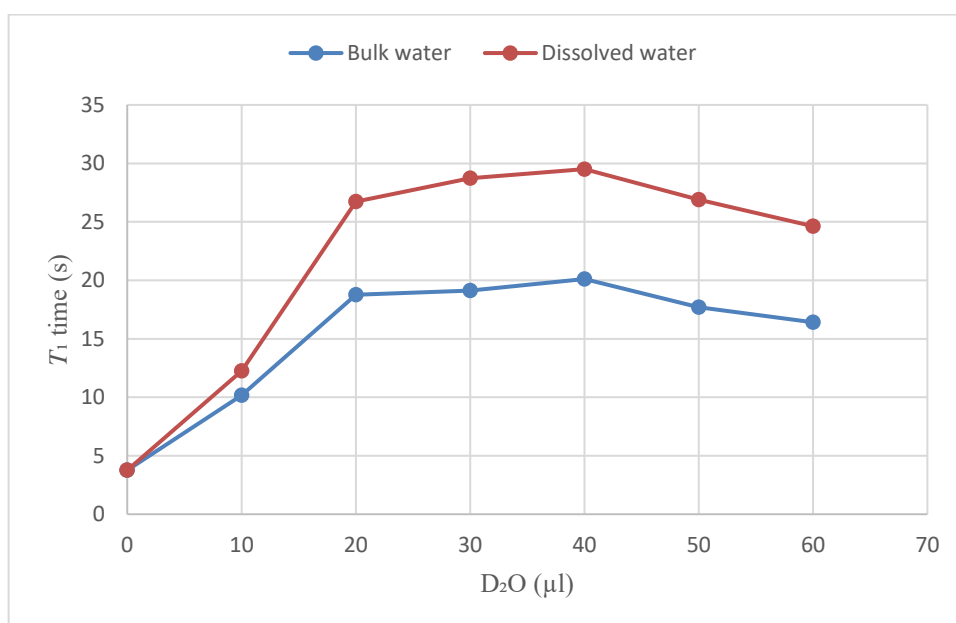
Given that DNP has demonstrated that a mixture of H₂O and D₂O has an extended relaxation time, the effect of D₂O on the H₂O polarisation level was explored. This process will not be straightforward as it is expected to see bulk and dissolved water signals for the two different proton pools and the *T*₁ values are likely to be influenced by chemical exchange. It is after all chemical exchange that leads to SABRE-RELAY.

In order to assess effect of adding D₂O on the relaxation time, a series of 0.6 ml samples were prepared, with the same amount of reagents, but variable amounts of D₂O (10, 20, 30, 40, 50, and 60 μl) for the benzylamine system. The corresponding *T*₁ results are shown in (Figure 4.5). They reveal that when no D₂O is present, just H₂O (1 μl) a *T*₁ value at 400 MHz for the 1.66 ppm signal is 3.76 s. Adding 1 μl of D₂O increases this to 5.27 s. Hence, an increase in relaxation time can be observed with the addition of D₂O. This trend continues as the level of D₂O is increased by 10 μl to 12.25 s but a bulk water signal can now be seen and this has a *T*₁ value of 10.18 s. Increasing the level of D₂O further to 20 μl results in a further increase to 15.69 and 12.7 s respectively. When the corresponding 20 μl or D₂O measurement is repeated without the addition of the initial 1 μl of H₂O, the corresponding values are 21.09 and 16.93 s respectively. Hence it is clear the adding D₂O under SABRE-RELAY increases the signal lifetime for H₂O.

A similar set of measurements were then made in the presence of 3 μl d_6 -DMSO. Under these conditions, there was a further increase in T_1 such that the dissolved water signal reached a maximum value of 29.51 s as detailed in Figure 4.7. The bulk water signal followed a similar trend, maximising with a T_1 value of 20.11 s for the same 40 μl of D_2O . Comparison of the related data at a 20 μl revealed both the bulk and dissolved H_2O signals T_1 values increase with d_6 -DMSO (11% and 21% respectively).

Hence, it is concluded from these results that it is possible to prepare a hyperpolarised H_2O signal through SABRE-RELAY with a T_1 value of ~ 30 s.

Figure 4.7: Effect of D_2O amount on the T_1 relaxation time of the water response under SABRE.



4.2.6 SABRE Relay using $\text{IrCl}(\text{COD})(\text{IMes})$, NH_3 and H_2O .

Earlier work in this thesis demonstrated that the SABRE polarisation of NH_3 was better than that of BnNH_2 . In order to assess the hyperpolarisation of H_2O by NH_3 a sample of $\text{Ir}(\text{IMes})(\text{COD})\text{Cl}$ was prepared that contained a 5 mM loading of the iridium complex. In addition, an 8-fold excess of NH_3 was added relative to iridium. This process was also completed in dichloromethane- d_2 as the solvent. The solution was activated with *para*- H_2 over 5 minutes at 298 K and a ^1H NMR spectrum recorded. This NMR spectrum contained key ^1H NMR resonances at $\delta -23.61$ (singlet) for the hydride signal of the SABRE catalyst $[\text{Ir}(\text{H})_2(\text{IMes})(\text{NH}_3)_3]\text{Cl}$ which appears

alongside bound NH resonances at δ 2.84 and 2.21 for the two inequivalent resonances of the NH₂ protons that lie in an equatorially bound ligand (Table 2.8). A signal for free NH₃ appeared at δ 0.48.

When 20 μ l of D₂O was added the resulting T_1 values for the bulk and dissolved water were 15.79 and 19.25 s respectively.

When the corresponding measurements are made with *d*₆-DMSO, several hydride resonances appear suggestive of the formation of multiple products. These were not characterised, however the SABRE studies utilising 20 μ l of D₂O were completed. The corresponding T_1 's for the bulk and dissolved H₂O/HOD signals were 17.54 and 23.48 s respectively. This showed that the T_1 values of the bulk and dissolved H₂O signals increase with *d*₆-DMSO by (10% and 18%, respectively).

When 20 μ l of D₂O was added to this sample, the signal for the free NH₃ resonance at δ 0.48 almost disappeared, due to H/D exchange between NH₃ and D₂O. Additionally, as expected, two signals appear at δ 4.79 and 1.75 for bulk and dissolved H₂O.

When SABRE was undertaken, several of these resonances were enhanced. The signal for bulk H₂O at δ 4.79 proved to be enhanced by 707-fold, while the enhancement for the peak at δ 1.75 for dissolved water was 73-fold. The iridium catalyst resonances at δ 2.14, 2.39 and 7.06 were also enhanced by 4, 2 and 4-fold respectively. The corresponding T_1 values for the bulk H₂O/HOD signal and the corresponding dissolved water signal were 17.54 and 23.48 s. These are 7% and 16% smaller than the corresponding values seen with BnNH₂ and *d*₆-DSMO respectively. Hence NH₃ yields a much higher level of H₂O/HOD polarisation, presumably because of more rapid proton exchange, there is a negative impact on T_1 .

4.3 Conclusion

In this chapter the polarisation of water (H₂O) was examined through SABRE-RELAY. This was complicated by the fact that in dichloromethane two pools of water are observed, which are connected by chemical exchange. Both BnNH₂ and NH₃

proved to undergo SABRE in the presence of H₂O or D₂O. Furthermore, the addition of *d*₆-DSMO was found to increase the relaxation times of both the bulk and dissolved water. The resulting H₂O/HOD signal gains were found to be maximised for the NH₃ system which is consistent with it presenting the largest NH₃ polarisation. It is expected, therefore, that with further work this approach could be useful in preparing hyperpolarised water samples for further use in imaging. The limiting factor in these experiments would be the availability of *para*-H₂ which is easy to source and larger volumes could be deployed if the reactor were scaled from a 5-mm NMR tube. Hence it is likely that such an approach could produce a reasonable volume of polarised water. It is interesting to hypothesise that this could be completed using phase-transfer catalysis, which would allow a pool of water to separate from the bulk. With a lifetime of 37 seconds, it should be possible to use this material in a second step rather like DNP. There are clearly several opportunities to take this work forward that could have significant impact.

Chapter 5: Conclusions and future work

Since the start of the research programme leading to my thesis a number of developments have been made in the field of hyperpolarisation. These developments have seen para-hydrogen related research become much more widespread. Researchers have developed hydrogenative routes to SABRE-RELAY wherein an unsaturated molecule containing an exchangeable proton is first hydrogenated. This leads to the creation of a substrate that can polarise its exchangeable proton.⁶⁷ From then on, a SABRE-RELAY type approach is utilised to sensitise other substrates.¹¹⁶ Furthermore, DNP has been utilised to polarise water which has subsequently been used to enable in-vivo imaging with improved sensitivity.¹³⁴

In the SABRE field progress has been made on the polarisation of pyruvate with the group of Theis utilising fine temperature control to exceed the hyperpolarization levels initially described by Duckett *et al.*¹³⁵ The York group has extended SABRE further with the hyperpolarised pharmaceutical approach that has seen materials like NO_2^- become embedded in triazines after diazatisation.¹³⁶

Sellies *et al.* achieved the hyperpolarisation of α -amino acids, enabling the detection and quantification of these compounds in sub-micromolar quantities in complex mixtures. Testing was done on human urine, which, after being diluted with methanol, allowed for the detection and quantification of naturally occurring α -amino acids.⁷⁸

SABRE has become the most commonly used hyperpolarisation method for enhancing benchtop NMR sensitivity. The increased sensitivity makes it possible to use helpful approaches that would be impractical to apply with benchtop NMR spectroscopy (such as ^{13}C) due to the latter's low sensitivity.¹³⁷

Advancements in SABRE at ultralow-field have made it possible to produce hyperpolarised material continuously in relatively large quantities.¹³⁸

A PHIP technique, has also seen fumarate hyperpolarised and successfully purified and separated from the polarising reagents, which allowed the use of fumarate for *in vivo* imaging.¹³⁹

This research has focussed on the optimisation of SABRE-RELAY. It was found that it was possible to use a range of amines and NH_3 as polarisation sources, with NH_3 proving optimal in most circumstances and some of this work has been published.¹⁰⁸ By focussing on a range of plant oils like citronellol and nerol, it was proved that fully diagnostic proton signals could be readily collected in a single NMR scan after hyperpolarisation. These signal gains allowed for the rapid detection of the ^{13}C spectra of these materials. The levels of signal gain were attenuated by relaxation and transfer within the molecular scaffold and required a H-H coupling pathway to exist across the hyperpolarised spin network. This served to illustrate a limitation, in so far as transfer to protons remote to the OH entering group could be challenging. Similar findings were made when the substrates ^{13}C signals were examined. The result was that for nerol and geraniol only a subset of their ^{13}C -skeleton was polarised. Nonetheless the results are again diagnostic of the materials present and demonstrate that small amounts can be readily detected.

The total signal enhancements reported throughout this thesis yield insightful information on the relative success of SABRE as it hyperpolarises a range of different molecules. Hence it provides a comprehensive view on the suitability of the substrate to SABRE and in this case reviews citronellol was the most suitable material. In contrast, the maximum signal gain reported as an average enhancement per proton, is useful in deciding which molecules are most readily detected after SABRE-RELAY by NMR. Now the answer changes to geraniol which shows a 343-fold signal gain for the CH_2 resonance. This is reflective of the fact the enhancement is shared over few protons.

Then, the progression was made to hyperpolarise water, and it was demonstrated that this could be achieved through SABRE-RELAY. By using a mixture of H_2O and D_2O the high-field relaxation time of the protons was extended to 30 seconds from the more usual 3.7 seconds. This reflects a remarkable extension which will aid in future utility. Furthermore, it proved possible to probe dissolved and bulk water in dichloromethane. Using NH_3 allowed to enhance the HOD signals by 700-fold.

As a consequence of this there are substantial opportunities to take this work forward. The H_2O polarisation studies would have progressed by extending the volumes of

material and probed the results in an imaging system. This would have allowed the use of larger volumes of *para*-H₂ and was expected to deliver far larger enhancement values. The ultimate goal was to have this scaled up to provide 2 cm³ of material.

The plant oil studies demonstrated that good levels of ¹H and ¹³C nuclear spin polarisation can be achieved in them through SABRE-RELAY. However, the corresponding ¹H and ¹³C nuclei's T_1 values proved to be quite short, so it was impossible to record the weaker signals ¹³C T_1 values. If this research were continued, it would therefore be sensible to prepare these materials through appropriate synthetic methods in a ¹³C labelled form. This would require extensive synthetic efforts and be highly time consuming. The result would be much stronger ¹³C NMR signals which would make their detection far easier and hence the assessment of their T_1 values. By selecting the most appropriate long-lived signals, it should then be possible to achieve the in-vitro MRI monitoring of these agents in plants as set out in my initial aims. Ideally, the substrates should contain a single label to prevent more rapid relaxation as multiple ¹³C spins will interact together and this is not desirable. It might also be sensible to introduce ²H labels to increase these relaxation times, and focus the available hyperpolarization into fewer sites. This will result in even stronger ¹³C signals. Hence, the process of further optimisation will be inherently time consuming as multiple isotopologues will need preparing and examining.

Chapter 6: Experimental

6.1 Instrumentation

6.1.1 NMR spectrometers

A 500 MHz Bruker AVIII spectrometer, operating at 11.7 T, was used for NMR characterisation. The hyperpolarisation tests were performed on a 400 MHz Bruker AVIII operating at 9.4 T. All data was acquired and processed using Bruker Topspin 3.6.2. Differences in chemical shift are reported in ppm (parts per million) relative to the residual solvent signal. The solvent utilised for NMR measurements was dichloromethane- d_2 .

6.1.2 Generation of *para*-H₂

The *para*-H₂ was generated with a *para*-H₂ rig. In short, a closed-cycle helium refrigeration unit cools hydrogen gas to 25 K before passing it over paramagnetic iron oxide (Fe₂O₃), which changes *ortho*-H₂ into *para*-H₂ with 99% purity. For the SABRE hyperpolarisation experiments, *para*-H₂ pressure of 4 bar was used.

6.2 Summary of the SABRE NMR method

6.2.1 Preparation of a SABRE NMR sample

In order to prepare a sample for a SABRE experiment a specified amount of a selected substrate (typically a 5 fold-excess relative to metal) was added to a suitable SABRE precatalyst in an NMR solvent. The sample was housed in an NMR tube supplied with a J. Young valve. It was then degassed, using a high vacuum system. To degas a sample with dichloromethane- d_2 , it was connected it to a high vacuum system whilst immersed in liquid nitrogen to remove any gases. Acetone was then sprayed onto the external wall of the NMR tube to melt the sample. To ensure such a sample was fully degassed this process was repeated 3 times. After that, normal hydrogen was added to the sample and left it to activate, and hence became ready for a SABRE experiment. During this time, the sample was expected to become colourless as we form an Ir(III) product.

6.2.2 SABRE NMR measurement

Once a sample had become activated it was placed in a Bruker 400 MHz (9.4T) NMR spectrometer where a single (thermal) reference scan was recorded. This was completed in order to enable the determination of the level of NMR signal enhancement by comparison with the corresponding hyperpolarized NMR spectrum. In addition, such measurements were used to detect the hydride ligand signal of the catalyst and thereby confirm the successful activation of the sample. Signals for bound and free substrate are also expected.

At that point, *para*-H₂ is added to the sample to hyperpolarise it by SABRE. A series of SABRE measurements can then be undertaken. These routinely involved the shake and drop approach which involved vigorous sample shaking for ~ 10 seconds in an ~65 G field, prior to immediately dropping it into the NMR for hyperpolarized spectrum measurement. Such measurements were then repeated at least 3 times so an average enhancement can be quoted, and comparisons between measurements can be made.

6.2.3 SABRE enhancement calculations

The enhancement of NMR signal was determined by comparing the integrals of a hyperpolarised spectrum to those of a reference spectrum obtained from the same sample after thermal relaxation and polarisation. When taking the experimental spectra, both the reference and hyperpolarised versions were acquired using the same NMR scanner. The enhancement was calculated using Equation 6.1, where S_{hyp} is the integrated signal from the hyperpolarised spectrum and S_{therm} is the integrated signal from the thermally polarised sample, and E is the enhancement.

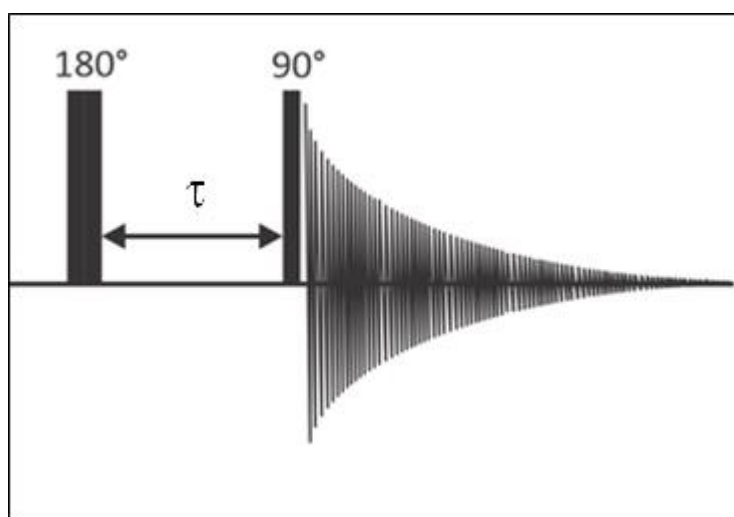
Equation 6.1: Equation for calculating signal enhancement.

$$E = \frac{S_{hyp}}{S_{therm}}$$

6.2.4 Measurement of T_1 relaxation time

For the measurements of T_1 the inversion recovery pulse was used. At equilibrium, the bulk magnetization (M_0) in NMR is along the z-axis. In inversion-recovery, a 180° pulse is used to change the magnetisation orientation from (z) to (-z) axis. Subsequently, a 90° radio-frequency (RF) pulse is applied after waiting for a delay time (τ), which turns the magnetisation into the x-y plane where signals are detected. As the amount of magnetisation in -z reduces over time, the visible signal intensity will also reduce due to the delay between the two pulses. Several iterations of this step are required to outline and reveal the T_1 relaxation time. After $5 T_1$ passes, the system is in thermal equilibrium.

Figure 6.1: Diagram of the inversion-recovery experiment's pulse sequence used for the measurements of T_1 .¹⁴⁰



6.2.5 Measurement of hyperpolarised T_1

This process involves exciting the enhanced signal by a series of low tip angle measurements which are separated in time by a variable delay. The resulting signal will consequently reduce according to the low tip angle value and the time delay which encodes relaxation.¹⁴¹ The resulting data was fit to an appropriate function in EXCEL and the difference between the predicted points and experimental points minimised. As a consequence, a T_1 value could be estimated.

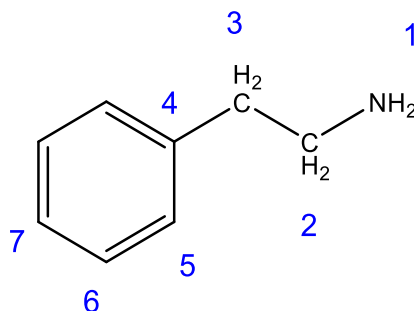
Appendix A

7.1 Characterisation of substrates

Phenylethylamine (see section (2.2.1))

Phenylethylamine was characterised by recording ^1H and ^{13}C NMR spectra in dichloromethane- d_2 solution at 400 MHz. The resulting ^1H NMR spectrum contains signals at δ 7.33 (m, 2H), 7.23 (m, 3H, significant overlap), 2.95 (t, 7 Hz, 2H), 2.75 (t, 7 Hz, 2H) and 1.15 (br, 2H) for this material. Table 2.1 outlines these NMR data and the assignments for phenylethylamine. During the SABRE studies efforts will be made to probe the signal enhancements that result for these NMR signals.

Table 6.1: NMR characterisation data for phenylethylamine in dichloromethane- d_2 at 298 K with labelling according to the inset structure.



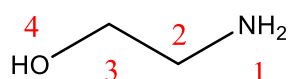
Resonance number	^1H (ppm)	^{13}C (ppm)
1	1.15 (br, 2H)	-
2	2.95 (t, $J = 7$ Hz, 2H)	43.74
3	2.75 (t, $J = 7$ Hz, 2H)	40.32
4	-	140.36
5	7.23 (m, 2H)*	128.3
6	7.33 (m, 2H)	128.8
7	7.22 (m, 1H)*	125.9

*Overlap

Ethanolamine (see section (2.4))

Ethanolamine was dissolved in dichloromethane- d_2 to record ^1H and ^{13}C NMR spectra at 400 MHz. The resulting ^1H NMR spectrum contains signals at δ 1.98 (br, 2H), 2.84 (t, 6.82 Hz, 2H), 3.58 (t, 7 Hz, 2H) and 1.98 (br, 2H) for this material. Table 2.5 outlines these NMR data and the assignments for ethanolamine.

Table 6.2: NMR characterisation data for ethanolamine in dichloromethane- d_2 at 298 K with labelling according to the inset structure.

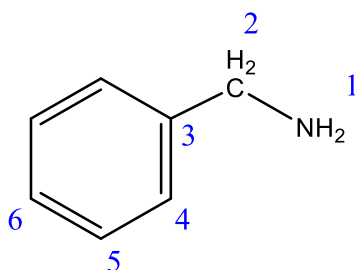


Resonance number	^1H (ppm)	^{13}C (ppm)
1	1.98 (3H, exchange weighted average of 1 and 4)	-
2	2.84 (t, $J = 6.82$ Hz, 2H)	63.74
3	3.58 (t, $J = 6.82$ Hz, 2H)	43.82

Benzylamine (see section (2.6))

To examine benzylamine (BnNH_2) it was first characterised by recording ^1H and ^{13}C NMR spectra in dichloromethane- d_2 solution at 400 MHz (Table 2.9).

Table 6.3: NMR characterisation data for benzylamine in dichloromethane- d_2 at 298 K.



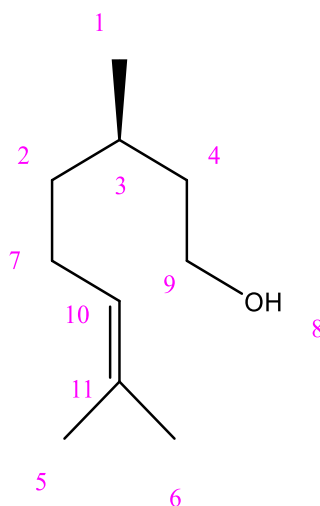
Resonance number	^1H (ppm)	^{13}C (ppm)
1	1.51 (br, 2H)	-
2	3.84 (s, 2H)	46.37
3	-	143.36
4	7.28 (m, 2H)	126.92
5	7.31 (m, 2H)*	128.34
6	7.32 (m, 1H)*	128.91

*Overlap

Citronellol (see section (3.1.1))

Citronellol was dissolved in dichloromethane- d_2 . The resulting ^1H NMR spectrum contains signals at δ 0.94 ($\text{CH}_3\text{-H}_1$), 1.20 ($\text{CH}_2\text{-H}_2$), 1.38 ($\text{CH}_2\text{-H}_4$), 1.59 (CH-H_3), 1.64 ($\text{CH}_3\text{-H}_5$), 1.71 ($\text{CH}_3\text{-H}_6$), 2.02 ($\text{CH}_2\text{-H}_7$), 2.14 (OH-H_8), 3.65 ($\text{CH}_2\text{-H}_9$), and 5.14 (CH-H_{10}) as listed and attributed in Table 3.1.

Table 6.4: NMR characterisation data for citronellol in dichloromethane- d_2 at 298 K.

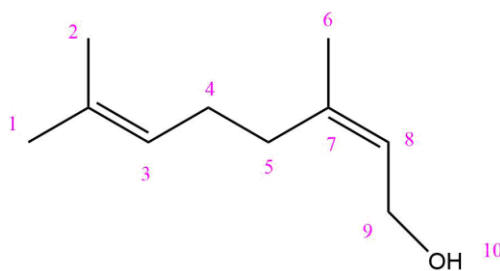


Resonance number	^1H (ppm)	^{13}C (ppm)
1	0.94 (d 6.6 Hz, 3H)	19.2 (q, 123 Hz)
2	1.22 (m, 1H), 1.38 (m, 1H)	37.2 (t, 126 Hz)
3	1.59 (m, 1H)	29.2 (d, 125 Hz)
4	1.39 (m, 1H), 1.64 (m, 1H)	39.9 (t, 124 Hz)
5	1.65 (s, 3H)	17.3 (q, 119 Hz)
6	1.72 (s, 3H)	25.4 (t, 123 Hz)
7	2.03 (m, 1H), 1.67 (m, 1H)	25.4 (t, 126 Hz)
8	2.14 (1H)	-
9	3.65 (m, 2H)	60.9 (t, 139 Hz)
10	5.14 (m, 1H)	124.6 (d, 149 Hz)
11	-	131.1 (s)

Nerol (see section (3.1.8))

Upon dissolving nerol in dichloromethane- d_2 the resulting ^1H NMR spectrum contained signals at δ 1.65 ($\text{CH}_3\text{-H}_1$), 1.78 ($\text{CH}_3\text{-H}_2$), 5.16 (CH-H_3), 2.18 ($\text{CH}_2\text{-H}_4$), 1.72 ($\text{CH}_3\text{-H}_6$), 5.45 (CH-H_8), 4.11 ($\text{CH}_2\text{-H}_9$) and 1.57 (OH-H_{10}) as detailed in Table 3.2.

Table 6.5: NMR characterisation data for nerol in dichloromethane- d_2 at 298 K.

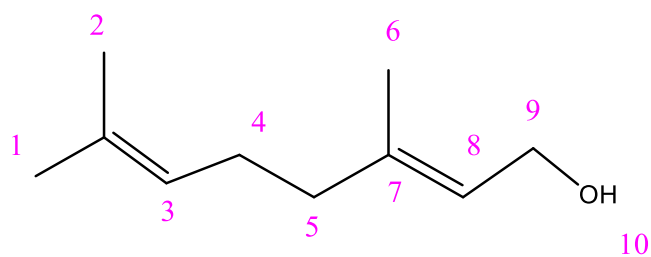


Resonance number	^1H (ppm)	^{13}C (ppm)
1	1.65 (s, 3H)	17.39
2	1.78 (s, 3H)	23.06
	-	132.19
3	5.16 (m, 1H)	123.94
4	2.18 (d, 2H)	26.54
5	2.18 (d, 2H)	31.91
6	1.72 (s, 3H)	25.44
7	-	139.55
8	5.45 (t, 1H)	124.54
9	4.11 (d, 2H)	58.84
10	1.57 (br, 1H)	-

Geraniol (see section (3.1.11))

When geraniol is dissolved in dichloromethane- d_2 the resulting ^1H NMR spectrum contained signals at δ 1.65 (H_1), 1.78 (H_2), 5.16 (H_3), 2.18 (H_4), 1.72 (H_6), 5.45 (H_8), 4.09 (H_9), and 1.57 (H_{10}) (Table 3.4).

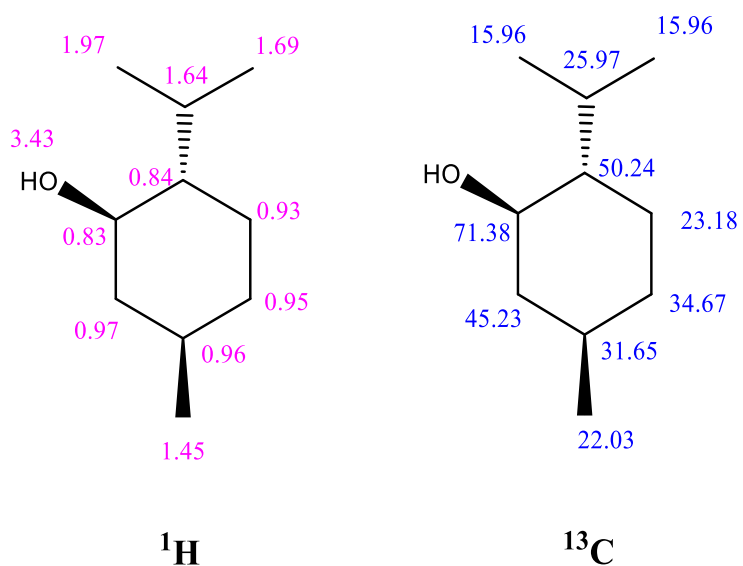
Table 6.6 : NMR characterisation data for geraniol in dichloromethane- d_2 at 298 K.



Resonance number	^1H (ppm)	^{13}C (ppm)
1	1.65 (s, 3H)	25.4
2	1.72 (s, 3H)	17.5
	-	131.6
3	5.15 (m, 1H)	124.0
4	2.17 (d, 2H)	26.5
5	2.08 (d, 2H)	39.5
6	1.70 (s, 3H)	16.0
7	-	139.3
8	5.42 (t, 1H)	123.7
9	4.14 (d, 2H)	59.3
10	1.57 (br, 1H)	-
11	-	-

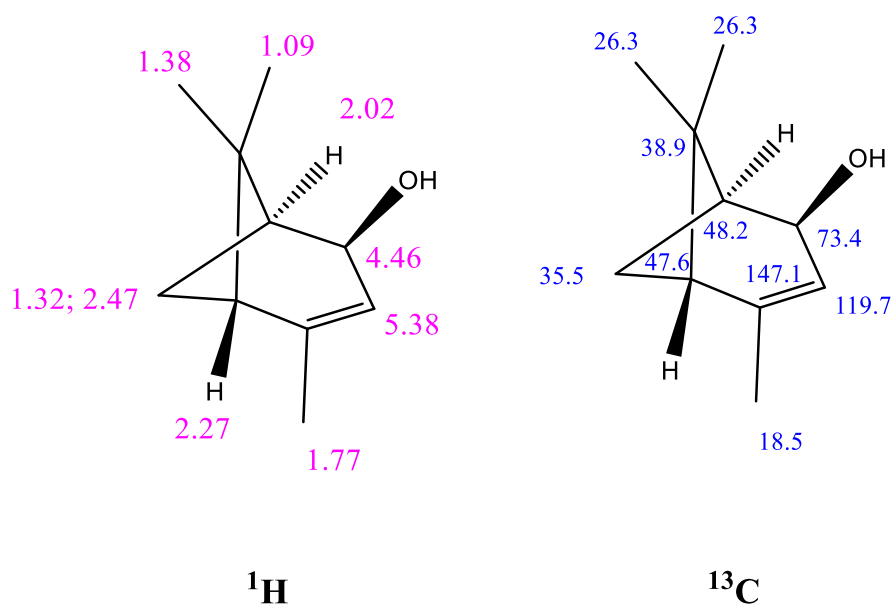
Menthol (see section (3.4.1))

Figure 6.2: NMR responses of menthol when dissolved in dichloromethane- d_2 at 298 K.



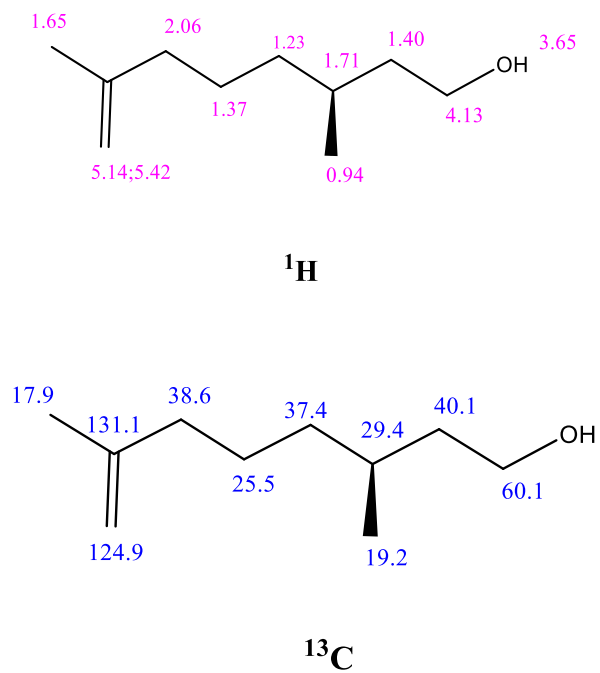
Verbenol (see section (3.4.2))

Figure 6.3: NMR responses of verbenol when dissolved in dichloromethane- d_2 at 298 K.



Rhodinol (see section (3.4.3))

Figure 6.4: NMR responses of rhodinol when dissolved in dichloromethane- d_2 at 298 K.

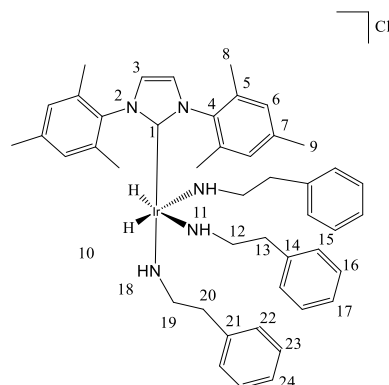


7.2 Characterisation of SABRE complexes

$[\text{Ir}(\text{H})_2(\text{IMes})(\text{phenethylamine})_3]\text{Cl}$

(see section (2.2.3))

Table 6.7: NMR characterisation data for octahedral $[\text{Ir}(\text{H})_2(\text{IMes})(\mathbf{1})_3]\text{Cl}$ (**3**) that forms when phenylethylamine (**1**) and H_2 react with $\text{Ir}(\text{Cl})(\text{COD})(\text{IMes})$ (**2**) in dichloromethane- d_2 at 298 K with the labels according to the inset structure.



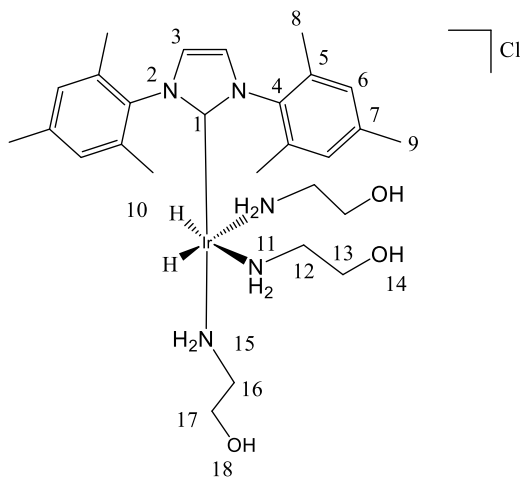
Resonance number	^1H (ppm)	^{13}C (ppm)	^{15}N (ppm)
1	--	153.8	--
2	--	--	192.21
3	6.75	121.73	--
4	--	138.14	--
5	--	135.06	--
6	7.0	129.4	--
7	--	138.64	--
8	2.17	18.30	--
9	2.21	21.10	--
10	-23.95	--	--
11	4.42 (t, $J_{\text{HH}} = 11$ Hz, 2H) * $J_{^{15}\text{NH}} = 68$ Hz 2.11 (br, t, $J_{\text{HH}} = 11$ Hz, 2H) * $J_{^{15}\text{NH}} = 68$ Hz	--	-7.2
12	2.41 (dt, $J_{\text{HH}} = 9$ and 11 Hz, 2 H) 3.30 (2H, overlap)	50.7	--
13	--	--	--
14	--	141.8	--
15	7.32 (dd, $J_{\text{HH}} = 7$ Hz)	128.33	--
16	7.25 (t, $J_{\text{HH}} = 7$ Hz)	126.88	--
17	~7.28 - overlap	-	--
18	3.685 (t, $J_{\text{HH}} = 5.9$ Hz, 2H) * $J_{^{15}\text{NH}} = 69$ Hz	--	-16.2
19	2.78 (t, $J_{\text{HH}} = 6.15$ Hz, 2H)	53.9	--
20	--	-	--
21	7.32	128.33	--
22	~7.2 - overlap	-	--
23	~7.12 - overlap	-	--

* ^{15}N coupling determined via 2D NMR spectrum on unlabelled sample

[Ir(H)₂(IMes)(ethanolamine)₃]Cl

see section (2.4.2)

Table 6.8: NMR characterisation data for [Ir(H)₂(ethanolamine)₃(IMes)]Cl (**4**) in dichloromethane-*d*₂ at 253 K alongside the labelled structure.



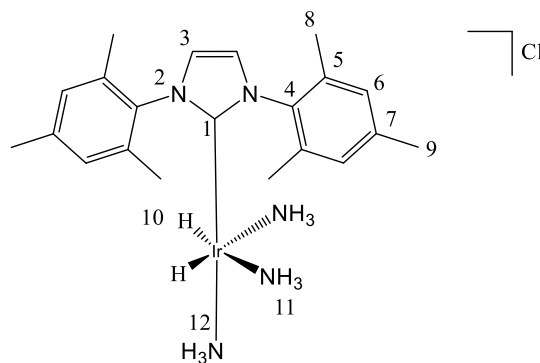
Resonance number	¹ H (ppm)	¹³ C (ppm)	¹⁵ N (ppm)
1	-	152.76	-
2	-	-	191.7
3	6.80 (2H)	121.75	-
4	-	137.6	-
5	-	135.81	-
6	7.04 (4H)	129.19	-
7	-	138.73	-
8	2.15 (12H)	18.2	-
9	2.33 (6H)	20.8	-
10	-23.91	--	-
11	3.36 (2H), 2.18 (2H)	--	-16.8
12	2.34 (2H), 1.68 (2H)	50.82	-
13	3.27 (2H), 3.16 (2H)	63.83	-
14	--	--	-
15	3.51 (2H)	--	-23.5
16	2.74 (2H)	54.43	-
17	3.42 (2H)	62.98	-
18	*	-	--

*Not observed

$[\text{Ir}(\text{H})_2(\text{IMes})(\text{NH}_3)_3]\text{Cl}$

see section (2.6)

Table 6.9: NMR characterisation data of $[\text{Ir}(\text{H})_2(\text{IMes})(\text{NH}_3)_3]\text{Cl}$ (**5**) in dichloromethane- d_2 at 298 K with resonances attributed according to the labelling of the inset structure.



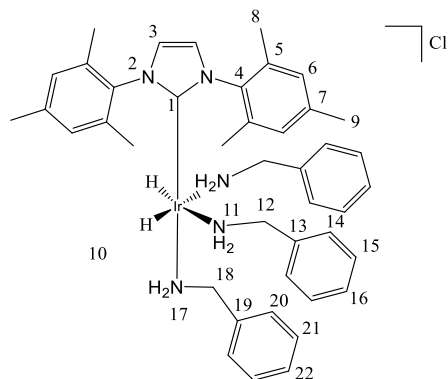
Resonance number	^1H (ppm)	^{13}C (ppm)	^{15}N (ppm)
1	--	153.8	--
2	--	--	190.83
3	6.80	121.5	--
4	--	138.11	--
5	--	135.25	--
6	7.00	129.00	--
7	--	138.64	--
8	2.10	18.30	--
9	2.35	20.78	--
10	-23.61	--	--
11	2.21 (br, s) * $J_{\text{NH}} = 67$ Hz	--	-34.9
12	2.84 (br, s) * $J_{\text{NH}} = 69$ Hz	--	-46.5

* ^{15}N coupling determined via 2D NMR spectrum on unlabelled sample

[Ir(H)₂(IMes)(BnNH₂)₃]Cl

see section (2.6)

Table 6.10: NMR characterisation data for [Ir(H)₂(IMes)(BnNH₂)₃]Cl (**6**) in dichloromethane-*d*₂ at 298 K with the labels according to the inset structure.



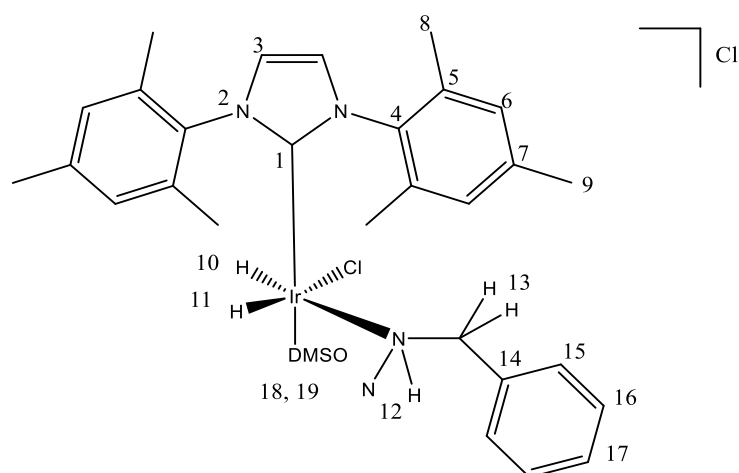
Resonance number	¹ H (ppm)	¹³ C (ppm)	¹⁵ N (ppm)
1	--	153.8	--
2	--	--	192.83
3	6.80	121.73	--
4	--	138.11	--
5	--	135.25	--
6	6.90	129.29	--
7	--	138.64	--
8	2.17	18.30	--
9	2.21	20.78	--
10	-23.95	--	--
11	5.00 (br, dt, J _{HH} = 5 and 11 Hz, 2H) *J _{15NH} = 68 Hz 2.30 (br, t, J _{HH} = 11 Hz, 2H) *J _{15NH} = 68 Hz	--	-6.4
12	3.65 (dt, J _{HH} = 5 and 15 Hz, 2H), 3.30 (ddd, J _{HH} = 3, 12 and 15 Hz, 2H)	53.14	--
13		141.8	--
14	7.35 (d, J _{HH} = 5 Hz)	128.33	--
15	7.25 (t, J _{HH} = 5 Hz)	126.88	--
16	~7.28 - overlap	--	--
17	4.25 (t, J _{HH} = 7 Hz, 2H) * J _{15NH} = 69 Hz	--	-13.4
18	3.85 (t, J _{HH} = 7 Hz, 2H)	57.26	--
19	--	-	--
20	7.30	128.35	--
21	~7.28 - overlap	-	--
22	~7.28 - overlap	-	--

*¹⁵N coupling determined via 2D NMR spectrum on unlabelled sample

[Ir(H)₂(IMes)(BnNH₂)₂(DMSO)]Cl



see section (4.2.4)

Table 6.11: Characterization of [Ir(H)₂(IMes)(BnNH₂)₂(DMSO)]Cl complex.



Resonance number	¹ H (ppm)	¹³ C (ppm)	¹⁵ N (ppm)
1	--	161.25	--
2	--	--	192.83
3	6.94	122.02	--
4	--	137.75	--
5	--	136.0, 135.82	--
6	6.93, 6.97	128.77	--
7	--	137.76	--
8	2.17	17.96	--
9	2.26	20.69	--
10	-23.32, d J _{HH} = 8.5 Hz	--	--
11	-23.76, d J _{HH} = 8.5	--	-6.4
12	2.275, 2.162	--	--
13	3.77, 3.30	51.9	--
14	--	*	--
15	*	*	--
16	*	*	--
17	*	*	--
18	3.11	46.20	--
19	3.17	58.38	--

*Not observed

Cite this: *Chem. Sci.*, 2018, 9, 3677Direct and indirect hyperpolarisation of amines using *parahydrogen*[†]Wissam Iali, Peter J. Rayner,  Adel Alshehri, A. Jonathan. Holmes, Amy J. Ruddlesden  and Simon B. Duckett *

Nuclear Magnetic Resonance (NMR) and Magnetic Resonance Imaging (MRI) are two widely used techniques for the study of molecules and materials. Hyperpolarisation methods, such as Signal Amplification By Reversible Exchange (SABRE), turn typically weak magnetic resonance responses into strong signals. In this article we detail how it is possible to hyperpolarise the ¹H, ¹³C and ¹⁵N nuclei of a range of amines. This involved showing how primary amines form stable but labile complexes of the type [Ir(H)₂(IMes)(amine)₂]Cl that allow *parahydrogen* to relay its latent polarisation into the amine. By optimising the temperature and *parahydrogen* pressure a 1000-fold per proton NH signal gain for deuterated benzylamine is achieved at 9.4 T. Additionally, we show that sterically hindered and electron poor amines that bind poorly to iridium can be hyperpolarised by either employing a co-ligand for complex stabilisation, or harnessing the fact that it is possible to exchange hyperpolarised protons between amines in a mixture, through the recently reported SABRE-RELAY method. These chemical refinements have significant potential to extend the classes of agent that can be hyperpolarised by readily accessible *parahydrogen*.

Received 1st February 2018
Accepted 6th March 2018

DOI: 10.1039/c8sc00526e

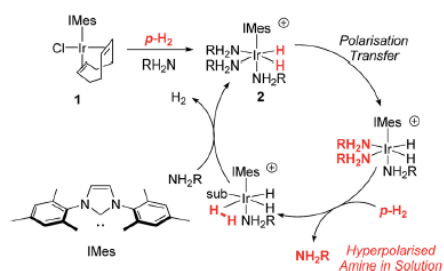
rsc.li/chemical-science

Introduction

Hyperpolarisation methods are used to overcome the inherent insensitivity of Nuclear Magnetic Resonance (NMR) spectroscopy and Magnetic Resonance Imaging (MRI) where their use may lead to dramatic time and cost savings. One such hyperpolarisation method, *Parahydrogen* Induced Polarisation (PHIP),¹ produces the required non-Boltzmann nuclear spin distribution by the incorporation of *parahydrogen* (*p*-H₂), an example of a nuclear singlet, into a suitable substrate molecule. This effect was shown to yield an enhanced NMR signal in 1987 (ref. 2) and has been the subject of intense investigation.^{1,3–6} A drawback of PHIP though, is the requirement for chemical change, caused by *p*-H₂ addition to an unsaturated centre such as an alkene. However, recently a *p*-H₂ technique that does not change the chemical identity of the sensitised molecule, called Signal Amplification By Reversible Exchange (SABRE), was reported.^{7,8} In this process, *p*-H₂ is not directly incorporated into the substrate. Instead, polarisation is transferred *via* the *J*-coupling network that exists within a metal complex that colocates *p*-H₂ derived hydride ligands and a weakly bound substrate (ligand).^{9–11} Ligand exchange with excess unbound

substrate and *p*-H₂ enables the build-up of a pool of polarised substrate molecules in solution in a catalytic fashion as shown in Scheme 1.¹² The SABRE polarisation of ¹H nuclei typically utilises a ⁴*J*_{HH} coupling between the catalysts hydride and substrate ligand protons. Tessari *et al.* have quantified these small spin–spin couplings to be ≈1.2 Hz.¹³ Alternatively, stronger ²*J*_{HN} couplings have now been used to achieve ¹⁵N polarisation transfer at micro-Tesla fields in a variant known as SABRE-SHEATH (SABRE-in shield enables alignment transfer to heteronuclei).^{14,15} Intra-molecular spin–spin coupling networks within the substrate subsequently enables transfer to remote spins which do not exhibit direct coupling to the hydride ligands.¹⁶

One of the most effective precatalysts for this process is [IrCl(COD)(IMes)] (1) [where IMes = 1,3-bis(2,4,6-trimethylphenyl)]

Scheme 1 Route to SABRE hyperpolarisation of an amine, NH₂R.

Centre for Hyperpolarisation in Magnetic Resonance (CHyM), Department of Chemistry, University of York, Heslington, YO10 5DD, UK. E-mail: simon.duckett@york.ac.uk

[†] Electronic supplementary information (ESI) available: Full experimental procedures, characterisation data and example spectra. See DOI: 10.1039/c8sc00526e



imidazol-2-ylidene, COD = *cis,cis*-1,5-cyclooctadiene] which, after reaction with H₂ and an excess of substrate, typically forms [Ir(H)₂(IMes)(substrate)₃]Cl in protic solvents such as methanol.¹⁷ Neutral active catalysts of the type [Ir(H)₂(Cl)(IMes)(substrate)₂] have also been reported to achieve similar results.¹⁸ These metal based polarisation transfer catalysts have been shown to act on a range of substrates that contain multiple bonds to nitrogen, such as nicotinamide,^{19,20} isoniazid,^{21,22} metronidazole,²³ pyrazole,²⁴ imines,²⁵ diazirines²⁶ and nitriles,²⁷ and lead to polarised ¹H, ¹³C, ¹⁵N, ¹⁹F, ²⁹Si, ³¹P, and ¹²⁹Sn nuclei that yield substantially enhanced NMR responses in just a few seconds.^{19,28–33} In fact, ¹H polarisations of 50% have been reported, while for ¹⁵N, values of over 20% have been achieved.^{19,23}

While SABRE-induced polarisation can also be achieved using in-field rf. transfer methods,^{34–37} whose efficiency varies with pulse sequence,^{37–39} spontaneous polarisation transfer occurs readily at low-field and it is this method we employ here. Moreover, as predicted,⁹ it has also been established that SABRE can be used to produce hyperpolarised singlet states⁴⁰ with long-lifetimes through transfer in ultra-low field, or after the implementation of rf. transfer.^{41–46} Hence the diversity of applications found for this approach is growing and it clearly reflects not only a successful medium to test hyperpolarisation concepts but a potential route to transform the analytical potential of NMR.^{47–50}

In this article, we introduce a new class of substrate into the SABRE repertoire, the amine. This is achieved by the formation of iridium-amine complexes of type [Ir(H)₂(IMes)(RNH₂)₃]Cl (2, Scheme 1), whose kinetic behaviour is determined. Whilst the synthesis and use of iridium-amine complexes has been reported for catalytic transformations such as hydrogenation,^{51–53} we use them here for polarisation transfer catalysis. We have recently shown a limited number of amines are amenable to SABRE.⁵⁴ Here, we start by detailing the hyperpolarisation of ammonia and benzylamine (BnNH₂) and its associated optimisation to achieve large NMR signal enhancements. We then show how hyperpolarisation can be achieved in a range of primary amines. Upon changing to sterically bulky primary amines, secondary amines or aromatic amines, we show that an active SABRE catalyst does not form upon reaction with 1. However, we exemplify co-ligand and relayed polarisation transfer protocols to overcome this limitation and hence expand further the range of amines amenable to polarisation by *p*-H₂.

Results and discussion

Direct ¹H hyperpolarisation of ammonia and BnNH₂ by SABRE

Our objective was to investigate the efficiency of the SABRE polarization of amines and ammonia and to determine their ligand exchange dynamics. A 5 mM solution of 1 in dry dichloromethane-*d*₂ containing an ≈ 6-fold excess of NH₃ relative to 1 at 298 K was therefore prepared. The aprotic solvent ensures that we maintain the necessary *J*-coupling network in [Ir(H)₂(IMes)(NH₃)₃]Cl (2-NH₃) during the study, as rapid ²H exchange results to form ND₃ in deuterated protic solvents. This complex yields a hydride signal at δ −23.8, alongside a broad

response at δ 0.47 for free NH₃. The corresponding equatorial and axial NH₃ ligand ¹H NMR signals of 2-NH₃ appear at δ 2.19 and 2.88 respectively. 2D ¹H-¹⁵N HMQC measurements were subsequently used to locate the corresponding ¹⁵N signals for these ligands at *d*_{axial} −47.8 and *d*_{equ} −35.5. Full characterisation data for 2-NH₃ is available in the ESI.[†] EXSY methods were then used to probe NH₃ and H₂ loss in 2-NH₃. At 298 K, the associated rate constant for NH₃ loss proved to be 1.64 s^{−1} while that of H₂ loss is 0.32 s^{−1}. For comparison, the dissociation rate for pyridine in [Ir(H)₂(IMes)(py)₃]Cl is 13.2 s^{−1} and suggests a higher stability for 2-NH₃ which agrees with the greater basicity of NH₃ relative to pyridine.⁵⁵

As 2-NH₃ undergoes both NH₃ and H₂ loss in solution, we sought to prove that it underwent SABRE catalysis. Thus, a 3 bar pressure of *p*-H₂ was introduced at 298 K and polarisation transfer was conducted at 60 G. A ¹H NMR spectrum at 9.4 T was then recorded which showed a 154-fold signal enhancement per proton for the free NH₃ response while the corresponding equatorial ligand signal, at δ 2.19, showed a 77-fold enhanced response (Fig. 1). Hence 2-NH₃ acts as a SABRE catalyst as it produces a hyperpolarised free ammonia response. In the presence of water, the observed signal enhancement of the protons in free NH₃ decreased to 40-fold per proton, matching that now observed for the equatorially bound NH₃ ligand. This drop is reflected in the signal at δ 1.88, for what is a H₂O response, exhibiting a 75-fold signal gain per proton due to concomitant proton exchange; the ratio of 2-NH₃ : H₂O : NH₃ in this sample was 1 : 5 : 17.5. Under these conditions, the *T*₁ value for free NH₃ in the presence of the active SABRE catalyst was measured by inversion recovery to be 5.5 s.

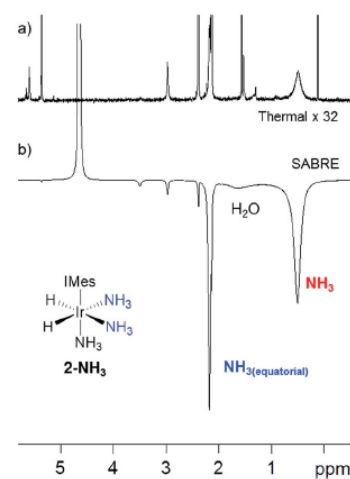


Fig. 1 (a) The thermally polarised ¹H NMR SABRE spectrum (× 32 vertical expansion) recorded of 2-NH₃ (formed by reaction of 1 with NH₃ and H₂) in dichloromethane-*d*₂ at 298 K. (b) The corresponding SABRE polarised 9.4 T ¹H NMR spectrum after transfer under *p*-H₂ at 60 G. The hyperpolarised responses of free NH₃ and Ir-NH₃(equatorial) of 2-NH₃ and residual H₂O are indicated.



The SABRE-induced hyperpolarisation of benzylamine (BnNH_2) was also investigated. A sample containing **1** (5 mM) and BnNH_2 (10 eq.) in dichloromethane- d_2 solution was exposed to 3 bar of H_2 . The immediate formation of $[\text{Ir}(\text{H})_2(\text{Imes})(\text{BnNH}_2)_3]\text{Cl}$ (**2-BnNH}_2) was observed. It gives a characteristic hydride resonance in the ^1H NMR spectrum at $\delta -23.97$. Full characterisation data for this product is available in the ESI.† Interestingly, the ^1H NMR spectrum of **2-BnNH}_2 showed that the BnNH_2 ligand that lies *trans* to hydride, yields inequivalent responses for its NH_2 protons at $\delta 4.92$ and 2.30 , and CH_2 protons at $\delta 3.60$ and 3.18 . This is due to hindered rotation around the Ir-N bond which results in an up/down distinction for the resonances of the equatorial ligand. In contrast, the axial ligand yields single responses which are equivalent at $\delta 4.24$ (NH_2) and $\delta 3.83$ (CH_2) due to free rotation on the NMR time-scale about the Ir-N bond. The corresponding EXSY-derived rate constant for equatorial BnNH_2 loss from **2-BnNH}_2 was 3.33 s^{-1} while the rate of H_2 loss was 2.83 s^{-1} at 298 K. Hence the rate of BnNH_2 loss is higher than that of NH_3 loss in **2-NH}_3**. This difference is due to NH_3 forming a stronger Ir-N bond as reflected in their relative pK_b values and suggests that it might perform better under SABRE than NH_3 .******

This was examined by $p\text{-H}_2$ -based polarisation transfer at 60 G which resulted in hyperpolarised free BnNH_2 in solution. The signal enhancements were quantified to be 72- (NH_2), 56- (CH_2) and 194-fold (Ph) per proton as shown in Fig. 2a. However, by using $d_7\text{-BnNH}_2$ instead we were able to focus the SABRE polarisation into the two amino protons alone and this led to an improved signal enhancement of 916-fold per proton (Fig. 2b).

In order to investigate the T_1 contribution to this effect we determined values for BnNH_2 and $d_7\text{-BnNH}_2$ at 9.4 T. BnNH_2 proved to have effective T_1 values of 1.1 s (NH_2) and 4.7 s (CH_2) respectively while its ^2H -labelled variant exhibited a similar 1.1 s T_1 value for the amino group in the presence of the active catalyst. Hence, the improved NH signal gain seen with $d_7\text{-BnNH}_2$ is due to a reduction in spin dilution which leads to

more efficient SABRE transfer. The relaxation rates for BnNH_2 and $d_7\text{-BnNH}_2$ are both slower in the absence of the active SABRE catalyst in agreement with earlier reports that the catalyst plays a role in reducing relaxation times due to reversible binding. Consequently, BnNH_2 now shows T_1 values of 9.0 s (NH_2) and 11.0 s (CH_2), whereas $d_7\text{-BnNH}_2$ has a T_1 value of 10.1 s for its NH_2 group.

Effect of catalyst to substrate ratio on SABRE polarisation

Previous studies have shown that the SABRE effect is dependent upon the catalyst to substrate ratio as a consequence of kinetic and relaxation effects.^{19,55} Therefore, we studied the effect of changing the ratio of BnNH_2 relative to **1** from 4-fold to 20-fold in a series of further experiments, undertaking the associated SABRE transfer studies at 60 G and 298 K. It was found that similar total polarisation levels result within experimental error during these experiments (see ESI†). Hence, we conclude that the observed signal enhancements under these conditions are essentially independent of ligand excess which suggests that slow exchange and fast relaxation within the catalyst restrict the maximum polarisation level.

Effect of $p\text{-H}_2$ pressure on SABRE polarisation of BnNH_2

As SABRE derives its polarisation from $p\text{-H}_2$, it could be the limiting reagent in this catalytic process and therefore affect the observed substrate polarisation level.¹⁹ Up until this point, we have been utilising 3 bar pressure of $p\text{-H}_2$ which reflects an *ca.* 6-fold excess when compared to the 50 mM substrate present in a 5 mm NMR tube. A sample containing **1** (5 mM), BnNH_2 (50 mM, 10 eq.) in dichloromethane- d_2 solution was therefore prepared and exposed to between 2 and 4 bar of $p\text{-H}_2$. The resulting signal gains, after polarisation transfer at 60 G, are shown in Fig. S14 (see ESI†) and a strong dependence on $p\text{-H}_2$ pressure is seen. This is consistent with the fact that H_2 exchange takes place after ligand dissociation and the remaining equatorially bound BnNH_2 ligand will experience a higher level of latent $p\text{-H}_2$ polarisation (see Scheme 1). When $d_7\text{-BnNH}_2$ is examined with 4 bar of $p\text{-H}_2$, the NH signal gain increases to 1079-fold per proton from the 916-fold signal gain achieved with 3 bar.

Effect of temperature on SABRE polarisation of BnNH_2

The temperature at which SABRE is conducted is also known to affect the efficiency of the polarisation transfer due to changes in the lifetime of the SABRE-active catalyst. We found here that cooling a dichloromethane- d_2 solution containing **1**, BnNH_2 and 3 bar $p\text{-H}_2$ to 288 K results in a reduction in the level of signal enhancement when compared to 298 K data (Fig. S15, ESI†). Conversely 308 K gave an improved response with the overall polarisation level increasing by ~40%. This fits with the observed rate constant for BnNH_2 dissociation increasing to 9.85 s^{-1} from the 3.33 s^{-1} value at 298 K. We therefore conclude the retained polarisation level in BnNH_2 is improved by the faster rate of substrate dissociation and shorter catalyst lifetime. For NH_3 , a 251-fold ^1H signal gain per NH proton is observed at 308 K when compared to the 154-fold value at 298 K. This is consistent

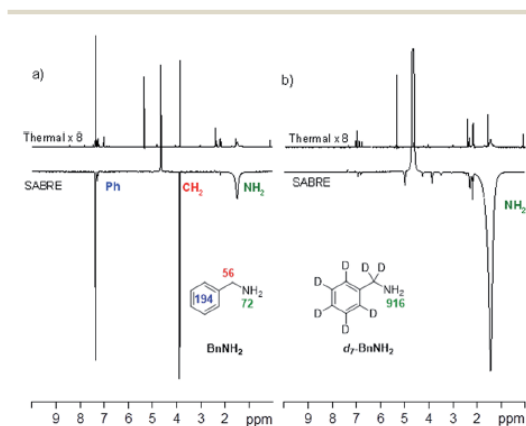


Fig. 2 (a) ^1H NMR spectra of BnNH_2 , thermally polarised, top, and hyperpolarised, bottom. (b) ^1H NMR spectra for $d_7\text{-BnNH}_2$, thermally polarised, top, and hyperpolarised, bottom.

with the increase in the NH_3 dissociation rate constant to 10.42 s^{-1} at 308 K when compared to 1.64 s^{-1} at 298 K.

SABRE transfer to ^{13}C and ^{15}N

SABRE-induced hyperpolarisation of ^{13}C was also observed for BnNH_2 . Whilst polarisation transfer into the *ortho* phenyl carbon was readily observed using a standard ^{13}C acquisition sequence after polarisation transfer 60 G under 4 bar $p\text{-H}_2$, the other ^{13}C resonances had poor signal-to-noise ratios. We overcame this by using a ^1H - ^{13}C refocused INEPT experiment that gave rise to a spectrum showing all 5 carbon environments after polarisation transfer at 60 G. We utilised long-range $J\text{-H-C}$ couplings to transfer this polarisation. ^{13}C signal gains of up to 65-fold were achieved using this method (Fig. 3a). We further note that there is a very strong polarisation transfer field dependence on the BnNH_2 ^{13}C signal intensities which is consistent with earlier reports on pyridine.³⁰

When $\text{Bn}^{15}\text{NH}_2$ is used instead of BnNH_2 , the detection of a hyperpolarised ^{15}N response is readily evident as shown in Fig. 3b. The ^{15}N signal gain for the free material in solution proved to be ~ 880 -fold after polarisation transfer at 60 G and 308 K. The equatorially bound ^{15}N resonance at $\delta -5.59$, is 4 times larger than the free amine signal. As the ratio of free amine to equatorially bound $\text{Bn}^{15}\text{NH}_2$ in solution is actually 7 : 2, the rate of $\text{Bn}^{15}\text{NH}_2$ loss must be relatively slow, even at 308 K. Under this 60 G condition, polarisation transfer is likely to occur *via* the $^3J_{\text{HH}}$ coupling between the $\text{Bn}^{15}\text{NH}_2$ and the hydride ligands. To investigate the effect of using a $^2J_{\text{HN}}$ coupling we repeated this measurement after polarization

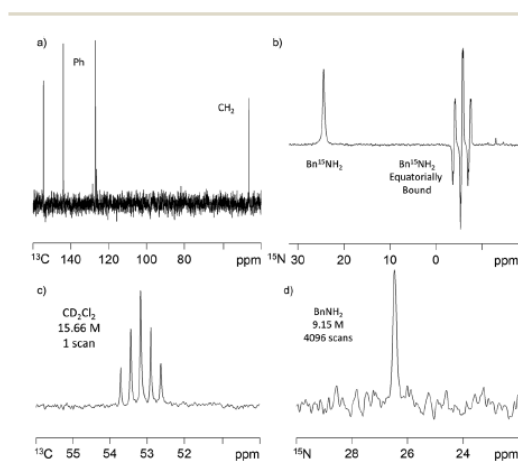


Fig. 3 (a) ^1H - ^{13}C refocused INEPT NMR spectrum of hyperpolarised BnNH_2 (35 mM) achieved *via* 2-BnNH_2 (5 mM) under SABRE in dichloromethane- d_2 solution after transfer at 60 G and 308 K; (b) ^{15}N NMR spectrum of ^{15}N -labelled $\text{Bn}^{15}\text{NH}_2$ (35 mM) after SABRE transfer *via* 2-BnNH_2 (5 mM) at 60 G and 308 K which gives rise to hyperpolarised resonances for free (δ 24.42) and equatorially bound ($\delta -5.59$) substrate; (c) single scan thermally polarised ^{13}C NMR spectrum in CD_2Cl_2 (15.66 M) and (d) 4096 scan thermally polarised ^{15}N NMR spectrum of BnNH_2 (9.15 M).

transfer within a μ -metal shield (*ca.* 350-fold shielding). Under these SABRE-SHEATH type conditions,^{14,15} an ~ 800 -fold ^{15}N -signal gain was observed and further optimisation may therefore be needed to maximise this response. The corresponding ^1H signal gains with this ^{15}N labelled material after transfer at 60 G were now 33-(NH_2), 34-(CH_2) and 52-fold (Ph). These compare to the analogous values of 72-, 56- and 192-fold respectively with $\text{Bn}^{14}\text{NH}_2$. Interestingly, the ^1H polarisation levels therefore decrease with ^{15}N addition and we propose that this is an example of spin dilution.

Expanding the substrate range

In order to test the generality of amine polarisation *via* SABRE, we prepared a series of samples containing 1 (5 mM) and 10 eq. of the substrates shown in Fig. 4 in dichloromethane- d_2 solution. These substrates include a number of primary amines and each is successfully hyperpolarised after transfer at 60 G upon reaction with 1 and $p\text{-H}_2$. In fact, SABRE polarisation of phenylethylamine (PEA) and phenylpropylamine (PPA) results in strong signal enhancements and transfer is found to proceed across the corresponding C_2 and C_3 carbon chains into their phenyl rings. For PEA we found that the NH_2 ^1H signal gain is actually increased to 108-fold per proton compared to the 72-fold BnNH_2 value, and that the CH_2CH_2 bridge gave 50-fold (NCH_2) and 45-fold (CH_2) enhancements per proton. The 5-proton containing phenyl group gave a 92-fold gain per proton.

Spin-isolation of the phenyl group, by introducing an ether linkage, as in phenoxyethylamine (POEA) resulted in signal enhancements of 99-(NH_2), 47-(NCH_2), 147-(CH_2O) and as expected, just 8-fold (Ph) per proton for our test sample. We therefore conclude that polarisation transfer across the oxygen linker is inefficient at 60 G and a stronger aliphatic proton response results. The amines isobutylamine, allylamine and tryptamine were also studied as shown in Fig. 4. In all cases, the formation of $[\text{Ir}(\text{H})_2(\text{IMes})(\text{amine})_3]\text{Cl}$ was indicated (see ESI †) and polarisation transfer results.

When secondary amines, such as dibenzylamine, were examined, no evidence for the formation of an active SABRE catalyst was observed. A similar result was observed for

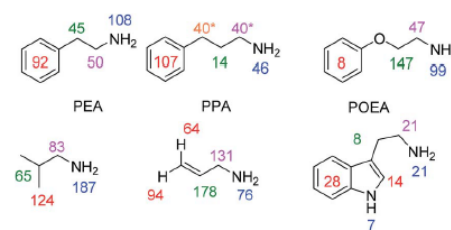


Fig. 4 Amine substrates polarised by SABRE using precatalyst 1 in dichloromethane- d_2 solution. Per proton signal gains are given for the indicated ^1H sites (* average across two sites due to peak overlap) observed at 9.4 T. Corresponding ^1H NMR spectra for thermally polarised and SABRE polarised experiments are given in the ESI † .



sterically hindered primary amines, such as isopropylamine and aromatic amines, such as aniline. Sterically demanding substrates, such as 2,6-lutidine, have been previously shown to be unable to be polarised using SABRE.⁵⁶ A full list of the amines probed in this study is available in the ESI.† We therefore postulate that sterically demanding or electron deficient amines fail to activate and form the necessary $[\text{Ir}(\text{H})_2(\text{IMes})(\text{amine})_3]\text{Cl}$ SABRE catalyst.

This problem could be overcome for aniline by the addition of the co-ligand 1-methyl 1,2,3-triazole (mtz) or CH_3CN . For the corresponding sample containing **1** (5 mM), aniline (10 eq.) and mtz (3 eq.) in dichloromethane- d_2 we achieved signal enhancements of 51-fold for the NH_2 group and 17-fold for the phenyl group, per proton. These signal gains are summarised in Fig. 5. When CH_3CN (8 eq.) is used instead of mtz, the polarisation levels increase to 306- (NH_2) and 193-fold (Ph) per proton. The active complex in this SABRE process was characterised as $[\text{Ir}(\text{H})_2(\text{IMes})(\text{aniline})_2(\text{CH}_3\text{CN})]\text{Cl}$ and yields a distinctive hydride resonance at $\delta -24.78$ (see ESI†). Utilisation of such a co-substrate strategy was however unsuccessful for the secondary amines as detailed in the ESI.†

Indirect hyperpolarisation of amines by SABRE-RELAY

As expected, substrate binding to the metal centre is needed for polarisation transfer to occur. We hypothesised that these amines might also be hyperpolarised indirectly. In this scenario, hyperpolarisation of a primary amine or ammonia is achieved and subsequent proton exchange, which may be mediated by residual water, allows for a polarised proton to be shuttled into the non-SABRE-active amine. Subsequent intra-substrate polarisation transfer then relays the signal gain more widely in this agent (Scheme 2).

In order to test this hypothesis, a series of samples containing **1** (5 mM), target amine (10 eq.) and NH_3 (3–5 eq.) were prepared in dichloromethane- d_2 solution. 2-NH_3 formed in all cases as confirmed by the presence of a hydride resonance in the corresponding ^1H NMR spectra at $\delta -23.8$. Polarisation transfer was then conducted at 60 G, and the resulting signal gains that were observed at 9.4 T are presented in Fig. 6.

For isopropylamine ($i\text{PrNH}_2$), the SABRE-RELAY polarised NH_2 signal showed a 220-fold signal gain while 27- and 150-fold enhancements were seen for the CH and CH_3 resonances respectively. This reflects a breakthrough as $i\text{PrNH}_2$ was unable to be directly polarised by SABRE due to its steric bulk preventing adequate binding. Dibenzylamine (Bn_2NH) was also successfully polarised using this method, and yields ^1H signal gains of 274- (NH) , 200- (CH_2) and 395-fold (Ph) per proton.

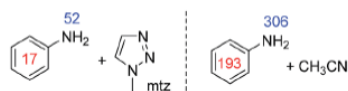
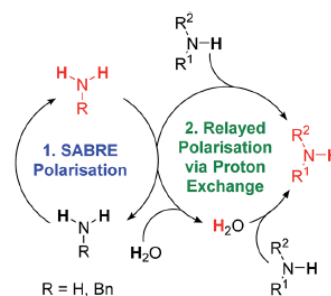


Fig. 5 ^1H NMR signal gains per proton observed for the indicated aniline resonances when hyperpolarised by SABRE in the presence of the described co-ligand at 9.4 T.



Scheme 2 SABRE-RELAY polarisation of amines. (1) SABRE polarisation of an intermediary transfer agent, in this case a primary amine or ammonia. (2) Polarisation is then relayed into the target amine via proton exchange, either directly or via residual water present in the sample.

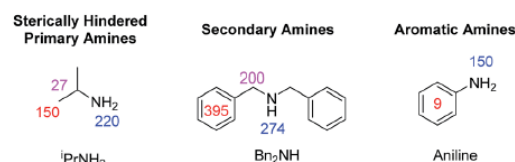


Fig. 6 ^1H NMR signal gains observed per proton for the indicated amine resonances when hyperpolarised by SABRE-RELAY using 2-NH_3 at 9.4 T.

Additionally, a ^{13}C spectrum can be acquired in a single scan on these materials after polarisation transfer at 60 G such that a 475-fold signal gain for the CH_2 resonance is observed. Full NMR spectra are available in the ESI.† Furthermore, the aromatic amine, aniline, now exhibits a 150-fold NH_2 proton signal enhancement and a 9-fold signal gain for the phenyl ring under analogous conditions. We note that these signal gains are lower than those seen when CH_3CN is used as a co-ligand to achieve direct SABRE transfer as detailed in Fig. 5. We suggest that this difference in behaviour arises because a 60 G polarisation transfer field is no-longer optimal for intra-molecular polarisation transfer after proton exchange. This is clearly not the case for transfer via directly bound aniline and the complex scalar coupling network which is in fact commonly maximised for ^1H transfer at 60 G.

From these results we can conclude that the SABRE-RELAY effect is able to polarise sterically hindered primary amines, secondary amines and aromatic amines that are not themselves accessible to SABRE. Thus, the scope of amine polarisation is vastly increased.

Conclusions

In summary, we have shown here how SABRE can be used to hyperpolarise a series of primary amines. This substrate extension opens up the SABRE approach to operate with a much wider range of analytes than was previously thought possible, as



we extend beyond the original aromatic N-heterocycles, imines and nitriles. Activity is achieved by the formation of a series of complexes of the form $[\text{Ir}(\text{H})_2(\text{IMes})(\text{amine})_3]\text{Cl}$. Relaxation studies, in conjunction with ligand dissociation rate measurements were used to demonstrate that the high relative stability of these complexes acts to limit the degree of SABRE signal gain. This hypothesis is consistent with the fact that increasing the $p\text{-H}_2$ pressure or reaction temperature leads to improved signal gains. Therefore, significant catalyst optimisation will be important if very high levels of hyperpolarisation are to be achieved by this route in the future.

Nonetheless, in the case of BnNH_2 , ^1H NMR signal enhancement values of ~ 100 -fold per NH proton were achieved for benzylamine using $[\text{IrCl}(\text{COD})(\text{IMes})]$. Consequently, when d_7 -benzylamine was used, the resulting focusing of the hyperpolarisation into the NH_2 resonance resulted in a 900-fold signal enhancement per proton at 9.4 T with a $p\text{-H}_2$ pressure of 3 bar. This value reduced to 33-fold for $\text{Bn}^{15}\text{NH}_2$ after transfer at 60 G. Hence, we predict that further improvements can be made through a more detailed study of the effect of isotopic labelling.^{18,19,57} We have also demonstrated transfer to ^{13}C and ^{15}N with diagnostic NMR spectra being collected at a 35 mM concentration in a single scan. We predict that application of high-field SABRE transfer techniques,^{34–37,39} such as the LIGHT-SABRE³⁸ approach, might subsequently enable this process to work inside the magnet, but note that a rigorous study of the effect the polarisation transfer field plays on the resulting signal enhancement levels is justified.

In the course of these studies we found that sterically hindered primary amines, secondary amines and aromatic amines were unable to form an active SABRE catalyst of the type $[\text{Ir}(\text{H})_2(\text{IMes})(\text{amine})_3]\text{Cl}$. This meant that direct polarisation transfer *via* such a complex was not possible. We found for aniline that the addition of a co-ligand such as CH_3CN overcame this problem *via* the formation of $[\text{Ir}(\text{H})_2(\text{IMes})(\text{aniline})_2(\text{CH}_3\text{CN})]\text{Cl}$ such that signal enhancements of up to 306-fold per NH proton could be achieved.

An indirect route was described to overcome this limitation more generally, such that hindered primary amines, secondary amines and aromatic amines can be hyperpolarised by SABRE-RELAY.⁵⁴ Now, a SABRE-hyperpolarised intermediary, such as ammonia, is able to readily transfer polarisation into agents such as isopropylamine, benzylamine and aniline *via* either direct proton exchange or mediated by residual water present in the sample. This approach expands the range of amines that can be hyperpolarised without changing their chemical identity through interactions with $p\text{-H}_2$.

Given the increase in signal intensity that is observed for the amines in this study, we are now working towards their use as agents for mechanistic study^{58–64} in transfer hydrogenation,^{65,66} hydroamination,^{67,68} and vitally important N_2 fixation reactions.^{69–71} Additionally, since phenylethylamine is a naturally occurring monoamine based alkaloid that acts as a promoter of catecholamine (dopamine and norepinephrine) release in plants and animals we expect these observations to be of wide interest.^{72,73} Furthermore, the SABRE-RELAY method⁵⁴ has recently been shown to offer a route to hyperpolarise an even

larger range of hydrogen transfer acceptors using OH functional groups. Optimisation of the intermediaries NH polarisation level reflects a key part to optimisation of this technique and hence these results will be of interest to any potential developer.

Conflicts of interest

The authors declare no conflicts of interest.

Acknowledgements

This work was supported by The Wellcome Trust (Grants 092506 and 098335), the EPSRC (EP/R51181X/1) and the University of York.

References

- 1 S. B. Duckett and R. E. Mewis, *Acc. Chem. Res.*, 2012, 45, 1247–1257.
- 2 C. R. Bowers and D. P. Weitekamp, *J. Am. Chem. Soc.*, 1987, 109, 5541–5542.
- 3 J. Natterer and J. Bargon, *Prog. Nucl. Magn. Reson. Spectrosc.*, 1997, 31, 293–315.
- 4 R. A. Green, R. W. Adams, S. B. Duckett, R. E. Mewis, D. C. Williamson and G. G. R. Green, *Prog. Nucl. Magn. Reson. Spectrosc.*, 2012, 67, 1–48.
- 5 C. R. Bowers and D. P. Weitekamp, *Phys. Rev. Lett.*, 1986, 57, 2645–2648.
- 6 J. Colell, P. Türschmann, S. Glöggler, P. Schleker, T. Theis, M. Ledbetter, D. Budker, A. Pines, B. Blümich and S. Appelt, *Phys. Rev. Lett.*, 2013, 110, 137602.
- 7 R. W. Adams, J. A. Aguilar, K. D. Atkinson, M. J. Cowley, P. I. P. Elliott, S. B. Duckett, G. G. R. Green, I. G. Khazal, J. Lopez-Serrano and D. C. Williamson, *Science*, 2009, 323, 1708–1711.
- 8 P. J. Rayner and S. Duckett, *Angew. Chem., Int. Ed.*, 2018, DOI: 10.1002/anie.201710406.
- 9 R. W. Adams, S. B. Duckett, R. A. Green, D. C. Williamson and G. G. R. Green, *J. Chem. Phys.*, 2009, 131, 194505.
- 10 A. N. Pravdivtsev, A. V. Yurkovskaya, H. M. Vieth, K. L. Ivanov and R. Kaptein, *ChemPhysChem*, 2013, 14, 3327–3331.
- 11 A. N. Pravdivtsev, K. L. Ivanov, A. V. Yurkovskaya, P. A. Petrov, H. H. Limbach, R. Kaptein and H. M. Vieth, *J. Magn. Reson.*, 2015, 261, 73–82.
- 12 K. D. Atkinson, M. J. Cowley, P. I. P. Elliott, S. B. Duckett, G. G. R. Green, J. Lopez-Serrano and A. C. Whitwood, *J. Am. Chem. Soc.*, 2009, 131, 13362–13368.
- 13 N. Eshuis, R. Aspers, B. J. A. van Weerdenburg, M. C. Feiters, F. Rutjes, S. S. Wijmenga and M. Tessari, *J. Magn. Reson.*, 2016, 265, 59–66.
- 14 M. L. Truong, T. Theis, A. M. Coffey, R. V. Shchepin, K. W. Waddell, F. Shi, B. M. Goodson, W. S. Warren and E. Y. Chekmenev, *J. Phys. Chem. C*, 2015, 119, 8786–8797.
- 15 T. Theis, M. L. Truong, A. M. Coffey, R. V. Shchepin, K. W. Waddell, F. Shi, B. M. Goodson, W. S. Warren and E. Y. Chekmenev, *J. Am. Chem. Soc.*, 2015, 137, 1404–1407.



- 16 R. V. Shchepin, L. Jaigirdar, T. Theis, W. S. Warren, B. M. Goodson and E. Y. Chekmenev, *J. Phys. Chem. C*, 2017, 121, 28425–28434.
- 17 M. J. Cowley, R. W. Adams, K. D. Atkinson, M. C. R. Cockett, S. B. Duckett, G. G. R. Green, J. A. B. Lohman, R. Kerssebaum, D. Kilgour and R. E. Mewis, *J. Am. Chem. Soc.*, 2011, 133, 6134–6137.
- 18 M. Fekete, O. Bayfield, S. B. Duckett, S. Hart, R. E. Mewis, N. Pridmore, P. J. Rayner and A. Whitwood, *Inorg. Chem.*, 2013, 52, 13453–13461.
- 19 P. J. Rayner, M. J. Burns, A. M. Oлару, P. Norcott, M. Fekete, G. G. R. Green, L. A. R. Highton, R. E. Mewis and S. B. Duckett, *Proc. Natl. Acad. Sci. U. S. A.*, 2017, 114, E3188–E3194.
- 20 R. V. Shchepin, D. A. Barskiy, D. M. Mikhaylov and E. Y. Chekmenev, *Bioconjugate Chem.*, 2016, 27, 878–882.
- 21 H. F. Zeng, J. D. Xu, J. Gillen, M. T. McMahon, D. Artemov, J. M. Tyburn, J. A. B. Lohman, R. E. Mewis, K. D. Atkinson, G. G. R. Green, S. B. Duckett and P. C. M. van Zijl, *J. Magn. Reson.*, 2013, 237, 73–78.
- 22 P. Norcott, P. J. Rayner, G. G. R. Green and S. B. Duckett, *Chem.–Eur. J.*, 2017, 23, 16990–16997.
- 23 D. A. Barskiy, R. V. Shchepin, A. M. Coffey, T. Theis, W. S. Warren, B. M. Goodson and E. Y. Chekmenev, *J. Am. Chem. Soc.*, 2016, 138, 8080–8083.
- 24 E. B. Ducker, L. T. Kuhn, K. Munnemann and C. Griesinger, *J. Magn. Reson.*, 2012, 214, 159–165.
- 25 A. W. J. Logan, T. Theis, J. F. P. Colell, W. S. Warren and S. J. Malcolmson, *Chem.–Eur. J.*, 2016, 22, 10777–10781.
- 26 T. Theis, G. X. Ortiz, A. W. J. Logan, K. E. Claytor, Y. Feng, W. P. Huhn, V. Blum, S. J. Malcolmson, E. Y. Chekmenev, Q. Wang and W. S. Warren, *Sci. Adv.*, 2016, 2, e1501438.
- 27 R. E. Mewis, R. A. Green, M. C. R. Cockett, M. J. Cowley, S. B. Duckett, G. G. R. Green, R. O. John, P. J. Rayner and D. C. Williamson, *J. Phys. Chem. B*, 2015, 119, 1416–1424.
- 28 R. E. Mewis, K. D. Atkinson, M. J. Cowley, S. B. Duckett, G. G. R. Green, R. A. Green, L. A. R. Highton, D. Kilgour, L. S. Lloyd, J. A. B. Lohman and D. C. Williamson, *Magn. Reson. Chem.*, 2014, 52, 358–369.
- 29 J. F. P. Colell, A. W. J. Logan, Z. J. Zhou, R. V. Shchepin, D. A. Barskiy, G. X. Ortiz, Q. Wang, S. J. Malcolmson, E. Y. Chekmenev, W. S. Warren and T. Theis, *J. Phys. Chem. C*, 2017, 121, 6626–6634.
- 30 D. A. Barskiy, R. V. Shchepin, C. P. N. Tanner, J. F. P. Colell, B. M. Goodson, T. Theis, W. S. Warren and E. Y. Chekmenev, *ChemPhysChem*, 2017, 18, 1493–1498.
- 31 V. V. Zhivonitko, I. V. Skovpin and I. V. Koptuyug, *Chem. Commun.*, 2015, 51, 2506–2509.
- 32 M. J. Burns, P. J. Rayner, G. G. R. Green, L. A. R. Highton, R. E. Mewis and S. B. Duckett, *J. Phys. Chem. B*, 2015, 119, 5020–5027.
- 33 A. M. Oлару, A. Burt, P. J. Rayner, S. J. Hart, A. C. Whitwood, G. G. R. Green and S. B. Duckett, *Chem. Commun.*, 2016, 52, 14482–14485.
- 34 K. D. Atkinson, M. J. Cowley, S. B. Duckett, P. I. P. Elliott, G. G. R. Green, J. Lopez-Serrano, I. G. Khazal and A. C. Whitwood, *Inorg. Chem.*, 2009, 48, 663–670.
- 35 D. A. Barskiy, K. V. Kovtunov, I. V. Koptuyug, P. He, K. A. Groome, Q. A. Best, F. Shi, B. M. Goodson, R. V. Shchepin, A. M. Coffey, K. W. Waddell and E. Y. Chekmenev, *J. Am. Chem. Soc.*, 2014, 136, 3322–3325.
- 36 S. Knecht, A. S. Kiryutin, A. V. Yurkovskaya and K. L. Ivanov, *J. Magn. Reson.*, 2018, 287, 74–81.
- 37 S. S. Roy, G. Stevanato, P. J. Rayner and S. B. Duckett, *J. Magn. Reson.*, 2017, 285, 55–60.
- 38 T. Theis, M. Truong, A. M. Coffey, E. Y. Chekmenev and W. S. Warren, *J. Magn. Reson.*, 2014, 248, 23–26.
- 39 A. N. Pravdivtsev, A. V. Yurkovskaya, H.-M. Vieth and K. L. Ivanov, *J. Phys. Chem. B*, 2015, 119, 13619–13629.
- 40 M. Carravetta, O. G. Johannessen and M. H. Levitt, *Phys. Rev. Lett.*, 2004, 92, 1177–1182.
- 41 T. Theis, G. X. Ortiz, A. W. J. Logan, K. E. Claytor, Y. Feng, W. P. Huhn, V. Blum, S. J. Malcolmson, E. Y. Chekmenev, Q. Wang and W. S. Warren, *Sci. Adv.*, 2016, 2, e1501438.
- 42 A. M. Oлару, S. S. Roy, L. S. Lloyd, S. Coombes, G. G. R. Green and S. B. Duckett, *Chem. Commun.*, 2016, 52, 7842–7845.
- 43 S. S. Roy, P. Norcott, P. J. Rayner, G. G. R. Green and S. B. Duckett, *Angew. Chem., Int. Ed.*, 2016, 55, 15642–15645.
- 44 S. S. Roy, P. J. Rayner, P. Norcott, G. G. R. Green and S. B. Duckett, *Phys. Chem. Chem. Phys.*, 2016, 18, 24905–24911.
- 45 S. S. Roy, P. Norcott, P. J. Rayner, G. G. R. Green and S. B. Duckett, *Chem.–Eur. J.*, 2017, 23, 10496–10500.
- 46 Z. Zhou, J. Yu, J. F. P. Colell, R. Laasner, A. Logan, D. A. Barskiy, R. V. Shchepin, E. Y. Chekmenev, V. Blum, W. S. Warren and T. Theis, *J. Phys. Chem. Lett.*, 2017, 8, 3008–3014.
- 47 V. Daniele, F.-X. Legrand, P. Berthault, J.-N. Dumez and G. Huber, *ChemPhysChem*, 2015, 16, 3413–3417.
- 48 N. Eshuis, B. J. A. van Weerdenburg, M. C. Feiters, F. P. J. T. Rutjes, S. S. Wijmenga and M. Tessari, *Angew. Chem., Int. Ed.*, 2015, 54, 1481–1484.
- 49 L. S. Lloyd, R. W. Adams, M. Bernstein, S. Coombes, S. B. Duckett, G. G. R. Green, R. J. Lewis, R. E. Mewis and C. J. Sleight, *J. Am. Chem. Soc.*, 2012, 134, 12904–12907.
- 50 I. Reile, R. L. E. G. Asperts, J.-M. Tyburn, J. G. Kempf, M. C. Feiters, F. P. J. T. Rutjes and M. Tessari, *Angew. Chem., Int. Ed.*, 2017, 56, 9174–9177.
- 51 W. N. O. Wylie, A. J. Lough and R. H. Morris, *Organometallics*, 2013, 32, 3808–3818.
- 52 Y. Sato, Y. Kayaki and T. Ikariya, *Organometallics*, 2016, 35, 1257–1264.
- 53 M.-L. Yuan, J.-H. Xie, S.-F. Zhu and Q.-L. Zhou, *ACS Catal.*, 2016, 6, 3665–3669.
- 54 W. Iali, P. J. Rayner and S. B. Duckett, *Sci. Adv.*, 2018, 4, eaa06250.
- 55 L. S. Lloyd, A. Asghar, M. J. Burns, A. Charlton, S. Coombes, M. J. Cowley, G. J. Dear, S. B. Duckett, G. R. Genov, G. G. R. Green, L. A. R. Highton, A. J. J. Hooper, M. Khan, I. G. Khazal, R. J. Lewis, R. E. Mewis, A. D. Roberts and A. J. Ruddlesden, *Catal. Sci. Technol.*, 2014, 4, 3544–3554.
- 56 R. V. Shchepin, M. L. Truong, T. Theis, A. M. Coffey, F. Shi, K. W. Waddell, W. S. Warren, B. M. Goodson and E. Y. Chekmenev, *J. Phys. Chem. Lett.*, 2015, 6, 1961–1967.



- 57 M. Fekete, P. J. Rayner, G. G. R. Green and S. B. Duckett, *Magn. Reson. Chem.*, 2017, 55, 944–957.
- 58 O. G. Salnikov, K. V. Kovtunov, D. A. Barskiy, A. K. Khudorozhkov, E. A. Inozemtseva, I. P. Prosvirin, V. I. Bukhtiyarov and I. V. Kopyug, *ACS Catal.*, 2014, 4, 2022–2028.
- 59 M. Leutzsch, L. M. Wolf, P. Gupta, M. Fuchs, W. Thiel, C. Fares and A. Furstner, *Angew. Chem., Int. Ed.*, 2015, 54, 12431–12436.
- 60 R. V. Shchepin, D. A. Barskiy, A. M. Coffey, B. M. Goodson and E. Y. Chekmenev, *ChemistrySelect*, 2016, 1, 2552–2555.
- 61 C. Godard, S. B. Duckett, S. Polas, R. Tooze and A. C. Whitwood, *Dalton Trans.*, 2009, 2496–2509.
- 62 D. J. Fox, S. B. Duckett, C. Flaschenriem, W. W. Brennessel, J. Schneider, A. Gunay and R. Eisenberg, *Inorg. Chem.*, 2006, 45, 7197–7209.
- 63 D. Blazina, S. B. Duckett, P. J. Dyson and J. A. B. Lohman, *Angew. Chem., Int. Ed.*, 2001, 40, 3874–3877.
- 64 S. A. Colebrooke, S. B. Duckett, J. A. B. Lohman and R. Eisenberg, *Chem.–Eur. J.*, 2004, 10, 2459–2474.
- 65 J. S. M. Samec, J. E. Backvall, P. G. Andersson and P. Brandt, *Chem. Soc. Rev.*, 2006, 35, 237–248.
- 66 S. E. Clapham, A. Hadzovic and R. H. Morris, *Coord. Chem. Rev.*, 2004, 248, 2201–2237.
- 67 M. Patel, R. K. Saunthwal and A. K. Verma, *Acc. Chem. Res.*, 2017, 50, 240–254.
- 68 T. E. Muller, K. C. Hultsch, M. Yus, F. Foubelo and M. Tada, *Chem. Rev.*, 2008, 108, 3795–3892.
- 69 J. S. Anderson, J. Rittle and J. C. Peters, *Nature*, 2013, 501, 84–87.
- 70 H. P. Jia and E. A. Quadrelli, *Chem. Soc. Rev.*, 2014, 43, 547–564.
- 71 S. Kuriyama, K. Arashiba, K. Nakajima, H. Tanaka, N. Kamaru, K. Yoshizawa and Y. Nishibayashi, *J. Am. Chem. Soc.*, 2014, 136, 9719–9731.
- 72 R. T. Premont, R. R. Gainetdinov and M. G. Caron, *Proc. Natl. Acad. Sci. U. S. A.*, 2001, 98, 9474–9475.
- 73 I. A. Paterson, A. V. Juorio and A. A. Boulton, *J. Neurochem.*, 1990, 55, 1827–1837.



Abbreviations

μl – microliter

μm – micrometre

B – Boltzmann distribution

μl – microliter

br – broad

BnNH₂ - Benzylamine

COD – 1,5-cyclooctadiene

COPD - Chronic Obstructive
Pulmonary Disease

d – deuterated

d – doublet

COD – 1,5-cyclooctadiene

DMSO – dimethylsulfoxide

DNP – Dynamic Nuclear Polarisation

d-DNP - dissolution-DNP

G – Gauss

Hz – hertz

IMes - 1,3-bis(2,4,6-
trimethylphenyl)imidazole-2-ylidene

INEPT – Insensitive Nuclei Enhanced
by Polarisation Transfer

J – scalar coupling

K – Kelvin

m – multiplet

k_B – Boltzmann constant

mM – millimoles per dm³

min – minute

MRI – Magnetic Resonance Imaging

mT – millitesla

M_{xy} – Magnetisation in the xy plane

M_z – Magnetisation in the z direction

N_α – number of spins in alpha state

N_β – number of spins in beta state

NMR – Nuclear Magnetic Resonance

PEA – phenethylamine

Para-H₂ – parahydrogen

PC – phosphatidylcholine

PE – phosphatidylethanolamine

PHIP – Parahydrogen Induced
Polarisation

ppm – parts per million

PTF – polarisation transfer field

RF – radiofrequency

SABRE – Signal Amplification by
Reversible Exchange

SABRE-SHEATH – SABRE in
shield enables alignment transfer to
heteronuclei)

S_{hyp} – hyperpolarised signal

S_{therm} – thermal signal

T - temperature

T – Tesla

T₁ – longitudinal relaxation time

ΔE – energy difference

References

1. Li, L.; Zhang, Q.; Huang, D., A review of imaging techniques for plant phenotyping. *Sensors* **2014**, *14* (11), 20078-20111.
2. Holzgrabe, U.; Deubner, R.; Schollmayer, C.; Waibel, B., Quantitative NMR spectroscopy—applications in drug analysis. *Journal of pharmaceutical and biomedical analysis* **2005**, *38* (5), 806-812.
3. Jones, C.; Ravenscroft, N., NMR assays for carbohydrate-based vaccines. *NMR spectroscopy in pharmaceutical analysis* **2008**, 341-368.
4. Kirtil, E.; Oztop, M. H., ¹H nuclear magnetic resonance relaxometry and magnetic resonance imaging and applications in food science and processing. *Food Engineering Reviews* **2016**, *8* (1), 1-22.
5. Pauli, G. F.; Jaki, B. U.; Lankin, D. C., Quantitative ¹H NMR: development and potential of a method for natural products analysis. *Journal of natural products* **2005**, *68* (1), 133-149.
6. Politi, M.; Zloh, M.; Pintado, M. E.; Castro, P. M.; Heinrich, M.; Prieto, J. M., Direct metabolic fingerprinting of commercial herbal tinctures by nuclear magnetic resonance spectroscopy and mass spectrometry. *Phytochemical Analysis* **2009**, *20* (4), 328-334.
7. d'Avila, M.; Powell, R.; Phillips, R.; Shapley, N.; Walton, J.; Dungan, S., Magnetic resonance imaging (MRI): a technique to study flow and microstructure of concentrated emulsions. *Brazilian Journal of Chemical Engineering* **2005**, *22* (1), 49-60.
8. Borisjuk, L.; Rolletschek, H.; Neuberger, T., Surveying the plant's world by magnetic resonance imaging. *The Plant Journal* **2012**, *70* (1), 129-146.
9. Windt, C. W.; Vergeldt, F. J.; De Jager, P. A.; Van As, H., MRI of long-distance water transport: a comparison of the phloem and xylem flow characteristics and dynamics in poplar, castor bean, tomato and tobacco. *Plant, Cell & Environment* **2006**, *29* (9), 1715-1729.
10. Kim, H. K.; Choi, Y. H.; Verpoorte, R., NMR-based metabolomic analysis of plants. *Nature protocols* **2010**, *5* (3), 536-549.
11. Moradi, A.; Oswald, S.; Nordmeyer-Massner, J.; Pruessmann, K.; Robinson, B.; Schulin, R., Analysis of nickel concentration profiles around the roots of the hyperaccumulator plant *Berkheya coddii* using MRI and numerical simulations. *Plant and soil* **2010**, *328* (1-2), 291-302.
12. Melkus, G.; Rolletschek, H.; Fuchs, J.; Radchuk, V.; Grafahrend-Belau, E.; Sreenivasulu, N.; Rutten, T.; Weier, D.; Heinzl, N.; Schreiber, F., Dynamic ¹³C/¹H NMR imaging uncovers sugar allocation in the living seed. *Plant biotechnology journal* **2011**, *9* (9), 1022-1037.
13. Schroeder, M. A.; Lau, A. Z.; Chen, A. P.; Gu, Y.; Nagendran, J.; Barry, J.; Hu, X.; Dyck, J. R.; Tyler, D. J.; Clarke, K., Hyperpolarized ¹³C magnetic resonance reveals early- and late-onset changes to in vivo pyruvate metabolism in the failing heart. *European journal of heart failure* **2013**, *15* (2), 130-140.
14. Fujiwara, T.; Ramamoorthy, A., How far can the sensitivity of NMR be increased? *Annual Reports on NMR Spectroscopy* **2006**, *58*, 155-175.
15. Duckett, S. B.; Wood, N. J., Parahydrogen-based NMR methods as a mechanistic probe in inorganic chemistry. *Coordination Chemistry Reviews* **2008**, *252* (21-22), 2278-2291.

16. Duckett, S. B.; Mewis, R. E., Application of para hydrogen induced polarization techniques in NMR spectroscopy and imaging. *Accounts of chemical research* **2012**, *45* (8), 1247-1257.
17. Hore, P. J., *Nuclear magnetic resonance*. Oxford University Press, USA: 2015.
18. Walker, T. G.; Happer, W., Spin-exchange optical pumping of noble-gas nuclei. *Reviews of modern physics* **1997**, *69* (2), 629.
19. Schroeder, M. A.; Cochlin, L. E.; Heather, L. C.; Clarke, K.; Radda, G. K.; Tyler, D. J., In vivo assessment of pyruvate dehydrogenase flux in the heart using hyperpolarized carbon-13 magnetic resonance. *Proceedings of the National Academy of Sciences* **2008**, *105* (33), 12051-12056.
20. Viale, A.; Aime, S., Current concepts on hyperpolarized molecules in MRI. *Current opinion in chemical biology* **2010**, *14* (1), 90-96.
21. Gorter, C., Kernentmagnetisierung. *Phys. Z* **1934**, *35*, 923.
22. Kaindl, G.; Bacon, F.; Shirley, D., Magnetic Moment and Spin of 6.9-h Mo m 93. *Physical Review C* **1973**, *8* (1), 315.
23. Brewer, W.; Kopp, M., Brute-force nuclear orientation. *Hyperfine Interactions* **1976**, *2* (2), 299-305.
24. Aime, S.; Dastru, W.; Gobetto, R.; Santelia, D.; Viale, A., Agents for polarization enhancement in MRI. *Molecular Imaging I* **2008**, 247-272.
25. Halse, M. E., Perspectives for hyperpolarisation in compact NMR. *TrAC Trends in Analytical Chemistry* **2016**, *83*, 76-83.
26. Månsson, S.; Johansson, E.; Magnusson, P.; Chai, C.-M.; Hansson, G.; Petersson, J. S.; Ståhlberg, F.; Golman, K., 13C imaging—a new diagnostic platform. *European radiology* **2006**, *16* (1), 57-67.
27. Owers-Bradley, J. R.; Horsewill, A. J.; Peat, D. T.; Goh, K. S.; Gadian, D. G., High polarization of nuclear spins mediated by nanoparticles at millikelvin temperatures. *Physical Chemistry Chemical Physics* **2013**, *15* (25), 10413-10417.
28. Hirsch, M. L.; Kalechofsky, N.; Belzer, A.; Rosay, M.; Kempf, J. G., Brute-force hyperpolarization for NMR and MRI. *Journal of the American Chemical Society* **2015**, *137* (26), 8428-8434.
29. Happer, W., Optical pumping. *Reviews of Modern Physics* **1972**, *44* (2), 169.
30. Suter, D., Sensitivity of optically excited and detected magnetic resonance. *Journal of Magnetic Resonance (1969)* **1992**, *99* (3), 495-506.
31. Albert, M.; Cates, G.; Driehuys, B.; Happer, W.; Saam, B.; Springer, C.; Wishnia, A., Biological magnetic resonance imaging using laser-polarized 129Xe. *Nature* **1994**, *370* (6486), 199-201.
32. van Beek, E. J.; Wild, J. M.; Kauczor, H. U.; Schreiber, W.; Mugler, J. P.; de Lange, E. E., Functional MRI of the lung using hyperpolarized 3-helium gas. *Journal of Magnetic Resonance Imaging* **2004**, *20* (4), 540-554.
33. Kirby, M.; Svenningsen, S.; Owrangi, A.; Wheatley, A.; Farag, A.; Ouriadov, A.; Santyr, G. E.; Etemad-Rezai, R.; Coxson, H. O.; McCormack, D. G., Hyperpolarized 3He and 129Xe MR imaging in healthy volunteers and patients with chronic obstructive pulmonary disease. *Radiology* **2012**, *265* (2), 600-610.
34. Wild, J. M.; Paley, M. N.; Kasuboski, L.; Swift, A.; Fischele, S.; Woodhouse, N.; Griffiths, P. D.; van Beek, E. J., Dynamic radial projection MRI of inhaled hyperpolarized 3He gas. *Magnetic Resonance in Medicine: An Official Journal of the International Society for Magnetic Resonance in Medicine* **2003**, *49* (6), 991-997.
35. Martin, C. C.; Williams, R. F.; Gao, J. H.; Nickerson, L. D.; Xiong, J.; Fox, P. T., The pharmacokinetics of hyperpolarized xenon: implications for cerebral MRI. *Journal of Magnetic Resonance Imaging* **1997**, *7* (5), 848-854.

36. Bartik, K.; Luhmer, M.; Dutasta, J.-P.; Collet, A.; Reisse, J., ¹²⁹Xe and ¹H NMR study of the reversible trapping of xenon by cryptophane-A in organic solution. *Journal of the American Chemical Society* **1998**, *120* (4), 784-791.
37. Spence, M. M.; Rubin, S. M.; Dimitrov, I. E.; Ruiz, E. J.; Wemmer, D. E.; Pines, A.; Yao, S. Q.; Tian, F.; Schultz, P. G., Functionalized xenon as a biosensor. *Proceedings of the National Academy of Sciences* **2001**, *98* (19), 10654-10657.
38. Maly, T.; Debelouchina, G. T.; Bajaj, V. S.; Hu, K.-N.; Joo, C.-G.; Mak-Jurkauskas, M. L.; Sirigiri, J. R.; Van Der Wel, P. C.; Herzfeld, J.; Temkin, R. J., Dynamic nuclear polarization at high magnetic fields. *The Journal of chemical physics* **2008**, *128* (5), 02B611.
39. Overhauser, A. W., Polarization of nuclei in metals. *Physical Review* **1953**, *92* (2), 411.
40. Carver, T. R.; Slichter, C. P., Polarization of nuclear spins in metals. *Physical Review* **1953**, *92* (1), 212.
41. Hovav, Y.; Levinkron, O.; Feintuch, A.; Vega, S., Theoretical aspects of dynamic nuclear polarization in the solid state: the influence of high radical concentrations on the solid effect and cross effect mechanisms. *Applied Magnetic Resonance* **2012**, *43* (1), 21-41.
42. Hovav, Y.; Feintuch, A.; Vega, S., Theoretical aspects of dynamic nuclear polarization in the solid state—spin temperature and thermal mixing. *Physical Chemistry Chemical Physics* **2013**, *15* (1), 188-203.
43. Banerjee, D.; Shimon, D.; Feintuch, A.; Vega, S.; Goldfarb, D., The interplay between the solid effect and the cross effect mechanisms in solid state ¹³C DNP at 95 GHz using trityl radicals. *Journal of Magnetic Resonance* **2013**, *230*, 212-219.
44. Abragam, A.; Goldman, M., *Rep. Prog. Phys.* **1978**.
45. Wollan, D. S., Dynamic nuclear polarization with an inhomogeneously broadened ESR line. I. Theory. *Physical Review B* **1976**, *13* (9), 3671.
46. Ardenkjær-Larsen, J. H.; Fridlund, B.; Gram, A.; Hansson, G.; Hansson, L.; Lerche, M. H.; Servin, R.; Thaning, M.; Golman, K. J. P. o. t. N. A. o. S., Increase in signal-to-noise ratio of > 10,000 times in liquid-state NMR. **2003**, *100* (18), 10158-10163.
47. Kim, Y.; Hilty, C., Applications of Dissolution-DNP for NMR Screening. In *Methods in enzymology*, Elsevier: 2019; Vol. 615, pp 501-526.
48. Slichter, C. P., The discovery and renaissance of dynamic nuclear polarization. *Reports on Progress in Physics* **2014**, *77* (7), 072501.
49. Zhang, G.; Hilty, C., Applications of dissolution dynamic nuclear polarization in chemistry and biochemistry. *Magnetic Resonance in Chemistry* **2018**, *56* (7), 566-582.
50. Flori, A.; Frijia, F.; Lionetti, V.; Ardenkjaer-Larsen, J. H.; Positano, V.; Giovannetti, G.; Schulte, R. F.; Wiesinger, F.; Recchia, F. A.; Landini, L., DNP methods for cardiac metabolic imaging with hyperpolarized [1-¹³C] pyruvate large dose injection in pigs. *Applied Magnetic Resonance* **2012**, *43* (1), 299-310.
51. Lumata, L.; Merritt, M. E.; Malloy, C. R.; Sherry, A. D.; Kovacs, Z., Impact of Gd³⁺ on DNP of [1-¹³C] pyruvate doped with trityl OX063, BDPA, or 4-oxo-TEMPO. *The journal of physical chemistry A* **2012**, *116* (21), 5129-5138.
52. Balzan, R.; Fernandes, L.; Pidial, L.; Comment, A.; Tavitian, B.; Vasos, P. R., Pyruvate cellular uptake and enzymatic conversion probed by dissolution DNP-NMR: the impact of overexpressed membrane transporters. *Magnetic Resonance in Chemistry* **2017**, *55* (6), 579-583.
53. Hu, S.; Larson, P. E.; VanCrickinge, M.; Leach, A. M.; Park, I.; Leon, C.; Zhou, J.; Shin, P. J.; Reed, G.; Keselman, P., Rapid sequential injections of hyperpolarized [1-¹³C] pyruvate in vivo using a sub-kelvin, multi-sample DNP polarizer. *Magnetic resonance imaging* **2013**, *31* (4), 490-496.
54. Warburg, O.; Wind, F.; Negelein, E., The metabolism of tumors in the body. *The Journal of general physiology* **1927**, *8* (6), 519.

55. Kurhanewicz, J.; Vigneron, D. B.; Brindle, K.; Chekmenev, E. Y.; Comment, A.; Cunningham, C. H.; DeBerardinis, R. J.; Green, G. G.; Leach, M. O.; Rajan, S. S., Analysis of cancer metabolism by imaging hyperpolarized nuclei: prospects for translation to clinical research. *Neoplasia* **2011**, *13* (2), 81-97.
56. Fernie, A. R.; Carrari, F.; Sweetlove, L. J., Respiratory metabolism: glycolysis, the TCA cycle and mitochondrial electron transport. *Current opinion in plant biology* **2004**, *7* (3), 254-261.
57. Jannin, S.; Dumez, J.-N.; Giraudeau, P.; Kurzbach, D., Application and methodology of dissolution dynamic nuclear polarization in physical, chemical and biological contexts. *Journal of Magnetic Resonance* **2019**, *305*, 41-50.
58. Adams, R. W.; Aguilar, J. A.; Atkinson, K. D.; Cowley, M. J.; Elliott, P. I.; Duckett, S. B.; Green, G. G.; Khazal, I. G.; López-Serrano, J.; Williamson, D. C., Reversible interactions with para-hydrogen enhance NMR sensitivity by polarization transfer. *Science* **2009**, *323* (5922), 1708-1711.
59. Hövener, J. B.; Pravdivtsev, A. N.; Kidd, B.; Bowers, C. R.; Glögler, S.; Kovtunov, K. V.; Plaumann, M.; Katz-Brull, R.; Buckenmaier, K.; Jerschow, A., Parahydrogen-based hyperpolarization for biomedicine. *Angewandte Chemie International Edition* **2018**, *57* (35), 11140-11162.
60. Adams, R. W.; Duckett, S. B.; Green, R. A.; Williamson, D. C.; Green, G. G., A theoretical basis for spontaneous polarization transfer in non-hydrogenative para hydrogen-induced polarization. *The Journal of chemical physics* **2009**, *131* (19), 194505.
61. Theis, T.; Truong, M. L.; Coffey, A. M.; Shchepin, R. V.; Waddell, K. W.; Shi, F.; Goodson, B. M.; Warren, W. S.; Chekmenev, E. Y., Microtesla SABRE enables 10% nitrogen-15 nuclear spin polarization. *Journal of the American Chemical Society* **2015**, *137* (4), 1404-1407.
62. Barskiy, D. A.; Shchepin, R. V.; Tanner, C. P.; Colell, J. F.; Goodson, B. M.; Theis, T.; Warren, W. S.; Chekmenev, E. Y., The absence of quadrupolar nuclei facilitates efficient ¹³C hyperpolarization via reversible exchange with parahydrogen. *ChemPhysChem* **2017**, *18* (12), 1493-1498.
63. Shchepin, R. V.; Goodson, B. M.; Theis, T.; Warren, W. S.; Chekmenev, E. Y., Toward hyperpolarized ¹⁹F molecular imaging via reversible exchange with parahydrogen. *ChemPhysChem* **2017**, *18* (15), 1961-1965.
64. Cowley, M. J.; Adams, R. W.; Atkinson, K. D.; Cockett, M. C.; Duckett, S. B.; Green, G. G.; Lohman, J. A.; Kerssebaum, R.; Kilgour, D.; Mewis, R. E., Iridium N-heterocyclic carbene complexes as efficient catalysts for magnetization transfer from para-hydrogen. *Journal of the American Chemical Society* **2011**, *133* (16), 6134-6137.
65. Lloyd, L. S.; Asghar, A.; Burns, M. J.; Charlton, A.; Coombes, S.; Cowley, M. J.; Dear, G. J.; Duckett, S. B.; Genov, G. R.; Green, G. G., Hyperpolarisation through reversible interactions with para hydrogen. *Catalysis Science & Technology* **2014**, *4* (10), 3544-3554.
66. Fekete, M.; Rayner, P. J.; Green, G. G.; Duckett, S. B., Harnessing polarisation transfer to indazole and imidazole through signal amplification by reversible exchange to improve their NMR detectability. *Magnetic Resonance in Chemistry* **2017**, *55* (10), 944-957.
67. Iali, W.; Rayner, P. J.; Duckett, S. B., Using parahydrogen to hyperpolarize amines, amides, carboxylic acids, alcohols, phosphates, and carbonates. *Science Advances* **2018**, *4* (1), eaao6250.
68. Dücker, E. B.; Kuhn, L. T.; Münnemann, K.; Griesinger, C., Similarity of SABRE field dependence in chemically different substrates. *Journal of magnetic resonance* **2012**, *214*, 159-165.
69. Rayner, P. J.; Duckett, S. B., Signal amplification by reversible exchange (SABRE): From discovery to diagnosis. *Angewandte Chemie International Edition* **2018**, *57* (23), 6742-6753.

70. Levitt, M. H., *Spin dynamics: basics of nuclear magnetic resonance*. John Wiley & Sons: 2013.
71. Rayner, P. J.; Burns, M. J.; Oлару, A. M.; Norcott, P.; Fekete, M.; Green, G. G.; Highton, L. A.; Mewis, R. E.; Duckett, S. B., Delivering strong ¹H nuclear hyperpolarization levels and long magnetic lifetimes through signal amplification by reversible exchange. *Proceedings of the National Academy of Sciences* **2017**, *114* (16), E3188-E3194.
72. Holmes, A. J.; Rayner, P. J.; Cowley, M. J.; Green, G. G.; Whitwood, A. C.; Duckett, S. B., The reaction of an iridium PNP complex with para hydrogen facilitates polarisation transfer without chemical change. *Dalton transactions* **2015**, *44* (3), 1077-1083.
73. Richardson, P. M.; John, R. O.; Parrott, A. J.; Rayner, P. J.; Iali, W.; Nordon, A.; Halse, M. E.; Duckett, S. B., Quantification of hyperpolarisation efficiency in SABRE and SABRE-Relay enhanced NMR spectroscopy. *Physical Chemistry Chemical Physics* **2018**, *20* (41), 26362-26371.
74. Norcott, P.; Burns, M. J.; Rayner, P. J.; Mewis, R. E.; Duckett, S. B., Using ²H Labelling to Improve the NMR Detectability of Pyridine and its Derivatives by SABRE. *Magnetic Resonance in Chemistry* **2018**, *56* (7), 663-671.
75. Iali, W.; Roy, S. S.; Tickner, B. J.; Ahwal, F.; Kennerley, A. J.; Duckett, S. B., Hyperpolarising pyruvate through signal amplification by reversible exchange (SABRE). *Angewandte Chemie* **2019**, *131* (30), 10377-10381.
76. Salnikov, O. G.; Chukanov, N. V.; Svyatova, A.; Trofimov, I. A.; Kabir, M. S.; Gelovani, J. G.; Kovtunov, K. V.; Koptuyug, I. V.; Chekmenev, E. Y., ¹⁵N NMR Hyperpolarization of Radiosensitizing Antibiotic Nimorazole by Reversible Parahydrogen Exchange in Microtesla Magnetic Fields. *Angewandte Chemie* **2021**, *133* (5), 2436-2443.
77. Birchall, J. R.; Kabir, M. S.; Salnikov, O. G.; Chukanov, N. V.; Svyatova, A.; Kovtunov, K. V.; Koptuyug, I. V.; Gelovani, J. G.; Goodson, B. M.; Pham, W., Quantifying the effects of quadrupolar sinks via ¹⁵N relaxation dynamics in metronidazoles hyperpolarized via SABRE-SHEATH. *Chemical Communications* **2020**, *56* (64), 9098-9101.
78. Sellies, L.; Aspers, R. L.; Feiters, M. C.; Rutjes, F. P.; Tessari, M., Parahydrogen Hyperpolarization Allows Direct NMR Detection of α -Amino Acids in Complex (Bio) mixtures. *Angewandte Chemie* **2021**, *133* (52), 27160-27165.
79. Richardson, P. M.; Iali, W.; Roy, S. S.; Rayner, P. J.; Halse, M. E.; Duckett, S. B., Rapid ¹³C NMR hyperpolarization delivered from para-hydrogen enables the low concentration detection and quantification of sugars. *Chemical science* **2019**, *10* (45), 10607-10619.
80. Ratajczyk, T.; Gutmann, T.; Bernatowicz, P.; Buntkowsky, G.; Frydel, J.; Fedorczyk, B., NMR signal enhancement by effective SABRE labeling of oligopeptides. *Chemistry—A European Journal* **2015**, *21* (36), 12616-12619.
81. Barskiy, D. A.; Kovtunov, K. V.; Koptuyug, I. V.; He, P.; Groome, K. A.; Best, Q. A.; Shi, F.; Goodson, B. M.; Shchepin, R. V.; Coffey, A. M., The feasibility of formation and kinetics of NMR signal amplification by reversible exchange (SABRE) at high magnetic field (9.4 T). *Journal of the American Chemical Society* **2014**, *136* (9), 3322-3325.
82. Appleby, K. M.; Mewis, R. E.; Oлару, A. M.; Green, G. G.; Fairlamb, I. J.; Duckett, S. B., Investigating pyridazine and phthalazine exchange in a series of iridium complexes in order to define their role in the catalytic transfer of magnetisation from para-hydrogen. *Chemical science* **2015**, *6* (7), 3981-3993.
83. Khan, M. Hyperpolarization using Parahydrogen. University of York, 2013.
84. Truong, M. L.; Shi, F.; He, P.; Yuan, B.; Plunkett, K. N.; Coffey, A. M.; Shchepin, R. V.; Barskiy, D. A.; Kovtunov, K. V.; Koptuyug, I. V., Irreversible catalyst activation enables hyperpolarization and water solubility for NMR signal amplification by reversible exchange. *The Journal of Physical Chemistry B* **2014**, *118* (48), 13882-13889.
85. Lawrence, S. A., *Amines: synthesis, properties and applications*. Cambridge University Press: 2004.

86. Gloria, M. B. A., Bioactive amines. *Hui, YH Handbook of Food Science, Technology and* **2005**.
87. Marieb, E. N.; Hoehn, K., *Human anatomy & physiology*. Pearson education: 2007.
88. Ohtsu, H., Histamine synthesis and lessons learned from histidine decarboxylase deficient mice. In *Histamine in Inflammation*, Springer: 2010; pp 21-31.
89. Nieto-Alamilla, G.; Márquez-Gómez, R.; García-Gálvez, A.-M.; Morales-Figueroa, G.-E.; Arias-Montaño, J.-A., The histamine H3 receptor: structure, pharmacology, and function. *Molecular pharmacology* **2016**, *90* (5), 649-673.
90. Voet, D.; Voet, J. G., *Biochimie*. De Boeck Supérieur: 2016.
91. Lou, H., Dopamine precursors and brain function in phenylalanine hydroxylase deficiency. *Acta Paediatrica* **1994**, *83*, 86-88.
92. Daubner, S. C.; Le, T.; Wang, S., Tyrosine hydroxylase and regulation of dopamine synthesis. *Archives of biochemistry and biophysics* **2011**, *508* (1), 1-12.
93. Berridge, K. C.; Robinson, T. E.; Aldridge, J. W., Dissecting components of reward: 'liking', 'wanting', and learning. *Current opinion in pharmacology* **2009**, *9* (1), 65-73.
94. Bhatt-Mehta, V.; Nahata, M. C., Dopamine and dobutamine in pediatric therapy. *Pharmacotherapy: The Journal of Human Pharmacology and Drug Therapy* **1989**, *9* (5), 303-314.
95. Noori, S.; Friedlich, P.; Seri, I., Pharmacology review: developmentally regulated cardiovascular, renal, and neuroendocrine effects of dopamine. *NeoReviews* **2003**, *4* (10), e283-e288.
96. Wong, L.; Hendeles, L.; Weinberger, M., Pharmacologic prophylaxis of allergic rhinitis: relative efficacy of hydroxyzine and chlorpheniramine. *Journal of Allergy and Clinical Immunology* **1981**, *67* (3), 223-228.
97. Gunanathan, C.; Milstein, D., Selective synthesis of primary amines directly from alcohols and ammonia. *Angewandte Chemie* **2008**, *120* (45), 8789-8792.
98. Bohnet, M., *Ullmann's encyclopedia of industrial chemistry*. Wiley-Vch: 2003.
99. Heacock, R.; Marion, L., The infrared spectra of secondary amines and their salts. *Canadian Journal of Chemistry* **1956**, *34* (12), 1782-1795.
100. Gohlke, R.; McLafferty, F., Mass Spectrometric Analysis. Aliphatic Amines. *Analytical Chemistry* **1962**, *34* (10), 1281-1287.
101. Irsfeld, M.; Spadafore, M.; Prüß, B. M., β -phenylethylamine, a small molecule with a large impact. *WebmedCentral* **2013**, *4* (9).
102. Sun, P.; Schuurink, R. C.; Caissard, J.-C.; Huguency, P.; Baudino, S., My way: noncanonical biosynthesis pathways for plant volatiles. *Trends in plant science* **2016**, *21* (10), 884-894.
103. Kamata, S.; Imura, K.; Okada, A.; Kawashima, Y.; Yamatodani, A.; Watanabe, T.; Wada, H., Simultaneous analyses of phenethylamine, phenylethanolamine, tyramine and octopamine in rat brain using fluorecamine. *Journal of Chromatography B: Biomedical Sciences and Applications* **1982**, *231* (2), 291-299.
104. Zhao, J.; Wang, M.; Avula, B.; Khan, I. A., Detection and quantification of phenethylamines in sports dietary supplements by NMR approach. *Journal of pharmaceutical and biomedical analysis* **2018**, *151*, 347-355.
105. Kwon, Y.; Yu, S.-i.; Lee, H.; Yim, J. H.; Zhu, J.-K.; Lee, B.-h., Arabidopsis serine decarboxylase mutants implicate the roles of ethanolamine in plant growth and development. *International journal of molecular sciences* **2012**, *13* (3), 3176-3188.
106. Rontein, D.; Nishida, I.; Tashiro, G.; Yoshioka, K.; Wu, W.-l.; Voelker, D. R.; Basset, G.; Hanson, A. D., Plants synthesize ethanolamine by direct decarboxylation of serine using a pyridoxal phosphate enzyme. *Journal of Biological Chemistry* **2001**, *276* (38), 35523-35529.

107. Patel, D.; Witt, S. N., Ethanolamine and phosphatidylethanolamine: partners in health and disease. *Oxidative medicine and cellular longevity* **2017**, 2017.
108. Iali, W.; Rayner, P. J.; Alshehri, A.; Holmes, A. J.; Ruddlesden, A. J.; Duckett, S. B., Direct and indirect hyperpolarisation of amines using para hydrogen. *Chemical science* **2018**, 9 (15), 3677-3684.
109. Atkinson, K. D.; Cowley, M. J.; Elliott, P. I.; Duckett, S. B.; Green, G. G.; López-Serrano, J. n.; Whitwood, A. C., Spontaneous Transfer of Para hydrogen Derived Spin Order to Pyridine at Low Magnetic Field. *Journal of the American Chemical Society* **2009**, 131 (37), 13362-13368.
110. Zeng, H.; Xu, J.; Gillen, J.; McMahon, M. T.; Artemov, D.; Tyburn, J.-M.; Lohman, J. A.; Mewis, R. E.; Atkinson, K. D.; Green, G. G., Optimization of SABRE for polarization of the tuberculosis drugs pyrazinamide and isoniazid. *Journal of magnetic resonance* **2013**, 237, 73-78.
111. Mewis, R. E.; Atkinson, K. D.; Cowley, M. J.; Duckett, S. B.; Green, G. G.; Green, R. A.; Highton, L. A.; Kilgour, D.; Lloyd, L. S.; Lohman, J. A., Probing signal amplification by reversible exchange using an NMR flow system. *Magnetic Resonance in Chemistry* **2014**, 52 (7), 358-369.
112. Chen, W.; Viljoen, A., Geraniol—a review of a commercially important fragrance material. *South African Journal of Botany* **2010**, 76 (4), 643-651.
113. Bauer, K.; Garbe, D.; Surburg, H., *Common fragrance and flavor materials: preparation, properties and uses*. John Wiley & Sons: 2008.
114. Bakkali, F.; Averbeck, S.; Averbeck, D.; Idaomar, M., Biological effects of essential oils—a review. *Food and chemical toxicology* **2008**, 46 (2), 446-475.
115. Tozoni, D.; Zacaria, J.; Vanderlinde, R.; Delamare, A. P. L.; Echeverrigaray, S., Degradation of citronellol, citronellal and citronellyl acetate by *Pseudomonas mendocina* IBPse 105. *Electronic Journal of Biotechnology* **2010**, 13 (2), 2-3.
116. Rayner, P. J.; Tickner, B. J.; Iali, W.; Fekete, M.; Robinson, A. D.; Duckett, S. B., Relayed hyperpolarization from para-hydrogen improves the NMR detectability of alcohols. *Chemical science* **2019**, 10 (33), 7709-7717.
117. Morris, G. A., Sensitivity enhancement in nitrogen-15 NMR: polarization transfer using the INEPT pulse sequence. *Journal of the American Chemical Society* **1980**, 102 (1), 428-429.
118. Lapczynski, A.; Bhatia, S.; Letizia, C.; Api, A., Fragrance material review on rhodinol. *Food and chemical toxicology* **2008**, 46 (11), S259-S262.
119. Alshehri, A.; Tickner, B. J.; Iali, W.; Duckett, S. B., Enhancing the NMR signals of plant oil components using hyperpolarisation relayed via proton exchange. *Chemical Science* **2023**.
120. Aung, K.; Jiang, Y.; He, S. Y. J. T. P. J., The role of water in plant–microbe interactions. **2018**, 93 (4), 771-780.
121. Mengel, K.; Kirkby, E. A.; Kosegarten, H.; Appel, T., Plant Water Relationships. In *Principles of Plant Nutrition*, Mengel, K.; Kirkby, E. A.; Kosegarten, H.; Appel, T., Eds. Springer Netherlands: Dordrecht, 2001; pp 181-242.
122. Sterling, T. M. J. J. o. N. R.; Education, L. S., Transpiration: Water Movement through Plants. **2005**, 34, 123.
123. McCarney, E. R.; Armstrong, B. D.; Lingwood, M. D.; Han, S. J. P. o. t. N. A. o. S., Hyperpolarized water as an authentic magnetic resonance imaging contrast agent. **2007**, 104 (6), 1754-1759.
124. Van As, H.; Scheenen, T.; Vergeldt, F. J. J. P. R., MRI of intact plants. **2009**, 102 (2-3), 213.
125. Harris, T.; Szekely, O.; Frydman, L. J. T. J. o. P. C. B., On the potential of hyperpolarized water in biomolecular NMR studies. **2014**, 118 (12), 3281-3290.

126. Lipsø, K. W.; Bowen, S.; Rybalko, O.; Ardenkjær-Larsen, J. H. J. o. M. R., Large dose hyperpolarized water with dissolution-DNP at high magnetic field. **2017**, *274*, 65-72.
127. Olsen, G.; Markhasin, E.; Szekely, O.; Bretschneider, C.; Frydman, L. J. J. o. M. R., Optimizing water hyperpolarization and dissolution for sensitivity-enhanced 2D biomolecular NMR. **2016**, *264*, 49-58.
128. Ardenkjær-Larsen, J. H.; Laustsen, C.; Bowen, S.; Rizi, R., Hyperpolarized H₂O MR angiography. *Magnetic resonance in medicine* **2014**, *71* (1), 50-56.
129. Lipsø, K. W.; Hansen, E. S. S.; Tougaard, R. S.; Laustsen, C.; Ardenkjær-Larsen, J. H., Dynamic coronary MR angiography in a pig model with hyperpolarized water. *Magnetic Resonance in Medicine* **2018**, *80* (3), 1165-1169.
130. Wigh Lipsø, K.; Hansen, E. S. S.; Tougaard, R. S.; Laustsen, C.; Ardenkjær-Larsen, J. H., Renal MR angiography and perfusion in the pig using hyperpolarized water. *Magnetic resonance in medicine* **2017**, *78* (3), 1131-1135.
131. Anderson, W. A.; Arnold, J. T., Proton relaxation times in H₂O—D₂O mixtures. *Physical Review* **1956**, *101* (2), 511.
132. Pinon, A. C.; Capozzi, A.; Ardenkjær-Larsen, J. H., Hyperpolarized water through dissolution dynamic nuclear polarization with UV-generated radicals. *Communications Chemistry* **2020**, *3* (1), 1-9.
133. Oka, K.; Shibue, T.; Sugimura, N.; Watabe, Y.; Winther-Jensen, B.; Nishide, H., Long-lived water clusters in hydrophobic solvents investigated by standard NMR techniques. *Scientific reports* **2019**, *9* (1), 1-6.
134. El Daraï, T.; Jannin, S., Sample formulations for dissolution dynamic nuclear polarization. *Chemical Physics Reviews* **2021**, *2* (4), 041308.
135. TomHon, P.; Abdulmojeed, M.; Adelabu, I.; Nantogma, S.; Kabir, M. S. H.; Lehmkühl, S. r.; Chekmenev, E. Y.; Theis, T., Temperature Cycling Enables Efficient ¹³C SABRE-SHEATH Hyperpolarization and Imaging of [1-¹³C]-Pyruvate. *Journal of the American Chemical Society* **2021**, *144* (1), 282-287.
136. Adams, R. W.; John, R. O.; Blazina, D.; Eguillor, B.; Cockett, M. C.; Dunne, J. P.; López-Serrano, J.; Duckett, S. B., Contrasting Photochemical and Thermal Catalysis by Ruthenium Arsine Complexes Revealed by Parahydrogen Enhanced NMR Spectroscopy. *European Journal of Inorganic Chemistry* **2022**, *2022* (5), e202100991.
137. Yu, H.-Y.; Myoung, S.; Ahn, S., Recent Applications of Benchtop Nuclear Magnetic Resonance Spectroscopy. *Magnetochemistry* **2021**, *7* (9), 121.
138. Blanchard, J. W.; Ripka, B.; Suslick, B. A.; Gelevski, D.; Wu, T.; Münnemann, K.; Barskiy, D. A.; Budker, D., Towards large-scale steady-state enhanced nuclear magnetization with in situ detection. *Magnetic Resonance in Chemistry* **2021**, *59* (12), 1208-1215.
139. Knecht, S.; Blanchard, J. W.; Barskiy, D.; Cavallari, E.; Dagys, L.; Van Dyke, E.; Tsukanov, M.; Bliemel, B.; Münnemann, K.; Aime, S., Rapid hyperpolarization and purification of the metabolite fumarate in aqueous solution. *Proceedings of the National Academy of Sciences* **2021**, *118* (13), e2025383118.
140. Barbosa, T. T₁ relaxation: definition, measurement and practical implications! <https://www.nanalysis.com/nmready-blog/part-1-t1-relaxation-definition-measurement-and-practical-implications> (accessed 16-11-2022).
141. Semenova, O.; Richardson, P. M.; Parrott, A. J.; Nordon, A.; Halse, M. E.; Duckett, S. B., Reaction monitoring using SABRE-hyperpolarized benchtop (1 T) NMR spectroscopy. *Analytical chemistry* **2019**, *91* (10), 6695-6701.